times a factor $[1 + O(v^2/c^2)]$. Now we use the identities

$$(\mathbf{T}^{l-2}_{lm})_{ij} = \left[\frac{l(l-1)}{(2l-1)(2l+1)}\right]^{1/2} \mathcal{Y}^{lm}_{iji_1\dots i_{l-2}}\, n_{i_1}\cdots n_{i_{l-2}}\,, \tag{3.363}$$

$$(\mathbf{T}^{l-1}_{lm})_{ij} = i\left[\frac{2l(l-1)}{(l+1)(2l+1)}\right]^{1/2} \epsilon_{pq(i}\mathcal{Y}^{lm}_{j)qi_1\dots i_{l-2}}\, n_p n_{i_1}\cdots n_{i_{l-2}}\,, \tag{3.364}$$

where the parentheses on the indices, in eq. (3.364), denotes the symmetrization over the indices i, j (i.e. $A_{(ij)} \equiv (1/2)(A_{ij} + A_{ji})$). These identities can be obtained (with quite some work) inserting eq. (3.234) into the definition of the spin-2 tensor harmonics. Inserting the explicit values of a_{33}, b_{22} from Table 3.1 (and recalling the change of notation $j \to l$ that we made in between, see Note 47), we get

$$\begin{aligned} u_{lm} &= \left[\frac{(l+1)(l+2)}{2(2l-1)(2l+1)}\right]^{1/2} \frac{4}{(l-2)!} \left[\frac{l(l-1)}{(2l-1)(2l+1)}\right]^{1/2} \\ &\quad\times \left(\partial_0^{l-2} S^{ij,i_1\dots i_{l-2}}\right) \mathcal{Y}^{lm*}_{ijj_1\dots j_{l-2}} \int d\Omega\, n_{i_1}\cdots n_{i_{l-2}}\, n_{j_1}\cdots n_{j_{l-2}} \\ &= \left[\frac{1}{2}\, l(l-1)(l+1)(l+2)\right]^{1/2} \frac{4}{(l-2)!}\, \frac{1}{(2l-1)(2l+1)} \\ &\quad\times \frac{4\pi}{(2l-3)!!}(l-2)!\, \left(\partial_0^{l-2} S^{ij,i_1\dots i_{l-2}}\right) \mathcal{Y}^{lm*}_{iji_1\dots i_{l-2}} \\ &= \frac{16\pi}{(2l+1)!!} \left[\frac{1}{2}\, l(l-1)(l+1)(l+2)\right]^{1/2} \left(\partial_0^{l-2} S^{ij,i_1\dots i_{l-2}}\right) \mathcal{Y}^{lm*}_{iji_1\dots i_{l-2}}\,. \end{aligned} \tag{3.365}$$

where the final integral as been performed using eq. (3.23). The integral for v_{lm} is performed similarly using eqs. (3.363) and (3.364), with the final result given in the text.

Further reading

- The quadrupole radiation is discussed in all general relativity textbooks, see in particular Weinberg (1972), Misner, Thorne and Wheeler (1973), Landau and Lifshitz, Vol. II (1979) and Straumann (2004).
- The radiation from sources with arbitrary velocity is discussed in Weinberg (1972), Section 10.4. Gravitational wave generation is also discussed in detail in the reviews Thorne (1983) and (1987).
- Radiation reaction for slow-motion sources is discussed in Misner, Thorne and Wheeler (1973), Sections 36.8 and 36.11.
- The multipole expansion for time-dependent fields in terms of STF tensors was introduced by Sachs (1961) and Pirani (1964). Thorne (1980) derived the slow-motion expansion of the mass and spin multipole moments, both in STF and in spherical tensor form. The closed-form expression for these moments in STF form is derived in Damour and Iyer (1991a). A detailed review of the multipole expansion for GWs, as well as a historical overview of the relevant literature, is Thorne (1980). A physical discussion of current quadrupole radiation is given in Schutz and Ricci (2001).

Applications

4

In this chapter we apply the formalism that we have developed to various instructive problems. The systems that we examine here are still somewhat idealized, compared to real astrophysical sources. This allows us to understand the essence of the physical mechanisms with a minimum of complications, and forms the basis for a more detailed study of realistic sources, which will be the subject of Vol. 2.

We begin, in Section 4.1, with the study of binary systems, taking the bodies as point-like and moving at first on a Newtonian trajectory. We will compute how the back-reaction of GWs affects the motion of the sources, inducing the inspiral and coalescence of the binary system, and we will see how this, in turn, affects the emission of the GWs themselves.

In Section 4.2 we will compute the radiation emitted by spinning rigid bodies, which are a first idealization of rotating neutron stars.

In Section 4.3 we compute the radiation emitted by a body falling radially into a black hole. A full resolution of this problem requires expansion over the Schwarzschild metric, rather than over flat space-time of linearized theory, and will be deferred to Vol. 2. However, we will see that the low-frequency part of the spectrum can be computed using a flat space-time background, so we can perform here this part of the computation. We will also compare the situation in which the infalling particle is point-like with that of a real star, which can be disrupted by the tidal gravitational force of the black hole. This is particularly instructive because it allows us to compare the coherent and the incoherent emission of GWs.

In Section 4.4 we study the radiation emitted by a mass accelerated by an external force. It will be interesting to compare the results with the electromagnetic radiation from an accelerated charge. We will see that, while the electromagnetic field of a relativistic charge is beamed into a small angle in the forward direction, this does not happen in the gravitational case. Finally, some computational details are collected in a Solved Problems section, at the end of the chapter.

4.1 Inspiral of compact binaries

In this section we consider a binary system made of two compact stars, such as neutron stars or black holes, and we treat them as point-like, with masses m_1, m_2, and positions $\mathbf{r}_1$ and $\mathbf{r}_2$. In the Newtonian approximation, and in the center-of-mass frame (CM), the dynamics reduces to a one-body problem with mass equal to the reduced mass

$\mu = m_1 m_2/(m_1+m_2)$, and equation of motion $\ddot{\mathbf{r}} = -(Gm/r^3)\mathbf{r}$, where $m = m_1 + m_2$ is the total mass and $\mathbf{r} = \mathbf{r}_2 - \mathbf{r}_1$ the relative coordinate. We consider first the case of circular orbits. Then the orbital frequency ω_s is related to the orbital radius R by $v^2/R = Gm/R^2$ with $v = \omega_s R$, so we have Kepler's law

$$\omega_s^2 = \frac{Gm}{R^3}\,. \tag{4.1}$$

We already studied this system in Problem 3.2, and the corresponding gravitational wave amplitudes are given in eqs. (3.330) and (3.331). In these expressions, we eliminate R in favor of ω_s using eq. (4.1), and we introduce the *chirp mass*

$$\boxed{M_c = \mu^{3/5} m^{2/5} = \frac{(m_1 m_2)^{3/5}}{(m_1+m_2)^{1/5}}\,.} \tag{4.2}$$

Then eqs. (3.330) and (3.331) become

$$\boxed{\begin{aligned} h_+(t) &= \frac{4}{r}\left(\frac{GM_c}{c^2}\right)^{5/3}\left(\frac{\pi f_{\rm gw}}{c}\right)^{2/3}\frac{1+\cos^2\theta}{2}\cos(2\pi f_{\rm gw} t_{\rm ret} + 2\phi)\,,\\ h_\times(t) &= \frac{4}{r}\left(\frac{GM_c}{c^2}\right)^{5/3}\left(\frac{\pi f_{\rm gw}}{c}\right)^{2/3}\cos\theta\,\sin(2\pi f_{\rm gw} t_{\rm ret} + 2\phi)\,, \end{aligned}} \tag{4.3}$$

where we expressed the result in terms of $f_{\rm gw} = \omega_{\rm gw}/(2\pi)$, with $\omega_{\rm gw} = 2\omega_s$. Observe that, in this lowest-order Newtonian approximation, the amplitudes h_+ and $h_\times$ of the GWs emitted depend on the masses m_1, m_2 only through the combination M_c.

The factors in eq. (4.3) are possibly more expressive if we write them in terms of ratios of quantities with dimension of length, introducing the Schwarzschild radius associated to the chirp mass,

$$R_c \equiv \frac{2GM_c}{c^2}\,, \tag{4.4}$$

and using the reduced wavelength of the GW, $\lambda\!\!\!^{-} = c/\omega_{\rm gw}$. Then, eq. (4.3) reads

$$h_+(t) = \mathcal{A}\,\frac{1+\cos^2\theta}{2}\cos(\omega_{\rm gw} t_{\rm ret} + 2\phi)\,, \tag{4.5}$$

$$h_\times(t) = \mathcal{A}\,\cos\theta\,\sin(\omega_{\rm gw} t_{\rm ret} + 2\phi)\,, \tag{4.6}$$

where

$$\mathcal{A} = \frac{1}{2^{1/3}}\left(\frac{R_c}{r}\right)\left(\frac{R_c}{\lambda\!\!\!^{-}}\right)^{2/3}\,. \tag{4.7}$$

From eq. (3.337) we can write the power radiated in GWs, per unit solid angle, as

$$\frac{dP}{d\Omega} = \frac{2}{\pi}\frac{c^5}{G}\left(\frac{GM_c\omega_{\rm gw}}{2c^3}\right)^{10/3} g(\theta)\,, \tag{4.8}$$

where

$$g(\theta) = \left(\frac{1+\cos^2\theta}{2}\right)^2 + \cos^2\theta\,. \tag{4.9}$$

Observe that $\langle\cos^2(2\omega t + 2\phi)\rangle = 1/2$ is independent of ϕ, so the angular distribution of the radiated power, which is proportional to $\langle \dot{h}_+^2 + \dot{h}_\times^2\rangle$, is also independent of ϕ. The angular average of $g(\theta)$ is

$$\int \frac{d\Omega}{4\pi}\, g(\theta) = \frac{4}{5}\,, \tag{4.10}$$

where, as usual, $d\Omega = d\cos\theta\, d\phi$. The total radiated power P is therefore[1]

$$P = \frac{32}{5}\frac{c^5}{G}\left(\frac{GM_c\omega_{\rm gw}}{2c^3}\right)^{10/3}\,. \tag{4.12}$$

4.1.1 Circular orbits. The chirp amplitude

Equation (4.3) gives the amplitude of the GWs, assuming that the motion of the sources is on a given, fixed, circular Keplerian orbit. However, the emission of GWs costs energy. The source for the radiated energy is the sum of kinetic plus potential energy of the orbit, which is

$$\begin{aligned} E_{\rm orbit} &= E_{\rm kin} + E_{\rm pot}\\ &= -\frac{Gm_1 m_2}{2R}\,, \end{aligned} \tag{4.13}$$

and therefore, to compensate for the loss of energy to GWs, R must decrease in time, so that $E_{\rm orbit}$ becomes more and more negative.[2]

According to eq. (4.1), if R decreases, ω_s increases. On the other hand, if ω_s increases, also the power radiated in GWs increases, as we see from eq. (4.12). Then R must decrease further, and we have a runaway process which, on a sufficiently long time-scale, leads to the coalescence of the binary system. As long as

$$\dot{\omega}_s \ll \omega_s^2\,, \tag{4.14}$$

we are in the regime called of quasi-circular motion. In fact, using eq. (4.1) we see that the radial velocity $\dot{R}$ can be written as

$$\begin{aligned} \dot{R} &= -\frac{2}{3}R\frac{\dot{\omega}_s}{\omega_s}\\ &= -\frac{2}{3}(\omega_s R)\frac{\dot{\omega}_s}{\omega_s^2}\,. \end{aligned} \tag{4.15}$$

Then, as long as the condition $\dot{\omega}_s \ll \omega_s^2$ is fulfilled, $|\dot{R}|$ is much smaller than the tangential velocity $\omega_s R$, and the approximation of a circular orbit with a slowly varying radius is applicable. In the following, we compute the back-reaction of GWs when eq. (4.14) applies.

Using eq. (4.1), we eliminate R in favor of $\omega_{\rm gw}$ in eq. (4.13), and we get

$$E_{\rm orbit} = -(G^2 M_c^5 \omega_{\rm gw}^2/32)^{1/3}\,. \tag{4.16}$$

[1] In Section 5.6, where we apply the post-Newtonian formalism to inspiraling binaries, we will see that, rather than using the source frequency ω_s, it is convenient to use the variable $x = (Gm\omega_s/c^3)^{2/3}$, which is dimensionless and of order v^2/c^2, where v is the typical orbital velocity. We also introduce the "symmetric mass ratio" $\nu = \mu/m$, so $M_c = \nu^{3/5} m$. Since here we are computing in the quadrupole approximation and we are considering a circular orbit, we have $\omega_{\rm gw} = 2\omega_s$, and the result (4.12) can be written as

$$P = \frac{32}{5}\frac{c^5}{G}\nu^2 x^5\,. \tag{4.11}$$

The corrections to this result in the post-Newtonian expansion are given in eq. (5.257).

[2] In our idealized setting of point-like particles, the two masses have no internal structure, so no degrees of freedom that can relax supplying, at least partially, the required energy, and the only possible source of energy is the orbital energy of the system. Even in a realistic system of two stars, however, at least in the early phase of the coalescence, the orbital frequency is much smaller than the frequencies of the normal modes of the star, and therefore the internal dynamics of the stars is decoupled from the orbital motion, and all the energy supplied to GWs again comes from the orbital energy of the system. We will see in Section 5.5 that, for compact objects, corrections that depend on the internal structure of the bodies enter only at the very high order 5PN in the post-Newtonian expansion, i.e. they are corrections of order $(v/c)^{10}$ to the equations of motion.

Observe that, at fixed $\omega_{\rm gw}$, the dependence on the masses is again only through the chirp mass. Equating P in eq. (4.12) to $-dE_{\rm orbit}/dt$ we find

$$\dot{\omega}_{\rm gw} = \frac{12}{5} 2^{1/3} \left(\frac{GM_c}{c^3}\right)^{5/3} \omega_{\rm gw}^{11/3} , \tag{4.17}$$

or, in terms of $f_{\rm gw} = \omega_{\rm gw}/(2\pi)$,

$$\dot{f}_{\rm gw} = \frac{96}{5} \pi^{8/3} \left(\frac{GM_c}{c^3}\right)^{5/3} f_{\rm gw}^{11/3} . \tag{4.18}$$

Integrating eq. (4.18) we see that $f_{\rm gw}$ formally diverges at a finite value of time, that we denote $t_{\rm coal}$. In terms of $\tau \equiv t_{\rm coal} - t$ (the time to coalescence), the solution of eq. (4.18) reads[3]

$$f_{\rm gw}(\tau) = \frac{1}{\pi} \left(\frac{5}{256} \frac{1}{\tau}\right)^{3/8} \left(\frac{GM_c}{c^3}\right)^{-5/8} . \tag{4.19}$$

The divergence is cut off by the fact that, when their separation becomes smaller than a critical distance, the two stars merge, as we discuss in more detail below, see eq. (4.38). Inserting in eq. (4.19) the numerical values we find

$$\boxed{f_{\rm gw}(\tau) \simeq 134\,{\rm Hz} \left(\frac{1.21 M_\odot}{M_c}\right)^{5/8} \left(\frac{1\,s}{\tau}\right)^{3/8} ,} \tag{4.20}$$

where, as reference value for M_c, we have taken $1.21 M_\odot$, which is the chirp mass of a system of two stars, each one with a mass of $1.4 M_\odot$. Equivalently, we can write eq. (4.20) as

$$\tau \simeq 2.18\,{\rm s} \left(\frac{1.21 M_\odot}{M_c}\right)^{5/3} \left(\frac{100\,{\rm Hz}}{f_{\rm gw}}\right)^{8/3} . \tag{4.21}$$

From this we find that (when $M_c = 1.21 M_\odot$) at 10 Hz (which is of the order of the lowest frequencies accessible to ground-based interferometers) we get the radiation emitted at about $\tau = 17$ min to coalescence; at 100 Hz we get the radiation from the last two seconds, and at 1 kHz we get the radiation from the last few milliseconds. From Kepler's law (4.1) we find that, when $f_{\rm gw} = 1$ kHz, the separation between two bodies with $m_1 = m_2 = 1.4 M_\odot$ is $R \simeq 33$ km. Such a small separation can be reached only by very compact bodies like neutron stars and black holes. Since the radius of a neutron star with $m = 1.4 M_\odot$ is about 10 km, for neutron stars and black holes the point-like approximation at this stage becomes inaccurate, but still not meaningless.

A useful quantity for assessing the sensitivity of detectors to inspiraling binaries is the number of cycles spent in the detector bandwidth $f \in [f_{\rm min}, f_{\rm max}]$. When the period $T(t)$ of the GW is a slowly varying function of time, the number of cycles in a time interval dt is given by

[3] If we denote by $(t_{\rm coal})_{\rm ret}$ the value of retarded time $t_{\rm ret}$ at coalescence, and by $t_{\rm coal}$ the value of the observer time t at coalescence, we have $\tau = (t_{\rm coal})_{\rm ret} - t_{\rm ret} = t_{\rm coal} - t$, since retarded time and the observer time differ only by a constant quantity, the time taken by the GW to propagate, at the speed of light, from the source (whose center-of-mass, to an excellent approximation, can be taken to be at a fixed position during the observation time) to the observer. Therefore, even if what we observe today on Earth depends on what happened millions of years ago in a far galaxy, when a quantity like $f_{\rm gw}$ depends on the difference τ we can express it simply in terms of the observer time t.

$d\mathcal{N}_{\rm cyc} = dt/T(t) = f_{\rm gw}(t) dt$, so

$$\mathcal{N}_{\rm cyc} = \int_{t_{\rm min}}^{t_{\rm max}} f_{\rm gw}(t) dt = \int_{f_{\rm min}}^{f_{\rm max}} df_{\rm gw} \frac{f_{\rm gw}}{\dot{f}_{\rm gw}} . \tag{4.22}$$

For the inspiral of a binary system we can express $\dot{f}_{\rm gw}$ as a function of $f_{\rm gw}$ using eq. (4.18), and we get

$$\begin{aligned} \mathcal{N}_{\rm cyc} &= \frac{1}{32\pi^{8/3}} \left(\frac{GM_c}{c^3}\right)^{-5/3} \left(f_{\rm min}^{-5/3} - f_{\rm max}^{-5/3}\right) \\ &\simeq 1.6 \times 10^4 \left(\frac{10\,{\rm Hz}}{f_{\rm min}}\right)^{5/3} \left(\frac{1.2 M_\odot}{M_c}\right)^{5/3} , \end{aligned} \tag{4.23}$$

where in the second line we assumed $f_{\rm min}^{-5/3} - f_{\rm max}^{-5/3} \simeq f_{\rm min}^{-5/3}$, as is typically the case. This means that ground-based interferometers can follow the evolution of the signal for thousands of cycles, and a space-borne interferometer sensitive to the mHz region can follow it for millions of cycles.[4] For this reason, accurate predictions of the waveform, going well beyond the Newtonian approximation used here, are very important, and will be discussed in Section 5.6.

As the frequency increases, the orbital radius shrinks. From eqs. (4.1) and (4.19) (recalling that $\tau = t_{\rm coal} - t$, so that $d/d\tau = -d/dt$, and using a dot denotes d/dt),

$$\begin{aligned} \frac{\dot{R}}{R} &= -\frac{2}{3} \frac{\dot{\omega}_{\rm gw}}{\omega_{\rm gw}} \\ &= -\frac{1}{4\tau} , \end{aligned} \tag{4.24}$$

which integrates to

$$\begin{aligned} R(\tau) &= R_0 \left(\frac{\tau}{\tau_0}\right)^{1/4} \\ &= R_0 \left(\frac{t_{\rm coal} - t}{t_{\rm coal} - t_0}\right)^{1/4} \end{aligned} \tag{4.25}$$

where R_0 is the value of R at the initial time t_0, and $\tau_0 = t_{\rm coal} - t_0$. The function $R(t)$ is shown in Fig. 4.1. We see that there is a long phase where R decreases smoothly, followed by a plunge phase, where our approximation of quasi-circular orbit is no longer valid.[5]

Inserting eq. (4.19), evaluated at an initial time t_0 when $\tau = \tau_0$, into eq. (4.1), we find the relation between the initial radius R_0 and the time to coalescence τ_0,

$$\tau_0 = \frac{5}{256} \frac{c^5 R_0^4}{G^3 m^2 \mu} . \tag{4.26}$$

[4] More precisely, a space interferometer such as LISA has $f_{\rm min} \sim 10^{-4}$ Hz, and signals in this frequency band are produced by the inspiral into supermassive BHs with a mass $O(10^6) M_\odot$. In a coalescence of two supermassive BHs with $m_1 = m_2 = 10^6 M_\odot$, we have $M_c \simeq 0.9 \times 10^6 M_\odot$ and $\mathcal{N}_c$ is only of order 600. However, in the infall of a stellar mass black hole into a supermassive black hole, taking $m_1 = 10^6 M_\odot$ and $m_2 = 10 M_\odot$, we have $M_c \simeq 10^3 M_\odot$ and $\mathcal{N}_c \simeq 5 \times 10^7$.

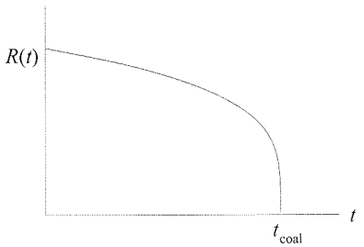

Fig. 4.1 The evolution of the separation $R(t)$ between the two bodies, in the lowest-order Newtonian approximation.

[5] Furthermore, in compact binaries made of black holes or neutron stars, the flat-space approximation is totally inadequate in the plunge phase, see the discussion around eq. (4.38) below. We will discuss the plunge phase for systems with BH or NS in Vol. 2.

Expressing the initial radius R_0 in terms of the initial orbital period $T_0 = 2\pi/\omega_s(\tau_0)$ through Kepler's law, $R_0^2 = Gm(T_0/2\pi)^2$, and plugging in the numerical values, we find

$$\boxed{\tau_0 \simeq 9.829 \times 10^6\,\mathrm{yr} \left(\frac{T_0}{1\,\mathrm{hr}}\right)^{8/3} \left(\frac{M_\odot}{m}\right)^{2/3} \left(\frac{M_\odot}{\mu}\right).} \tag{4.27}$$

Therefore, under our assumption of circular orbits and for masses of order $M_\odot$, only binaries which at formation had an initial orbital period of less than about one day can have coalesced by emission of GWs, within the present age of galaxies. We will discuss in Section 4.1.2 how this result is modified for elliptic orbits.

Until now we have studied how the GW frequency evolves in time, in a binary system. We next examine how the corresponding waveform of the GW changes. A particle that moves on a quasi-circular orbit in the (x, y) plane with a radius $R = R(t)$ and an angular velocity $\omega_s = \omega_s(t)$ has Cartesian coordinates $x(t) = R(t)\cos(\Phi(t)/2)$ and $y(t) = R(t)\sin(\Phi(t)/2)$, where we have defined

$$\begin{aligned}\Phi(t) &= 2\int_{t_0}^{t} dt'\,\omega_s(t') \\ &= \int_{t_0}^{t} dt'\,\omega_{\rm gw}(t')\,.\end{aligned} \tag{4.28}$$

When we compute the GW production in the quadrupole approximation, in the computation of the second time derivative of the quadrupole moment there are therefore three differences, compared to the case when ω_s and R constants, i.e. to the computation which gives eq. (4.3):

- in the argument of the trigonometric functions, $\omega_{\rm gw}t$ must be replaced by $\Phi(t)$;
- in the factors in front of the trigonometric functions, $\omega_{\rm gw}$ is replaced by $\omega_{\rm gw}(t)$;
- we should also include in the computation the contributions coming from the derivatives of $R(t)$ and of $\omega_{\rm gw}(t)$.

However, as we have seen above, the radial velocity $\dot{R}$ is negligible as long as $\dot{\omega}_s \ll \omega_s^2$. Using eq. (4.17), the condition $\dot{\omega}_s \ll \omega_s^2$ translates into $GM_c\omega_s/c^3 \ll 0.5$. In terms of $f_{\rm gw} = \omega_{\rm gw}/(2\pi)$, this means that $\dot{R}$ is negligible as long as $f_{\rm gw} \ll 13\,\mathrm{kHz}\,(1.2M_\odot/M_c)$. As we will see in eq. (4.40) below, the transition to the plunge phase takes place earlier, thus as long as we assume that we are in the inspiral phase we can simply neglect the terms proportional to $\dot{R}$ in the computation of the waveform, at least to lowest order, and similarly for the terms involving the derivative of $\omega_{\rm gw}(t)$. The only changes, therefore, are the replacement of $\omega_{\rm gw}t$ by $\Phi(t)$ in the argument of the sine and cosine, and of ω_s by $\omega_s(t)$ in the prefactor, all evaluated at the retarded time $t_{\rm ret}$.[6] Then,

[6] As discussed in Problem 3.2, we are interested in the radiation that a binary star emits in the direction which points from the star toward us. The angle θ is therefore equal to the angle ι between the normal to the orbit and the line-of-sight, while we can orient the axes so that $\phi = 0$ or, equivalently, we can reabsorb the fixed value of ϕ into a shift of the origin of time.

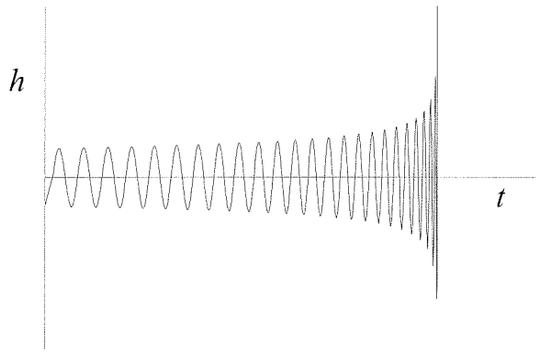

Fig. 4.2 The time evolution of the GW amplitude in the inspiral phase of a binary system.

$$\begin{aligned}h_+(t) &= \frac{4}{r}\left(\frac{GM_c}{c^2}\right)^{5/3}\left(\frac{\pi f_{\rm gw}(t_{\rm ret})}{c}\right)^{2/3}\left(\frac{1+\cos^2\iota}{2}\right)\cos[\Phi(t_{\rm ret})]\,, \\ h_\times(t) &= \frac{4}{r}\left(\frac{GM_c}{c^2}\right)^{5/3}\left(\frac{\pi f_{\rm gw}(t_{\rm ret})}{c}\right)^{2/3}\cos\iota\,\sin[\Phi(t_{\rm ret})]\,.\end{aligned} \tag{4.29}$$

Using the explicit expression (4.19) we find (recall that $d\tau = -dt$)

$$\Phi(\tau) = -2\left(\frac{5GM_c}{c^3}\right)^{-5/8}\tau^{5/8} + \Phi_0\,, \tag{4.30}$$

where $\Phi_0 = \Phi(\tau = 0)$ is an integration constant, equal to the value of Φ at coalescence. Then the GW amplitude can be expressed directly in terms of the time to coalescence τ measured by the observer,

$$h_+(t) = \frac{1}{r}\left(\frac{GM_c}{c^2}\right)^{5/4}\left(\frac{5}{c\tau}\right)^{1/4}\left(\frac{1+\cos^2\iota}{2}\right)\cos\left[\Phi(\tau)\right]\,, \tag{4.31}$$

$$h_\times(t) = \frac{1}{r}\left(\frac{GM_c}{c^2}\right)^{5/4}\left(\frac{5}{c\tau}\right)^{1/4}\cos\iota\,\sin\left[\Phi(\tau)\right]\,, \tag{4.32}$$

where

$$\tau = t_{\rm coal} - t\,, \tag{4.33}$$

t is the observer time (rather than retarded time) and $t_{\rm coal}$ is the value of t when the coalescence takes place (compare with Note 3). We see from the above equations that both the frequency and the amplitude increase as the coalescence is approached; this behavior is referred to as "chirping" (for its similarity with the chirp emitted by a bird). The functional dependence of h_+ (or of $h_\times$) on t is shown in Fig. 4.2.

As we will see in detail in Chapter 7, to compare the theoretical waveforms with the experimental sensitivities it is necessary to have the Fourier transform of the GW amplitudes. To compute the Fourier transform of the chirp signal is not completely straightforward, since $h_{+,\times}(t)$

are defined only on the interval $-\infty < t < t_{\rm coal}$, and we compute their Fourier transform explicitly in Problem 4.1. The result is

$$\tilde{h}_+(f) = A\, e^{i\Psi_+(f)}\, \frac{c}{r} \left(\frac{GM_c}{c^3}\right)^{5/6} \frac{1}{f^{7/6}} \left(\frac{1+\cos^2\iota}{2}\right), \qquad (4.34)$$

$$\tilde{h}_\times(f) = A\, e^{i\Psi_\times(f)}\, \frac{c}{r} \left(\frac{GM_c}{c^3}\right)^{5/6} \frac{1}{f^{7/6}} \cos\iota\,, \qquad (4.35)$$

where the constant A has the value

$$A = \frac{1}{\pi^{2/3}} \left(\frac{5}{24}\right)^{1/2}. \qquad (4.36)$$

The phases are given by $\Psi_\times = \Psi_+ + (\pi/2)$ and

$$\Psi_+(f) = 2\pi f\,(t_c + r/c) - \Phi_0 - \frac{\pi}{4} + \frac{3}{4}\left(\frac{GM_c}{c^3}\, 8\pi f\right)^{-5/3}, \qquad (4.37)$$

where Φ_0 is the value of the phase Φ at coalescence, see eq. (4.30). We will see in Sections 5.6 and 7.7 that an accurate computation of $\Psi_{+,\times}(f)$, going well beyond the Newtonian approximation, is crucial for discriminating the signal of a coalescing binary from the detector noise, and we will give in eq. (5.275) the post-Newtonian corrections to eq. (4.37).

The above computations have been performed in a flat background. For binary systems made of black holes or neutron stars, the gravitational field close to the stars is however strong, and this has important consequences on the dynamics of the binary system when the two objects get close. A full discussion of a realistic coalescence of compact binaries will be deferred to Vol. 2. However, the most important qualitative modification to the dynamics comes from the fact that, in the Schwarzschild geometry, there is a minimum value of the radial distance beyond which stable circular orbits are no longer allowed, i.e. an Innermost Stable Circular Orbit (ISCO). In Schwarzschild coordinates this is located at $r = r_{\rm ISCO}$, with

$$r_{\rm ISCO} = \frac{6Gm}{c^2}, \qquad (4.38)$$

where $m = m_1 + m_2$ is the total mass of the binary.[7] Therefore, for binaries made of BH or NS, a phase of slow adiabatic inspiral, going through a succession of quasi-circular orbit and driven by the emission of gravitational radiation, can only take place at distances $r \gtrsim r_{\rm ISCO}$. When the ISCO is approached, the dynamics is rather dominated by strong-field effects (namely, by the fact that the Schwarzschild geometry no longer allows for circular orbits), and the two stars plunge toward each other. Thus, the waveform computed above is only valid up to a maximum frequency $f_{\rm max}$, beyond which the inspiral phase ends and the two stars plunge toward each other and coalesce. From Kepler's law

[7] More precisely, this is valid in the test mass limit, when one of the two stars is much lighter than the other. For finite masses, this result receives corrections that can be expressed as an expansion in powers of the symmetric mass ratio $\nu = \mu/m$. The position of the ISCO is also affected by the spin of the bodies. We will discuss these effects in Vol. 2.

(4.1), this means that the inspiral phase ends when the source frequency f_s approaches the value

$$(f_s)_{\rm ISCO} = \frac{1}{6\sqrt{6}\,(2\pi)} \frac{c^3}{Gm}. \qquad (4.39)$$

Inserting the numerical values, this gives

$$\boxed{(f_s)_{\rm ISCO} \simeq 2.2\,{\rm kHz} \left(\frac{M_\odot}{m}\right).} \qquad (4.40)$$

For instance, for a NS-NS system with the typical masses $m_1 = m_2 \simeq 1.4 M_\odot$, so that $m \simeq 2.8 M_\odot$, we have $(f_s)_{\rm ISCO} \sim 800$ Hz, while for a BH-BH binary with a total mass $m = 10 M_\odot$ we have $(f_s)_{\rm ISCO} \sim 200$ Hz. The coalescence of two supermassive BHs with $m \sim 10^6 M_\odot$ takes place when f_s is in the mHz region.

Plugging eqs. (4.34) and (4.35) into eq. (1.160) and performing the angular integration we get the energy spectrum in the inspiral phase, in the Newtonian approximation,

$$\boxed{\frac{dE}{df} = \frac{\pi^{2/3}}{3G} (GM_c)^{5/3}\, f^{-1/3}.} \qquad (4.41)$$

Integrating up to the maximum GW frequency $f_{\rm max}$ for which we are still in the inspiral phase we can estimate the total energy radiated during the inspiral phase,

$$\Delta E_{\rm rad} \sim \frac{\pi^{2/3}}{2G} (GM_c)^{5/3}\, f_{\rm max}^{2/3}, \qquad (4.42)$$

or, inserting the numerical values,

$$\Delta E_{\rm rad} \sim 4.2 \times 10^{-2} M_\odot c^2 \left(\frac{M_c}{1.21 M_\odot}\right)^{5/3} \left(\frac{f_{\rm max}}{1\,{\rm kHz}}\right)^{2/3}. \qquad (4.43)$$

Setting $f_{\rm max} = 2(f_s)_{\rm ISCO}$ (as appropriate for quadrupole radiation) and using eq. (4.40) we see that the total energy radiated during the inspiral phase actually depends only on the reduced mass μ of the system, and is

$$\Delta E_{\rm rad} \sim 8 \times 10^{-2} \mu c^2. \qquad (4.44)$$

For stellar mass objects this is a huge amount of energy, and this makes coalescing binaries one of the most interesting sources of GWs. Actually, the above numerical value only provides an order-of-magnitude estimate, since we performed a flat-space computation, and we cut off the result by hand at the value of $(f_s)_{\rm ISCO}$ obtained from the Schwarzschild geometry. A better approach consists in observing that, in the Schwarzschild metric, the binding energy of the ISCO is given by[8]

$$E_{\rm binding} = (1 - \sqrt{8/9})\mu c^2 \simeq 5.7 \times 10^{-2} \mu c^2, \qquad (4.45)$$

[8] See e.g. Landau and Lifshitz, Vol. II (1979), Section 102, Problem 1.

and this is the total energy radiated in GWs when the binary system is slowly inspiraling from an orbit with large relative separation down to the ISCO. We will see in Vol. 2 that the post-Newtonian corrections to this binding energy are of order of a few per cent. Thus, the order-of-magnitude estimate given in eq. (4.44) turns out to be reasonably close to the correct result.

4.1.2 Elliptic orbits. (I) Total power and frequency spectrum of the radiation emitted

We now consider the radiation emitted by masses in an elliptic Keplerian orbit. As before, we denote by m_1, m_2 the masses of the two stars, by $m = m_1 + m_2$ the total mass, and by μ the reduced mass. As usual, in the CM the problem reduces to a one-body problem for a particle of mass μ, subject to an acceleration $\ddot{\mathbf{r}} = -(Gm/r^2)\hat{\mathbf{r}}$. We first recall, from elementary mechanics, the solution of this equation of motion for an elliptic orbit, and then we compute the total power radiated in GWs and its frequency spectrum.

Elliptic Keplerian orbits

The general solution of the equation of motion is obtained by observing that there are two first integral of motion, the angular momentum $\mathbf{L}$, and the energy E. The conservation of $\mathbf{L}$ implies that the orbit lies in a plane; we then introduce polar coordinates (r, ψ) in the plane of the orbit, with origin on the position of the center-of-mass (we use ψ to denote the angular position along the orbit, since we reserve θ and ϕ to describe the angular distribution of the radiation emitted). Then, in terms of r and ψ, the modulus of the angular momentum is given by

$$L = \mu r^2 \dot{\psi} \,, \tag{4.46}$$

while the energy is given by

$$\begin{aligned} E &= \frac{1}{2}\mu(\dot{r}^2 + r^2\dot{\psi}^2) - \frac{G\mu m}{r} \\ &= \frac{1}{2}\mu\dot{r}^2 + \frac{L^2}{2\mu r^2} - \frac{G\mu m}{r} \,. \end{aligned} \tag{4.47}$$

From eq. (4.47) we get dr/dt as a function of r while from eq. (4.46) we get $d\psi/dt$; combining the two expressions we find $dr/d\psi$ as a function of r and, integrating this expression, we obtain the equation of the orbit,

$$\frac{1}{r} = \frac{1}{R}(1 + e\cos\psi) \,. \tag{4.48}$$

The length-scale R and the eccentricity e are constants of motion, and are related to the energy E of the system (with $E < 0$ for a bound orbit) and to the orbital angular momentum L by

$$R = \frac{L^2}{Gm\mu^2} \,, \tag{4.49}$$

and

$$e^2 = 1 + \frac{2EL^2}{G^2 m^2 \mu^3} \,. \tag{4.50}$$

The eccentricity e for an ellipse satisfies $0 \leqslant e < 1$; for $e = 0$ the ellipse becomes a circle, while $e = 1$ corresponds to a parabola. The two semiaxes of the ellipse are given by

$$a = \frac{R}{1 - e^2} \,, \tag{4.51}$$

$$b = \frac{R}{(1 - e^2)^{1/2}} \,. \tag{4.52}$$

The geometry is shown in Fig. 4.3. Inserting the explicit expression for e given in eq. (4.50), we see that

$$a = \frac{Gm\mu}{2|E|} \,. \tag{4.53}$$

Observe that a is independent of L, so orbits with the same energy have the same value of the semimajor axis a. In terms of a and e, we can rewrite the equation of the orbit (4.48) in the form

$$r = \frac{a(1 - e^2)}{1 + e\cos\psi} \,. \tag{4.54}$$

Combining eqs. (4.46) and (4.49), we see also that $r(t)$ and $\dot{\psi}(t)$ satisfy the relation

$$\dot{\psi} = \frac{(GmR)^{1/2}}{r^2} \,. \tag{4.55}$$

The explicit time dependence of $r(t)$ and $\psi(t)$ is obtained by integrating eqs. (4.46) and (4.47) (making use also of the equation of the orbit) and is given in parametric form by

$$r = a[1 - e\cos u] \,, \tag{4.56}$$

$$\cos\psi = \frac{\cos u - e}{1 - e\cos u} \,, \tag{4.57}$$

where u is called the eccentric anomaly, and is related to t by the famous Kepler equation

$$\beta \equiv u - e\sin u = \omega_0 t \,, \tag{4.58}$$

with

$$\omega_0^2 = \frac{Gm}{a^3} \,. \tag{4.59}$$

We have chosen the origin of time such that, at $t = 0$, we have $\psi = 0$. Making use of trigonometric identities, eq. (4.57) can also be rewritten as

$$\tan\frac{\psi}{2} = \left(\frac{1+e}{1-e}\right)^{1/2} \tan\frac{u}{2} \,, \tag{4.60}$$

i.e.

$$\psi = A_e(u) \equiv 2\arctan\left[\left(\frac{1+e}{1-e}\right)^{1/2} \tan\frac{u}{2}\right] \,. \tag{4.61}$$

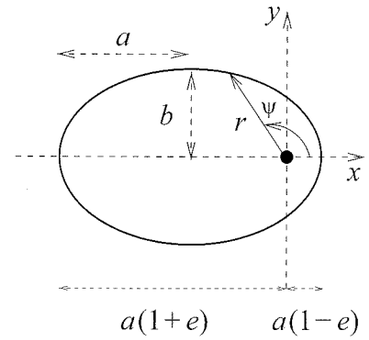

Fig. 4.3 The definitions used for an elliptic orbit. The polar coordinates (r, ψ), as well as the Cartesian coordinates (x, y), are centered on a focus of the ellipse (dark blob). The angle ψ is measured counterclockwise, from the x axis. The semiaxes a, b are indicated. The focus splits the major axis into two segments of length $a(1+e)$ and $a(1-e)$, respectively.

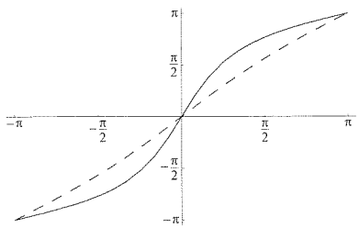

Fig. 4.4 The function $\psi(u)$ for $e = 0.2$ (dashed line) and for $e = 0.75$ (solid line).

The function $A_e(u)$ is called the true anomaly. Observe from eq. (4.58) that, if $t \to t + 2\pi/\omega_0$, we have $\beta \to \beta + 2\pi$ and $u \to u + 2\pi$, so the coordinates r, ψ are periodic functions of t, with period

$$T = \frac{2\pi}{\omega_0} \,. \tag{4.62}$$

As u runs between $-\pi$ and π, ψ also runs between $-\pi$ and π. A graph of $\psi(u)$ is shown in Fig. 4.4, for two different values of the ellipticity. Observe that, for $e = 0$, $\psi = u$. We will also use Cartesian coordinates (x, y) centered on the focus of the ellipse,

$$\begin{aligned} x &= r\cos\psi \\ &= a[\cos u(t) - e] \,, \end{aligned} \tag{4.63}$$

$$\begin{aligned} y &= r\sin\psi \\ &= b\sin u(t) \,. \end{aligned} \tag{4.64}$$

In terms of the original problem with two bodies of masses m_1 and m_2, the focus of the ellipse is the point where $\mathbf{x}_{\rm CM} = 0$, and the coordinates, measured from this point, are the relative coordinates in the CM system.[9]

[9]The equation of the ellipse in Cartesian coordinates would be slightly simpler if we choose the center of the ellipse, rather than a focus, as the origin, since in this case we simply have $x = a\cos u(t)$ and $y = b\sin u(t)$. However, recall from Section 3.3.5 that, if we want to compute the GW production using just the quadrupole moment for a particle with mass equal to the reduced mass of the system, we *must* choose the origin of our frame at the point where $\mathbf{x}_{\rm CM} = 0$.

Radiated power

We first compute the total power radiated in GWs, integrated over all frequencies and over the solid angle. We choose a reference frame where the orbit is in the (x, y) plane. In this frame the second mass moment is given by the 2×2 matrix

$$M_{ab} = \mu r^2 \begin{pmatrix} \cos^2\psi & \sin\psi\cos\psi \\ \sin\psi\cos\psi & \sin^2\psi \end{pmatrix}_{ab} \,, \tag{4.65}$$

where $a, b = 1, 2$ are indices in the (x, y) plane. To compute the total power emitted in the quadrupole approximation we must evaluate the third derivatives of M_{ab}, and we can then use the quadrupole formula in the form (3.76). In eq. (4.65) the time dependence is both in $r(t)$ and in $\psi(t)$. To compute these derivative, the simplest way is to write M_{ab} as a function of ψ only, eliminating r with the help of eq. (4.54), e.g.

$$\begin{aligned} M_{11} &= \mu r^2 \cos^2\psi \\ &= \mu a^2 (1-e^2)^2 \frac{\cos^2\psi}{(1+e\cos\psi)^2} \,. \end{aligned} \tag{4.66}$$

Now we can compute the time derivatives using

$$\begin{aligned} \dot\psi &= \frac{(GmR)^{1/2}}{r^2} \\ &= \left(\frac{Gm}{a^3}\right)^{1/2} (1-e^2)^{-3/2} (1+e\cos\psi)^2 \,, \end{aligned} \tag{4.67}$$

where we used eqs. (4.55), (4.54) and (4.51). Then a simple computation gives

$$\ddot M_{11} = \beta(1+e\cos\psi)^2 \left[2\sin 2\psi + 3e\sin\psi\cos^2\psi\right] , \tag{4.68}$$

$$\ddot M_{22} = \beta(1+e\cos\psi)^2 \left[-2\sin 2\psi - e\sin\psi(1+3\cos^2\psi)\right] , \tag{4.69}$$

$$\ddot M_{12} = \beta(1+e\cos\psi)^2 \left[-2\cos 2\psi + e\cos\psi(1-3\cos^2\psi)\right] , \tag{4.70}$$

with

$$\beta^2 \equiv \frac{4G^3\mu^2 m^3}{a^5(1-e^2)^5} \,. \tag{4.71}$$

Plugging this into eq. (3.76) we get the power radiated, in the quadrupole approximation, as a function of the position ψ along the orbit,

$$\begin{aligned} P(\psi) &= \frac{G}{5c^5}\left[\dddot M_{11}^2 + \dddot M_{22}^2 + 2\dddot M_{12}^2 - \frac{1}{3}(\dddot M_{11} + \dddot M_{22})^2\right] \\ &= \frac{2G}{15c^5}\left[\dddot M_{11}^2 + \dddot M_{22}^2 + 3\dddot M_{12}^2 - \dddot M_{11}\dddot M_{22}\right] \\ &= \frac{8G^4}{15c^5}\frac{\mu^2 m^3}{a^5(1-e^2)^5}(1+e\cos\psi)^4\left[12(1+e\cos\psi)^2 + e^2\sin^2\psi\right] . \end{aligned} \tag{4.72}$$

As explained in Chapter 1, the GW energy is only well defined by taking a temporal average over several periods of the wave. As we will see below, a particle in a Keplerian elliptic orbit emits GWs at frequencies which are integer multiple of the frequency ω_0 defined in eq. (4.59), and therefore the period of the GWs is a fraction of the orbital period T given in eq. (4.62). Then, a well defined quantity is the average of $P(\psi(t))$ over one period T. We can now perform this time average, writing

$$\begin{aligned} P &\equiv \frac{1}{T}\int_0^T dt\, P(\psi) \\ &= \frac{\omega_0}{2\pi}\int_0^{2\pi}\frac{d\psi}{\dot\psi}\,P(\psi) \\ &= (1-e^2)^{3/2}\int_0^{2\pi}\frac{d\psi}{2\pi}\,(1+e\cos\psi)^{-2}P(\psi) \\ &= \frac{8G^4\mu^2m^3}{15c^5a^5}(1-e^2)^{-7/2} \\ &\quad\times\int_0^{2\pi}\frac{d\psi}{2\pi}\left[12(1+e\cos\psi)^4 + e^2(1+e\cos\psi)^2\sin^2\psi\right] , \end{aligned} \tag{4.73}$$

where we used eq. (4.67). The integral is elementary and one finally obtains the total radiated power[10]

$$\boxed{P = \frac{32G^4\mu^2m^3}{5c^5a^5}f(e) \,,} \tag{4.74}$$

with

$$\boxed{f(e) = \frac{1}{(1-e^2)^{7/2}}\left(1 + \frac{73}{24}e^2 + \frac{37}{96}e^4\right) .} \tag{4.75}$$

[10]This classical formula is due to Peters and Mathews (1963).

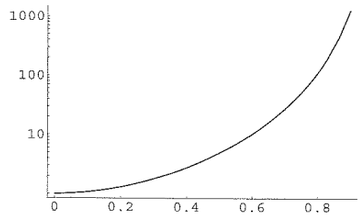

Fig. 4.5 The function $f(e)$, on a logarithmic scale.

Using eq. (4.59) we can eliminate m in favor of ω_0, and rewrite the above result as

$$P = \frac{32}{5}\,\frac{G\mu^2}{c^5}\,a^4\omega_0^6\,f(e)\,. \tag{4.76}$$

For $e = 0$, we have $f(e) = 1$, while a becomes the radius of the circular orbit and ω_0 becomes the same as ω_s, so we get back the result for circular orbits, eq. (3.339). The function $f(e)$ is plotted, on a logarithmic scale, in Fig. 4.5. For instance, for the Hulse–Taylor binary pulsar (that will be discussed in detail in Chapter 6) the eccentricity is quite large, $e \simeq 0.617$, and $f(e) \simeq 11.8$. The radiated power is therefore an order of magnitude larger than the power emitted in a circular orbit with radius a (i.e. with the same energy).

Combining eqs. (4.62), (4.59) and (4.53) we see that the orbital period T is related to the orbital energy E by $T = \text{const.} \times (-E)^{-3/2}$ and therefore

$$\frac{\dot T}{T} = -\frac{3}{2}\,\frac{\dot E}{E}\,. \tag{4.77}$$

From eq. (4.74) we find the energy loss (averaged over one orbital period) $\dot E = -P$ and therefore (using again eq. (4.53) to express E in terms of a) we get

$$\frac{\dot T}{T} = -\frac{96}{5}\,\frac{G^3\mu m^2}{c^5 a^4}\,f(e)\,, \tag{4.78}$$

where the average over an orbital period is understood. Expressing a in terms of T using eqs. (4.62) and (4.59) we can also rewrite this as

$$\boxed{\frac{\dot T}{T} = -\frac{96}{5}\,\frac{G^{5/3}\mu m^{2/3}}{c^5}\left(\frac{T}{2\pi}\right)^{-8/3} f(e)\,.} \tag{4.79}$$

This equation is of great importance, since it is at the basis of the first experimental evidence for gravitational radiation, as will be discussed in Chapter 6.

Coming back to eq. (4.74), we see that in the limit $e \to 1^-$ (with a fixed) the radiated power diverges. This is due to the fact that, if we send $e \to 1^-$ keeping a fixed, we get $R \to 0$ (see eq. (4.51)) and $b = a(1-e^2)^{1/2} \to 0$. Therefore, as the ellipticity $e \to 1^-$ at fixed a, the motion of the relative coordinates approaches more and more the point $r = 0$, where the acceleration Gm/r^2 diverges, and therefore the GW production formally diverges as well. However, clearly at this moment the approximation of point-like masses ceases to be valid, and we must take into account the finite size of the bodies.

The limit $e \to 1^-$ at fixed R corresponds instead to parabolic motion,

$$r = \frac{R}{1+\cos\psi}\,. \tag{4.80}$$

When $\psi \to -\pi$ the particle is at $r = \infty$; by increasing ψ the value of r decreases down to $r = R/2$ (reached for $\psi = 0$), and then increases again, until again $r \to \infty$ as $\psi \to \pi$ (see Fig. 4.6). In this limit, eliminating

a in favor of R using eq. (4.51), we obtain from eq. (4.72) the power radiated along the trajectory,

$$\begin{aligned} P(\psi) &= \frac{8G^4\mu^2m^3}{15c^5R^5}\,(1+\cos\psi)^4\,[12(1+\cos\psi)^2+\sin^2\psi] \\ &= \frac{16G^4\mu^2m^3}{15c^5}\,\frac{1}{r^5}\left(1+\frac{11R}{2r}\right). \end{aligned} \tag{4.81}$$

Then, $P(\psi)$ goes to zero quite fast as $r \to \infty$ or, equivalently, as $\psi \to \pm\pi$, see Fig. 4.7. This is of course expected, since the acceleration vanishes as $1/r^2$. As a result, the total energy radiated in GWs is finite

$$\begin{aligned} E_{\rm rad} &= \int_{-\infty}^{\infty} dt\,P(\psi(t)) \\ &= \int_{-\pi}^{\pi}\frac{d\psi}{\dot\psi}\,P(\psi) \\ &= \frac{85\pi}{48}\,\frac{G\mu^2}{R}\left(\frac{v_0}{c}\right)^5, \end{aligned} \tag{4.82}$$

where $v_0 = 2(Gm/R)^{1/2}$ is the velocity at $\psi = 0$ (which corresponds to $r = R/2$), i.e. is the maximum velocity attained along the trajectory. In this form, the result is similar to that found for a periodic source, compare, e.g. with eq. (3.319). Since this finite energy is emitted in a time $T = \infty$, if we take the average value of the power over a time T we find zero, as we can also check from eq. (4.74) writing $(1/a^5)f(e) = (1/R^5)(1-e^2)^5 f(e)$ and taking the limit $e \to 1^-$ at fixed R. Of course, this reflects simply the fact that the radiation is emitted basically between $-\pi/2 < \psi < \pi/2$, see Fig. 4.7; the radiation emitted when $\pi/2 < |\psi| < \pi$ is instead finite (and, indeed, even negligible), even if it takes an infinite time to get to $\psi = \pi$ or to come from $\psi = -\pi$.

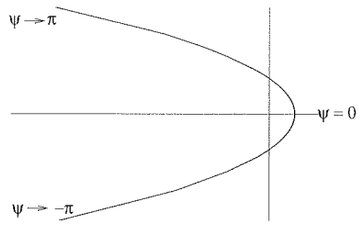

Fig. 4.6 The parabolic trajectory.

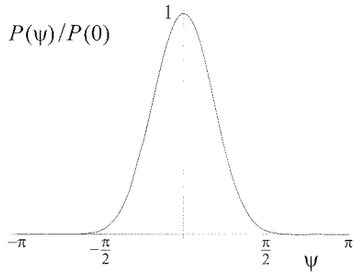

Fig. 4.7 The function $P(\psi)$, normalized to the value at $\psi = 0$, for parabolic motion.

Frequency spectrum

Above we have computed the total radiated power, integrated both over the frequency and over the solid angle. It is however very interesting to compute the frequency spectrum of the radiated power, $dP/d\omega$, for a Keplerian elliptic orbit.

Such a trajectory, given as a function of time by eqs. (4.63), (4.64) and (4.58), is of course not simple harmonic motion, and therefore the first step is to perform the Fourier decomposition of the trajectory. This can be done by observing, first of all, that $x(t)$ and $y(t)$ are periodic functions of the variable β defined in eq. (4.58), with period 2π. Therefore we can restrict β to the range $-\pi \leqslant \beta \leqslant \pi$, and we can perform a discrete Fourier transform,

$$x(\beta) = \sum_{n=-\infty}^{\infty} \tilde x_n e^{-in\beta}\,, \tag{4.83}$$

$$y(\beta) = \sum_{n=-\infty}^{\infty} \tilde y_n e^{-in\beta}\,, \tag{4.84}$$

with $\tilde{x}_n = \tilde{x}^*_{-n}$ and $\tilde{y}_n = \tilde{y}^*_{-n}$, since $x(\beta)$ and $y(\beta)$ are real functions. Furthermore, we have chosen the origin of time so that at $t = 0$ (i.e. at $\beta = 0$), we are at the point $x = a(1-e), y = 0$; with this choice, $x(-\beta) = x(\beta)$ while $y(-\beta) = -y(\beta)$. Therefore, writing $e^{-in\beta} = \cos(n\beta) - i\sin(n\beta)$, in the expansion of $x(\beta)$ contributes only $\cos(n\beta)$ while in the expansion of $y(\beta)$ contributes only $\sin(n\beta)$, and eqs. (4.83) and (4.84) simplify to

$$x(\beta) = \sum_{n=0}^{\infty} a_n \cos(n\beta)\,, \tag{4.85}$$

$$y(\beta) = \sum_{n=1}^{\infty} b_n \sin(n\beta)\,, \tag{4.86}$$

where, for $n \geqslant 1$, $a_n = 2\tilde{x}_n$ and $b_n = -2i\tilde{y}_n$, while $a_0 = \tilde{x}_0$. Since $\beta = \omega_0 t$, we can rewrite this as

$$x(t) = \sum_{n=0}^{\infty} a_n \cos\omega_n t\,, \tag{4.87}$$

$$y(t) = \sum_{n=1}^{\infty} b_n \sin\omega_n t\,, \tag{4.88}$$

where

$$\omega_n = n\omega_0\,. \tag{4.89}$$

We see that the Fourier decomposition of the Keplerian motion involves the fundamental frequency $\omega_0 = (Gm/a^3)^{1/2}$ and all its higher harmonics. The coefficients a_n and b_n are obtained by inverting eqs. (4.85) and (4.86), which gives, for $n \neq 0$,

$$a_n = \frac{2}{\pi}\int_0^{\pi} d\beta\, x(\beta)\cos(n\beta)\,, \tag{4.90}$$

$$b_n = \frac{2}{\pi}\int_0^{\pi} d\beta\, y(\beta)\sin(n\beta)\,, \tag{4.91}$$

$$\tag{4.92}$$

while, for $n = 0$,

$$a_0 = \frac{1}{\pi}\int_0^{\pi} d\beta\, x(\beta)\,. \tag{4.93}$$

With $x(\beta)$ and $y(\beta)$ given by eqs. (4.63), (4.64) and (4.58), these integrals are computed explicitly in Problem 4.2, and the result is given in terms of Bessel functions,[11]

$$a_n = \frac{a}{n}[J_{n-1}(ne) - J_{n+1}(ne)] \tag{4.94}$$

$$b_n = \frac{b}{n}[J_{n-1}(ne) + J_{n+1}(ne)]\,. \tag{4.95}$$

for $n \neq 0$, and $a_0 = -(3/2)ae$. The above result is interesting in itself but, to compute the spectrum of GWs, we are really interested in the

[11] Actually, Bessel functions were introduced for the first time just in this context, by Lagrange and, half a century later, in the more general solution for the Fourier transform of the Kepler problem given by Bessel. See Watson (1966).

Fourier decomposition of the second mass moment, and therefore of $x^2(t), y^2(t)$ and $x(t)y(t)$. This is again computed in Problem 4.2, where we show that

$$x^2(t) = \sum_{n=0}^{\infty} A_n \cos\omega_n t, \tag{4.96}$$

$$y^2(t) = \sum_{n=0}^{\infty} B_n \cos\omega_n t\,, \tag{4.97}$$

$$x(t)y(t) = \sum_{n=1}^{\infty} C_n \sin\omega_n t\,, \tag{4.98}$$

where

$$A_n = \frac{a^2}{n}\left[J_{n-2}(ne) - J_{n+2}(ne) - 2e(J_{n-1}(ne) - J_{n+1}(ne))\right], \tag{4.99}$$

$$B_n = \frac{b^2}{n}\left[J_{n+2}(ne) - J_{n-2}(ne)\right]\,, \tag{4.100}$$

$$C_n = \frac{ab}{n}\left[J_{n+2}(ne) + J_{n-2}(ne) - e(J_{n+1}(ne) + J_{n-1}(ne))\right]. \tag{4.101}$$

The second mass moment (4.65) therefore has the Fourier decomposition

$$\begin{aligned} M_{ab}(t) &= \mu\sum_{n=0}^{\infty}\begin{pmatrix} A_n\cos\omega_n t & C_n\sin\omega_n t \\ C_n\sin\omega_n t & B_n\cos\omega_n t\end{pmatrix}_{ab} \\ &\equiv \sum_{n=0}^{\infty} M^{(n)}_{ab}(t)\,. \end{aligned} \tag{4.102}$$

When we compute the radiated power, temporal averages such as

$$\langle \sin\omega_n t \sin\omega_m t\rangle$$

are non-vanishing only if $n = m$, so there is no interference term between the different harmonics, and

$$P = \sum_{n=1}^{\infty} P_n\,, \tag{4.103}$$

where P_n is the power radiated in the n-th harmonics. To compute P_n we use the quadrupole formula, written in the form

$$P = \frac{2G}{15c^5}\langle \dddot{M}^2_{11} + \dddot{M}^2_{22} + 3\dddot{M}^2_{12} - \ddddot{M}_{11}\ddddot{M}_{22}\rangle \tag{4.104}$$

(that takes into account that the orbit is in the (x, y) plane, compare with eq. (4.72)), and we replace M_{ab} by $M^{(n)}_{ab}$. Using

$$\dddot{M}^{(n)}_{ab} = \mu\,\omega_n^3\begin{pmatrix} A_n\sin\omega_n t & -C_n\cos\omega_n t \\ -C_n\cos\omega_n t & B_n\sin\omega_n t\end{pmatrix}_{ab}, \tag{4.105}$$

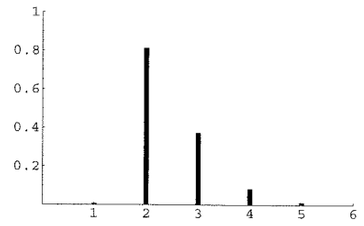

Fig. 4.8 The power P_n radiated at the GW frequency $\omega_n = n\omega_0$, as a function of n, for $e = 0.2$. P_n is normalized to the value for $e = 0$.

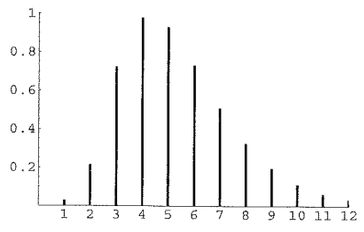

Fig. 4.9 The same as Fig. 4.8, for $e = 0.5$.

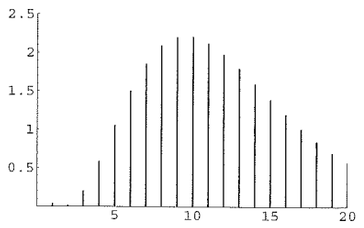

Fig. 4.10 The same as Fig. 4.8, for $e = 0.7$.

we get

$$P_n = \frac{G\mu^2\omega_0^6}{15c^5}\, n^6 (A_n^2 + B_n^2 + 3C_n^2 - A_n B_n)\,, \tag{4.106}$$

where we used $\langle \sin^2 \omega_n t\rangle = \langle \cos^2 \omega_n t\rangle = 1/2$. Recalling that $\omega_0^2 = Gm/a^3$, the above result can be rewritten as

$$\boxed{P_n = \frac{32 G^4 \mu^2 m^3}{5c^5 a^5}\, g(n,e)\,,} \tag{4.107}$$

where

$$\boxed{g(n,e) = \frac{n^6}{96a^4}[A_n^2(e) + B_n^2(e) + 3C_n^2(e) - A_n(e)B_n(e)]\,,} \tag{4.108}$$

where the notation stresses that A_n, B_n and C_n depends on the eccentricity e (recall also that $b^2/a^2 = (1-e^2)$).

First of all, we can check from this expression that, in the limit $e \to 0$, we get back the result for circular motion. If $e = 0$, the argument of the Bessel functions, in eqs. (4.99)–(4.101), vanishes. Since $J_m(0) = \delta_{m0}$, and since for us $n \geqslant 1$, we see from eqs. (4.99)–(4.101) that in this limit $A_n \to (a^2/2)\delta_{n2}$, $B_n \to (-a^2/2)\delta_{n2}$ (of course $b = a$ when $e = 0$) and $C_n \to (a^2/2)\delta_{n2}$. Then we get back the result that, for circular motion, only the harmonic with $n = 2$ contributes, and we find from eq. (4.108) that $g(0,n) = \delta_{n2}$, so we get back the correct value for the radiated power.

For a generic value of e (with $0 < e < 1$) all harmonics contribute, and we have radiation at all frequencies $\omega_n = n\omega_0$ for all integer values of n, including also $n = 1$. Increasing the ellipticity, increases also the value of $n = \bar{n}$ where $g(n,e)$ is maximum, as well as the value of P_n at $n = \bar{n}$, and the total radiated power. In Figs. 4.8–4.10 we show the power spectrum P_n, normalized to the power radiated when $e = 0$, for three different values of the ellipticity. Observe the change in the horizontal and vertical scales, among these figures.

4.1.3 Elliptic orbits. (II) Evolution of the orbit under back-reaction

The evolution equations

A binary system in a Keplerian orbit radiates both energy and angular momentum. In our approximation of point-like bodies (without an intrinsic spin) these are necessarily drained from the energy and angular momentum of the orbital motion, which therefore undergoes secular changes, both in its semimajor axis and in its ellipticity, until the system enters the merging phase and collapses. In this section we compute how the shape and size of the orbit evolve, for a generic elliptic orbit.

We already computed the energy radiated, in the quadrupole approximation, in eq. (4.74). We now compute the angular momentum radiated, again in the quadrupole approximation. We therefore start from eq. (3.99), which we write as

$$\frac{dL^i}{dt} = -\frac{2G}{5c^5}\,\epsilon^{ikl}\langle \dddot{M}_{ka}\ddot{M}_{la}\rangle\,, \tag{4.109}$$

where L^i is the orbital angular momentum of the binary system, and we replaced $\ddot{Q}_{ka}$ by $\ddot{M}_{ka}$ (because the difference gives a contribution to eq. (4.109) proportional to $\epsilon^{ikl}\delta_{ka}\dddot{Q}_{la} = \epsilon^{ikl}\dddot{Q}_{kl}$, which vanishes because $\dddot{Q}_{kl}$ is symmetric in (k,l) and ϵ^{ikl} is antisymmetric), and similarly we replaced $\dddot{Q}_{la}$ by $\dddot{M}_{la}$. As in the computation of the radiated energy, we put the orbit in the (x,y) plane, so M_{ab} is given by eq. (4.65), and we write $L_z = L$. Then, recalling that inside $\langle \ldots\rangle$ we can integrate by parts, eq. (4.109) gives

$$\begin{aligned}\frac{dL}{dt} &= -\frac{2G}{5c^5}\,\langle \dddot{M}_{1a}\ddot{M}_{2a} - \dddot{M}_{2a}\ddot{M}_{1a}\rangle \\ &= \frac{4G}{5c^5}\,\langle \dddot{M}_{12}(\ddot{M}_{11} - \ddot{M}_{22})\rangle\,.\end{aligned} \tag{4.110}$$

The third derivatives $\dddot{M}_{11}$ and $\dddot{M}_{22}$ have been computed in eqs. (4.68) and (4.69), while a similar computation gives

$$\begin{aligned}\dddot{M}_{12} = {} & \frac{G\mu m}{a(1-e^2)}\,\sin\psi \\ & \times\left[-4(1+e\cos\psi)^2\cos\psi + 2e(3\cos^2\psi - 1 + 2e\cos^3\psi)\right]\,.\end{aligned} \tag{4.111}$$

For periodic motion, the average over several periods of the wave is the same as the average over one orbital period T and, as in eq. (4.73), we transform the temporal average over one period into an integration over ψ, using

$$\int_0^T \frac{dt}{T}\,(\ldots) = (1-e^2)^{3/2}\int_0^{2\pi}\frac{d\psi}{2\pi}\,(1+e\cos\psi)^{-2}\,(\ldots)\,. \tag{4.112}$$

Then we get, for the angular momentum loss averaged over one period,

$$\begin{aligned}\frac{dL}{dt} = {} & \frac{8}{5}\,\frac{G^{7/2}\mu^2 m^{5/2}}{c^5 a^{7/2}}\,\frac{1}{(1-e^2)^2}\int_0^{2\pi}\frac{d\psi}{2\pi}\,\sin^2\psi \\ & \times[-4(1+e\cos\psi)^2\cos\psi + 2e(3\cos^2\psi - 1 + 2e\cos^3\psi)] \\ & \times[8\cos\psi + 6e\cos^2\psi + e]\,.\end{aligned} \tag{4.113}$$

The integral over ψ is elementary, and gives $-4(1+7e^2/8)$. In conclusion, from this result and eq. (4.74), the energy E and the angular momentum L of the orbit evolve as

$$\frac{dE}{dt} = -\frac{32}{5}\,\frac{G^4\mu^2 m^3}{c^5 a^5}\,\frac{1}{(1-e^2)^{7/2}}\left(1 + \frac{73}{24}e^2 + \frac{37}{96}e^4\right)\,, \tag{4.114}$$

$$\frac{dL}{dt} = -\frac{32}{5}\,\frac{G^{7/2}\mu^2 m^{5/2}}{c^5 a^{7/2}}\,\frac{1}{(1-e^2)^2}\left(1 + \frac{7}{8}e^2\right)\,, \tag{4.115}$$

and we recall again that these quantities are really averages over one period, rather than instantaneous energy and angular momentum losses. Using eqs. (4.50) and (4.53) we can rewrite these equations in terms of the evolution of the semimajor axis a and of the eccentricity e,

$$\frac{da}{dt} = -\frac{64}{5}\frac{G^3\mu m^2}{c^5 a^3}\frac{1}{(1-e^2)^{7/2}}\left(1+\frac{73}{24}e^2+\frac{37}{96}e^4\right), \quad (4.116)$$

$$\frac{de}{dt} = -\frac{304}{15}\frac{G^3\mu m^2}{c^5 a^4}\frac{e}{(1-e^2)^{5/2}}\left(1+\frac{121}{304}e^2\right). \quad (4.117)$$

From eq. (4.117) we see that, if $e = 0$, then $de/dt = 0$. Therefore a circular orbit remains circular. This could also have been seen directly from eqs. (4.114) and (4.115), observing that, for $e = 0$, they give

$$\frac{dE}{dt} = \omega_0 \frac{dL}{dt}, \quad (4.118)$$

where $\omega_0 = (Gm/a^3)^{1/2}$ is the frequency of the circular motion, see eq. (4.59). Equation (4.118) is just what is needed to maintain the relation between energy and angular momentum that holds for circular motion. In fact, for circular orbits, using eq. (4.59),

$$E = -\frac{Gm\mu}{2a} = -\frac{1}{2}(Gm)^{2/3}\mu\,\omega_0^{2/3}, \quad (4.119)$$

while

$$L = ma^2\omega_0 = (Gm)^{2/3}\mu\,\omega_0^{-1/3}, \quad (4.120)$$

and therefore

$$\frac{dE}{dt} = -\frac{1}{3}(Gm)^{2/3}\mu\,\omega_0^{-1/3}\dot{\omega}_0, \quad (4.121)$$

$$\frac{dL}{dt} = -\frac{1}{3}(Gm)^{2/3}\mu\,\omega_0^{-4/3}\dot{\omega}_0, \quad (4.122)$$

from which eq. (4.118) follows. For $e > 0$, eq. (4.117) gives $de/dt < 0$ instead, and therefore an elliptic orbit becomes more and more circular because of the emission of GWs.

A direct numerical integration of eqs. (4.116) and (4.117) is not as straightforward as one might think. The reason can be seen by putting the equations in dimensionless form. To do so, it is convenient to introduce a length-scale R_*, from $R_*^3 = 4G^3\mu m^2/c^6$. We have chosen the numerical factor so that when the masses of the two stars are equal, $m_1 = m_2 = M$, we have $R_* = 2GM/c^2$, so R_* becomes equal to the Schwarzschild radius of the stars. We then introduce the dimensionless variable $\tau = ct/R_*$, i.e. time measured in units of the light travel time across a distance R_*, and the dimensionless function $\tilde{a}(\tau) = a(\tau)/R_*$. Then eqs. (4.116) and (4.117) read

$$\frac{d\tilde{a}}{d\tau} = -\frac{16}{5}\frac{1}{\tilde{a}^3}\frac{1}{(1-e^2)^{7/2}}\left(1+\frac{73}{24}e^2+\frac{37}{96}e^4\right), \quad (4.123)$$

$$\frac{de}{d\tau} = -\frac{76}{15}\frac{1}{\tilde{a}^4}\frac{e}{(1-e^2)^{5/2}}\left(1+\frac{121}{304}e^2\right). \quad (4.124)$$

This shows that $\tau = ct/R_*$ is the natural adimensional time-scale in the differential equation. However, for typical solar-mass stars, $R_* \sim 3$ km and $R_*/c = O(10^{-5})$ s. Therefore, to follow the evolution of the orbit for a time $t \sim 1$ yr, we need to push the integration up to a dimensionless value $\tau \sim 10^{12}$, which is numerically difficult.

A better approach is to combine eqs. (4.116) and (4.117) to get da/de,

$$\frac{da}{de} = \frac{12}{19}\,a\,\frac{1+(73/24)e^2+(37/96)e^4}{e(1-e^2)[1+(121/304)e^2]}. \quad (4.125)$$

This equation can be integrated analytically, and gives

$$a(e) = c_0\,\frac{e^{12/19}}{1-e^2}\left(1+\frac{121}{304}e^2\right)^{870/2299}, \quad (4.126)$$

where c_0 is determined by the initial condition $a = a_0$ when $e = e_0$. It is convenient to define the function[12]

$$\boxed{g(e) = \frac{e^{12/19}}{1-e^2}\left(1+\frac{121}{304}e^2\right)^{870/2299}}, \quad (4.127)$$

so that $a(e) = c_0 g(e)$; c_0 is fixed by $a_0 = c_0 g(e_0)$, and therefore

$$\boxed{a(e) = a_0\frac{g(e)}{g(e_0)}}. \quad (4.128)$$

In particular, for $e \ll 1$, we have $g(e) \simeq e^{12/19}$ while, for e close to 1,

$$g(e) \simeq \frac{g_1}{1-e^2}, \quad (4.129)$$

where $g_1 = (425/304)^{870/2299} \simeq 1.1352$. A plot of the function $g(e)$ is shown in Fig. 4.11.

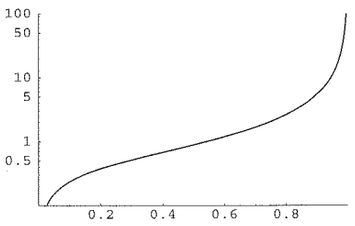

Fig. 4.11 The function $g(e)$, on a logarithmic scale, against e.

[12] This has nothing to do with the function $g(n, e)$ defined in eq. (4.108). Both the notation $g(e)$ for this function and the notation $g(n, e)$ for the function defined by eq. (4.108) are standard in the literature.

Orbit circularization

A consequence of the above result is that the eccentricity decreases quite fast, so the effect of the back-reaction of GWs is to circularize the orbit. Consider a compact binary system, say a NS-NS binary, that at an initial time has a_0 very large compared to the radius of the neutron stars, so we are still very far from coalescence, and an eccentricity e_0 not particularly small, neither especially close to one, so that $g(e_0) = O(1)$; let a and e be the values of the semiaxis and eccentricity at a much later time, say when the system is approaching the coalescence phase. Then e will be small and, from eq. (4.128) and the small e limit of $g(e)$, we have

$$a(e) \simeq a_0\,\frac{e^{12/19}}{g(e_0)}, \quad (4.130)$$

i.e.

$$e \simeq \left[\frac{a}{a_0}\,g(e_0)\right]^{19/12}. \quad (4.131)$$

For example, consider the Hulse–Taylor binary pulsar (which will be discussed in detail in Chapter 6). Today it has a semimajor axis $a_0 \simeq 2 \times 10^9$ m and a rather large eccentricity $e_0 \simeq 0.617$. By the time that the two stars reach a short separation a, say of the order of a hundred times the radius of the neutron stars, $a = O(10^2 R_{\rm NS}) \simeq 10^3$ km, we have $a/a_0 = O(5\times 10^{-4})$ and, since $g(e_0) = O(1)$, the eccentricity has become $e \sim (5 \times 10^{-4})^{19/12} \sim 6 \times 10^{-6}$. The conclusion is that (unless some external interaction perturbs the binary system), long before the two neutron stars approach the coalescence phase, the ellipticity has become zero to very high accuracy, and the two stars move on a circular orbit which shrinks adiabatically.

The time to coalescence

We now compute the time to coalescence, $\tau(a_0, e_0)$, of a binary system that, at an initial time $t_0 = 0$, has semimajor axis a_0 and eccentricity e_0. When $e_0 = 0$, we found the result in eq. (4.26),

$$\tau(a_0, e_0 = 0) \equiv \tau_0(a_0) = \frac{5}{256}\,\frac{c^5 a_0^4}{G^3 m^2 \mu}\,. \tag{4.132}$$

For an elliptic orbit, we can integrate eq. (4.116) requiring $a(t) = 0$ at $t = \tau(a_0, e_0)$ or, equivalently, we can integrate eq. (4.117) requiring $e(t) = 0$ at $t = \tau(a_0, e_0)$, since we have seen that at the coalescence e goes to zero. Since the analytic expression for $a(e)$ is simpler than the form of the inverse function $e(a)$, it is in fact better to use eq. (4.117), so we write

$$\int_0^{\tau(a_0,e_0)} dt = -\frac{15}{304}\,\frac{c^5}{G^3 m^2 \mu}\int_{e_0}^{0} de\,\frac{a^4(e)(1-e^2)^{5/2}}{e\,(1+\frac{121}{304}e^2)}\,, \tag{4.133}$$

that is,

$$\tau(a_0, e_0) = \frac{15}{304}\,\frac{c^5}{G^3 m^2 \mu}\int_{0}^{e_0} de\,\frac{a^4(e)(1-e^2)^{5/2}}{e\,(1+\frac{121}{304}e^2)}\,. \tag{4.134}$$

Using eq. (4.128) for $a(e)$, we get

$$\tau(a_0, e_0) = \tau_0(a_0)\,\frac{48}{19}\,\frac{1}{g^4(e_0)}\int_{0}^{e_0} de\,\frac{g^4(e)(1-e^2)^{5/2}}{e\,(1+\frac{121}{304}e^2)}\,. \tag{4.135}$$

Expressing $\tau_0(a_0)$ in terms of the orbital period as in eq. (4.27), we can write the result for $\tau_0(a_0, e_0)$ as

$$\boxed{\tau_0(a_0, e_0) \simeq 9.829\,{\rm Myr}\left(\frac{T_0}{1\,{\rm hr}}\right)^{8/3}\left(\frac{M_\odot}{m}\right)^{2/3}\left(\frac{M_\odot}{\mu}\right)F(e_0)\,,} \tag{4.136}$$

where $m = m_1 + m_2$ is the total mass, μ is the reduced mass,

$$\boxed{F(e_0) = \frac{48}{19}\,\frac{1}{g^4(e_0)}\int_0^{e_0} de\,\frac{g^4(e)(1-e^2)^{5/2}}{e\,(1+\frac{121}{304}e^2)}\,,} \tag{4.137}$$

and $g(e)$ is given in eq. (4.127). For example, the Hulse–Taylor binary pulsar has $e_0 \simeq 0.617$ and $F(e_0) \simeq 0.184$, so its time to coalescence is shorter by a factor $1/F(e_0) \simeq 5.4$, compared to a binary on a circular orbit with the same period. Using the values, $m_1 = m_2 \simeq 1.4 M_\odot$ and $T_0 \simeq 7.75$ hr we obtain the time to coalescence of the Hulse–Taylor binary pulsar, $\tau(a_0, e_0) \simeq 300$ Myr.

It can be useful to write some approximate, but more handy expression, for $F(e_0)$. In the limit $e_0 \ll 1$ the integrand can be approximated as $g^4(e)/e$, and $g(e) \simeq e^{12/19}$, see eq. (4.127). Then

$$\begin{aligned} F(e_0) &\simeq \frac{48}{19}\,\frac{1}{g^4(e_0)}\int_0^{e_0} de\, e^{48/19-1} \\ &= \frac{1}{g^4(e_0)}\,e_0^{48/19} \simeq 1\,, \end{aligned} \tag{4.138}$$

so for $e_0 = 0$ we have $F(0) = 1$ and we get back the result for circular orbit, eq. (4.27). In the opposite limit $e_0 \to 1^-$, the integral in eq. (4.134) is dominated by the region $e \simeq 1$, where $g(e)$ is given by eq. (4.129). Then we get

$$\begin{aligned} F(e_0) &\simeq \frac{48}{19}\left(\frac{1-e_0^2}{g_1}\right)^4\int^{e_0} de\,\frac{1}{[1+(121/304)]}\,\frac{g_1^4}{(1-e^2)^4}\,(1-e^2)^{5/2} \\ &\simeq \frac{768}{429}(1-e_0^2)^4\left[(1-e_0^2)^{-1/2} + O(1)\right] \\ &\simeq \frac{768}{429}(1-e_0^2)^{7/2}\,. \end{aligned} \tag{4.139}$$

Therefore, in this limit the time to coalescence is smaller than for a circular orbit with the same period, by a factor proportional to $(1-e_0^2)^{7/2}$. This dependence is easily understood from the fact that the system spends most of its lifetime near $a = a_0$, $e = e_0$, where the radiated energy is enhanced by a factor proportional to $(1-e_0^2)^{7/2}$, compared to the circular case, see eqs. (4.74) and (4.75). Comparing the limits $e \to 0$ and $e \to 1^-$, we see that it is convenient to define a function $G(e_0)$ from

$$F(e_0) \equiv G(e_0)(1-e_0^2)^{7/2}\,, \tag{4.140}$$

because $G(e_0)$ is a function everywhere close to one. A plot of $G(e_0)$ from the exact numerical integration of eq. (4.137) is shown in Fig. 4.12. We see that $G(e)$ is always very close to one, within a few per cent at least until $e = 0.6$, where $G(e) \simeq 0.982$, and then, approaching $e = 1$, it raises to reach the finite value $G(1) = 768/425 \simeq 1.80$.

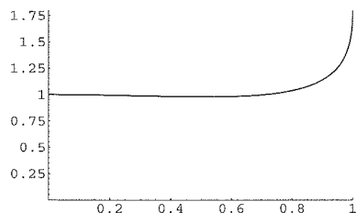

Fig. 4.12 The function $G(e)$, against e. At $e = 1$ $G(e)$ is finite, $G(1) = 768/425 \simeq 1.80$.

4.1.4 Binaries at cosmological distances

Until now, we have implicitly assumed that the binary system that coalesces is at a sufficiently small distance from us, so that the expansion of the Universe during the propagation of the GWs from the source to the detector can be neglected. However, some gravitational-wave detectors, in their advanced stage, have the potential of observing coalescing binaries out to cosmological distances: we will see that advanced ground-based interferometers could detect BH-BH coalescences out to distances of order 1–2 Gpc (corresponding to a redshift $z \sim 0.25$–0.5), while the space interferometer LISA could detect the coalescence of supermassive black-hole binaries out to redshifts $z \sim 5$–10. Actually, these will be among the most fascinating sources of GW astronomy. The rich cosmological information that could be extracted from such events will be discussed in Vol. 2. Here we prepare the necessary tools, discussing how the signal of a binary inspiral at a cosmological distance is affected by the expansion of the Universe.

First of all, we recall a few elementary notions of cosmology (see, e.g. Chapter 2 of Kolb and Turner (1990) for more details and derivations), also in order to fix our notation. The expert reader might wish to skip this part and move on to page 194.

A reminder of FRW kinematic

On the Gpc scale, the Universe is to a first approximation isotropic and homogeneous, and is described by the Friedmann–Robertson–Walker (FRW) metric,

$$ds^2 = -c^2 dt^2 + a^2(t) \left[\frac{dr^2}{1-kr^2} + r^2 d\theta^2 + r^2 \sin^2\theta d\phi^2 \right] , \qquad (4.141)$$

where the function $a(t)$ is called the scale factor and is determined by the Einstein equations. After an appropriate rescaling of the coordinates, k can take the values $k = 0$ (flat Universe[13]), $k = +1$ (closed Universe) or $k = -1$ (open Universe). We define $a(t)$ as adimensional, so the dimensions of length are carried by r. The coordinates (t, r, θ, ϕ) that appear above are called *comoving* coordinates. This name reflects the property that a test mass, initially at rest in the comoving frame, remains at a fixed value of its comoving coordinates r, θ, ϕ in spite of the expansion of the Universe. This can be proved writing down the geodesic equation in the metric (4.141) (just as we did in Section 1.3, when we understood the physical meaning of the TT gauge). From the $\mu = 0$ component, one finds

$$\frac{d|\mathbf{u}|}{dt} = -\frac{\dot{a}}{a} |\mathbf{u}| , \qquad (4.142)$$

where $|\mathbf{u}|^2 = g_{ij} u^i u^j$ is the squared modulus of the spatial part of the four-velocity u^μ. This equation shows that, in the comoving frame, if at $t = t_0$ the modulus of the four-velocity $|\mathbf{u}|$ is zero, then $d|\mathbf{u}|/dt$ also vanishes, so $|\mathbf{u}|$ remains zero at all times.[14] This explains why these coordinates are called comoving: they "stretch" themselves, following

[13] Here the word "flat" refers to the geometry of the *spatial* slices. As a four-dimensional space-time, the FRW metric with $k = 0$ *is* curved.

[14] Equation (4.142) also implies a much stronger result. If at $t = t_0$ the velocity has an initial value $\mathbf{u}_0$, the integration of eq. (4.142) gives

$$|\mathbf{u}(t)| = \frac{a(t_0)}{a(t)} |\mathbf{u}_0| , \qquad (4.143)$$

so spatial velocities are redshifted by the cosmological expansion. In a Universe which expands forever, even test masses with a non-vanishing initial value of $\mathbf{u}$ will eventually come to rest with respect to the observer that uses comoving coordinates.

the expansion of the Universe. If, at an initial time, a star has comoving spatial coordinates (r_1, θ_1, ϕ_1), and a second star has comoving spatial coordinates (r_2, θ_2, ϕ_2), and if both stars have zero velocity, then at any subsequent time their comoving spatial coordinates will still be (r_1, θ_1, ϕ_1) and (r_2, θ_2, ϕ_2), respectively, and in particular their coordinate distance will be unchanged, in spite of the expansion of the Universe. Comparing with the discussion in Section 1.3.3, we see that comoving coordinates in a FRW space-time play the same role as TT coordinates in the space-time generated by a gravitational wave.

A star at $r = r_1$ and a star at $r = r_2$ (and with the same values of θ and ϕ) have a *coordinate* distance $r = r_2 - r_1$. Of course, this quantity has no physical meaning, since coordinates are arbitrary in general relativity. The physical spatial distance is the *proper* spatial distance, $r_{\rm phys}(t)$, given by

$$dr^2_{\rm phys} = g_{ij} dx^i dx^j . \qquad (4.144)$$

If the first star is at the origin and the second is at comoving radial coordinate r, then eq. (4.141) gives $dr^2_{\rm phys} = a^2(t) dr^2/(1-kr^2)$, and therefore their physical distance is

$$r_{\rm phys}(t) = a(t) \int_0^r \frac{dr}{(1-kr^2)^{1/2}} . \qquad (4.145)$$

In particular, for a flat Universe ($k = 0$) we have $r_{\rm phys}(t) = a(t) r$.

Consider now a source located at comoving distance r, that emits signals (such as electromagnetic or gravitational waves) which travel at the speed of light, and are later received by an observer located at $r = 0$. Suppose that the source emits a wavecrest at a time $t_{\rm emis}$. The signal will be detected by the observer at a time $t_{\rm obs}$, which is obtained by imposing $ds^2 = 0$ in eq. (4.141). This gives

$$\int_{t_{\rm emis}}^{t_{\rm obs}} \frac{c\, dt}{a(t)} = \int_0^r \frac{dr}{(1-kr^2)^{1/2}} . \qquad (4.146)$$

Suppose that a second wavecrest is emitted at time $t_{\rm emis} + \Delta t_{\rm emis}$, and received at $t_{\rm obs} + \Delta t_{\rm obs}$. Then

$$\int_{t_{\rm emis}+\Delta t_{\rm emis}}^{t_{\rm obs}+\Delta t_{\rm obs}} \frac{c\, dt}{a(t)} = \int_0^r \frac{dr}{(1-kr^2)^{1/2}} . \qquad (4.147)$$

Observe that the right-hand side is always the same, since the source is at a fixed comoving distance. Then, taking the difference between these two equations, the right-hand sides cancel and, to linear order in $\Delta t_{\rm emis}$, one finds

$$\Delta t_{\rm obs} = \frac{a(t_{\rm obs})}{a(t_{\rm emis})} \Delta t_{\rm emis} . \qquad (4.148)$$

In an expanding Universe, there is therefore a dilatation of the time measured by the observer, with respect to the time of the source. The *redshift* of the source, z, is defined by

$$1 + z = \frac{a(t_{\rm obs})}{a(t_{\rm emis})} . \qquad (4.149)$$

Equation (4.148) means that the time $t_{\rm obs}$ measured by the observer's clock, and the time t_s measured by the source clock are related by

$$\boxed{dt_{\rm obs} = (1+z)dt_s\,.} \tag{4.150}$$

As a consequence, any frequency measured by the observer, $f^{(\rm obs)}$, is related to the corresponding frequency measured in the source frame, $f^{(s)}$, by

$$f^{(\rm obs)} = \frac{f^{(s)}}{1+z}\,, \tag{4.151}$$

and the wavelengths are related by

$$\lambda^{(\rm obs)} = (1+z)\lambda^{(s)}\,. \tag{4.152}$$

To complete our quick tour of kinematics in a FRW space-time, we need the definition of luminosity distance and the relation between the luminosity distance and the redshift. Let $\mathcal{F}$ be the energy flux (energy per unit time per unit area) measured in the observer's frame, and let $\mathcal{L}$ be the absolute luminosity of the source, i.e. the power that it radiates in its rest frame,

$$\mathcal{L} = \frac{dE_s}{dt_s}\,, \tag{4.153}$$

where E_s is the energy measured in the source proper frame. The luminosity distance d_L is then defined by

$$\boxed{\mathcal{F} = \frac{\mathcal{L}}{4\pi d_L^2}\,.} \tag{4.154}$$

In the absence of redshift, the energy $E_{\rm obs}$ measured in the observer frame is the same as the energy E_s measured in the source frame, and $dt_{\rm obs} = dt_s$, so

$$\frac{dE_{\rm obs}}{dt_{\rm obs}} = \frac{dE_s}{dt_s}\,. \tag{4.155}$$

When it arrives at the detector, the energy radiated by an isotropic source is distributed over an area $A = 4\pi r^2$, and therefore

$$\begin{aligned}\mathcal{F} &= \frac{1}{4\pi r^2}\frac{dE_{\rm obs}}{dt_{\rm obs}} \\ &= \frac{1}{4\pi r^2}\frac{dE_s}{dt_s} \\ &= \frac{\mathcal{L}}{4\pi r^2}\,,\end{aligned} \tag{4.156}$$

which shows that, in the absence of redshift, d_L is just equal to the distance r of the source. In an expanding Universe, however, the energy observed is redshifted,

$$E_{\rm obs} = \frac{E_s}{1+z} \tag{4.157}$$

(the quickest derivation of this result makes use of eq. (4.151), together with the quantum relation $E = \hbar\omega$, but this is a kinematic property that can also be derived purely classically), while $dt_{\rm obs} = (1+z)dt_s$. Therefore

$$\frac{dE_{\rm obs}}{dt_{\rm obs}} = \frac{1}{(1+z)^2}\frac{dE_s}{dt_s}\,. \tag{4.158}$$

Furthermore, using the FRW metric (4.141), we find that, at time t, the surface of a sphere with comoving radius r is $4\pi a^2(t)r^2$ (independently of k), so when the radiation arrives at the detector it is spread over an area $A = 4\pi a^2(t_{\rm obs})r^2$. Therefore

$$\mathcal{F} = \frac{\mathcal{L}}{4\pi a^2(t_{\rm obs})r^2(1+z)^2}\,, \tag{4.159}$$

which means that (setting $t_{\rm obs}$ equal to the present time t_0)

$$\boxed{d_L = (1+z)\,a(t_0)r\,.} \tag{4.160}$$

For small values of the redshift, we can express d_L as a function of z as follows. We perform a Taylor expansion of $a(t)$ around the present epoch $t = t_0$,

$$\frac{a(t)}{a(t_0)} = 1 + H_0(t-t_0) - \frac{1}{2}q_0H_0^2(t-t_0)^2 + \dots \tag{4.161}$$

where

$$H_0 \equiv \frac{\dot a(t_0)}{a(t_0)}\,, \tag{4.162}$$

is the *Hubble constant* (or, more appropriately, the present value of the Hubble parameter $H(t) = \dot a/a$), while

$$\begin{aligned}q_0 &\equiv -\frac{\ddot a(t_0)}{a(t_0)}\frac{1}{H_0^2} \\ &= -\frac{a(t_0)\ddot a(t_0)}{\dot a^2(t_0)}\end{aligned} \tag{4.163}$$

is called the *deceleration parameter.*[15] Using $a(t_0)/a(t) = 1+z$, eq. (4.161) can be inverted to give perturbatively $(t-t_0)$ as a function of z, while inserting the expansion (4.161) into eq. (4.146) gives $a(t_0)r$, as an expansion in powers of $(t-t_0)$ and therefore of z. The result is (see, e.g. Kolb and Turner (1990), pages 41–42 for the explicit calculation)

$$\boxed{\frac{H_0d_L}{c} = z + \frac{1}{2}(1-q_0)z^2 + \dots\,.} \tag{4.164}$$

The first term of this expansion just gives the Hubble law $z \simeq (H_0/c)d_L$, which states that redshifts are proportional to distances. The term $O(z^2)$ is the correction to the linear law for moderate redshifts. For large redshifts, the Taylor series is no longer appropriate, and the whole expansion

[15] This name is somewhat unfortunate, since it suggests that presently the expansion of the Universe is decelerating. Rather, we will see below that the evidence from the observation of type Ia supernovae indicates that presently the expansion of the Universe is accelerating, i.e. $q_0 < 0$.

history of the Universe is encoded in a function $d_L(z)$. As an example, for a flat Universe ($k = 0$), eq. (4.146) gives

$$\int_{t_{\rm emis}}^{t_{\rm obs}} \frac{c\,dt}{a(t)} = r_. \tag{4.165}$$

Differentiating the relation $1 + z(t) = a(t_0)/a(t)$ we get

$$\frac{dt}{a(t)} = -\frac{1}{a(t_0)}\,\frac{dz}{H(z)}\,, \tag{4.166}$$

so eq. (4.165) becomes

$$a(t_0)r = c\int_0^z \frac{dz'}{H(z')}\,, \tag{4.167}$$

where the upper limit in the integral is the redshift z corresponding to the emission time $t_{\rm emis}$ while, in the lower limit of the integral, we used the fact that at the present time $t = t_0$ we have $z = 0$. Then eq. (4.160) gives

$$\boxed{d_L(z) = c\,(1+z)\int_0^z \frac{dz'}{H(z')}\,,} \tag{4.168}$$

or, taking a derivative with respect to z,

$$\frac{c}{H(z)} = \frac{d}{dz}\left(\frac{d_L(z)}{1+z}\right)\,. \tag{4.169}$$

Thus, from the knowledge of $d_L(z)$, we can get the Hubble parameter $H(z)$. This shows that the luminosity distance function $d_L(z)$ is a very important quantity, which encodes the whole expansion history of the Universe.

From the definition (4.154) we see that, in order to determine the luminosity distance of a source, we need to know both $\mathcal{F}$ and $\mathcal{L}$. The flux $\mathcal{F}$ is the quantity that is directly measured by the observer. The problem is to know the intrinsic luminosity $\mathcal{L}$ of the source. This is possible if we have a "standard candle", that is, a source whose absolute luminosity is known. The redshift of an electromagnetic source can be determined from the redshift of its spectral lines, and then we get the corresponding value of $d_L(z)$. Up to distances of order 600 Mpc, standard candles are provided by Cepheid variable stars while, at larger cosmological distances, a standard candle is provided by Type Ia supernovae.[16] The Hubble constant is usually written as $H_0 = h_0 \times 100\,{\rm km\ s^{-1}\,Mpc^{-1}}$, and the most recent determination of h_0 is $h_0 = 0.73 \pm 0.03$, while the value of the deceleration parameter is $q_0 = -0.74 \pm 0.18$.

[16] Type Ia supernovae are modeled as carbon–oxygen white dwarfs, in a close binary system. They accrete matter from their companion until their mass reaches a critical value $\simeq 1.30 M_\odot$, and then they explode as supernovae. Since the mass of the star at the moment of the explosion is always the same, the light curves of Type Ia supernovae are sufficiently similar to each other and, after applying corrections that take into account a relation between the shape of the light curve and the peak luminosity, they can be used as standard candles.

Propagation of GWs in a FRW Universe

We can now discuss how the waveform produced by a binary inspiral is modified by the propagation across cosmological distances. First of all,

we can define a *local* wave zone, as the region where the distance to the source is sufficiently large so that the gravitational field already has the $1/r$ behavior characteristic of waves, but still sufficiently small, so that the expansion of the Universe is negligible. During the propagation of the GW in the local wave zone, the scale factor $a(t)$ does not change appreciably, so in the local wave zone physical distances can be written as $r_{\rm phys} = a(t_{\rm emis})r$, where r is the comoving distance and $t_{\rm emis}$ is (any) time of emission,[17] so $r_{\rm phys}$ differs from r by just a constant normalization factor. Using eq. (4.29) we see that the GW produced by a binary inspiral, at a distance $r_{\rm phys} = a(t_{\rm emis})r$ in the local wave zone, can be written as

$$h_+(t_s) = h_c(t_s^{\rm ret})\,\frac{1+\cos^2\iota}{2}\,\cos\left[2\pi\int^{t_s^{\rm ret}} dt'_s f_{\rm gw}^{(s)}(t'_s)\right]\,, \tag{4.170}$$

$$h_\times(t_s) = h_c(t_s^{\rm ret})\,\cos\iota\,\sin\left[2\pi\int^{t_s^{\rm ret}} dt'_s f_{\rm gw}^{(s)}(t'_s)\right]\,, \tag{4.171}$$

where

$$h_c(t_s^{\rm ret}) = \frac{4}{a(t_{\rm emis})r}\left(\frac{GM_c}{c^2}\right)^{5/3}\left(\frac{\pi f_{\rm gw}^{(s)}(t_s^{\rm ret})}{c}\right)^{2/3}\,. \tag{4.172}$$

Here time is the time t_s measured by the clock of the source (and $t_s^{\rm ret}$ is the corresponding value of retarded time) and the GW frequency $f_{\rm gw}$ is the one associated to this definition of time, that we denote by $f_{\rm gw}^{(s)}$. They are related to the quantities measured by the observer which is at a cosmological distance, very far from the local wave zone, by eqs. (4.150) and (4.151). The dependence of $f_{\rm gw}^{(s)}$ on t_s is given by eq. (4.19), that we rewrite as

$$f_{\rm gw}^{(s)}(\tau_s) = \frac{1}{\pi}\left(\frac{5}{256}\,\frac{1}{\tau_s}\right)^{3/8}\left(\frac{GM_c}{c^3}\right)^{-5/8}\,, \tag{4.173}$$

where τ_s is the time to coalescence measured by the source's clock.

To compute how this waveform propagates across cosmological distances to reach the observer, we should use eq. (1.179), that describes the propagation of GWs in a curved space-time, specializing it to the FRW metric. Actually, it is instructive to start from a simpler problem, namely the propagation of a *scalar* perturbation ϕ in the FRW metric. In this case, the propagation equation is simply $\Box\phi = 0$ where, on scalar functions, the curved-space d'Alembertian $\Box = D_\mu D^\mu$ can be written as

$$\Box = \frac{1}{\sqrt{-g}}\,\partial_\mu(\sqrt{-g}\,g^{\mu\nu}\partial_\nu)\,. \tag{4.174}$$

To solve this wave equation in the FRW metric, it is convenient to introduce the conformal time η , from

$$d\eta = \frac{dt}{a(t)}\,, \tag{4.175}$$

[17] We do not need to track the change of the scale factor during the observed part of the emission process, so we do not need to be more precise about $t_{\rm emis}$.

i.e.

$$\eta = \int^t \frac{dt'}{a(t')}\,, \tag{4.176}$$

so the FRW metric reads (limiting ourselves for simplicity to $k = 0$)

$$ds^2 = a^2(\eta)\,\left[-c^2 d\eta^2 + dr^2 + r^2 d\theta^2 + r^2 \sin^2\theta\, d\phi^2\right]\,. \tag{4.177}$$

We want to know how a solution which decreases as $1/r$ evolves in this space-time. We therefore search for spherically symmetric solutions of the form $\phi(r,\eta) = (1/r) f(r,\eta)$. The equation $\Box\phi = 0$ in this metric then becomes

$$\begin{aligned} 0 &= \partial_\mu(\sqrt{-g} g^{\mu\nu}\partial_\nu)\phi \\ &= -\frac{1}{c^2}\partial_\eta\left[a^2(\eta) r^2 \partial_\eta\phi\right] + \partial_r\left[a^2(\eta) r^2 \partial_r\phi\right] \\ &= \partial_r^2 f - f'' - 2\frac{a'}{a} f'\,, \end{aligned} \tag{4.178}$$

where the prime denotes derivation with respect to $c\eta$, $f' = (1/c)\partial f/\partial\eta$. It is convenient to search for the solution in the form

$$f(r,\eta) = \frac{1}{a(\eta)}\, g(r,\eta)\,. \tag{4.179}$$

Then $g(r,\eta)$ satisfies the equation

$$\partial_r^2 g - g'' + \frac{a''}{a}\, g = 0\,. \tag{4.180}$$

Now observe that $a''/a \sim \eta^{-2}$, for dimensional reasons.[18] Then we see that eq. (4.180) has the approximate solutions

$$g(r,\eta) \simeq e^{\pm i\omega(\eta - r/c)}\,, \tag{4.181}$$

as long as $\omega^2 \gg 1/\eta^2$, since in this case in eq. (4.180) the term $(a''/a)g \sim g/\eta^2$ is negligible with respect to $-g'' = \omega^2 g$, and we are left with a simple wave equation $\partial_r^2 g - g'' \simeq 0$. More generally, any function of the form $g(\eta - r/c)$ is a solution, as long as in Fourier space it contains only frequencies such that $\eta^2\omega^2 \gg 1$. In conclusion, we have the approximate solution

$$\phi(r,\eta) \simeq \frac{1}{r a(\eta)}\, g(\eta - r/c)\,. \tag{4.182}$$

We can normalize conformal time so that, at the present epoch, $\eta = t$. Then, the wave observed today at a detector reads[19]

$$\phi(r,t) \simeq \frac{1}{r a(t_0)}\, g(t - r/c)\,. \tag{4.183}$$

Thus, the propagation of a scalar wave through a FRW background is very simple. Compared to the solution in the absence of cosmological expansion, we just need to replace the factor $1/r$ with $1/[r a(t)]$.

Now we can turn to the propagation equation of a tensor perturbation $h_{\mu\nu}$, eq. (1.179). It is in principle straightforward to write down this

[18] More precisely, we are interested in the evolution in a matter-dominated Universe (since we need that stars already formed!). In this case the FRW scale factor evolves as $a(\eta) \sim \eta^2$ and $a''/a = 2/\eta^2$. Instead, in a radiation-dominated Universe, $a(\eta) \sim \eta$ and $a''/a = 0$.

[19] Obviously, since $a(\eta)$ evolves appreciably only on a cosmological time-scale, once we fix $\eta = t$ at one moment of time in the present epoch, we have $\eta = t$, with exceedingly good accuracy, over the whole time-scale relevant for GW observation at a detector, so we can write $g(\eta - r/c) = g(t - r/c)$ for all these values of time. For the same reason, $a(\eta)$ can be written simply as a constant factor $a(t_0)$.

equation explicitly in the FRW metric (4.177); we then find that, once we disregard all terms $O(1/\eta^2)h_{\mu\nu}$ with respect to the terms $O(\omega^2)h_{\mu\nu}$, we get back the same equation that we discussed for scalar perturbations. Of course, this is not surprising. Simply, the condition $\eta^2\omega^2 \gg 1$ demands that ω be large with respect to the typical scale of the background space-time and this is nothing but the condition that defines the geometrical optics approximation. In this approximation all massless particles follow null geodesics, independently of their spin, as we saw in Section 1.5.1.

Then we find that, to leading order:

- The two polarizations h_+ and $h_\times$ decouple, that is each one satisfies a wave equation which is independent of the other. This means that the propagation does not introduces a mixing among them. For instance, if we observe the binary edge-on ($\cos\iota = 0$), we see from eqs. (4.170) and (4.171) that in the local wave zone the GW has only the plus polarization; then, even after propagation across a cosmological distance, the wave will still have only the plus polarization. This is as expected, since we already saw in Section 1.5.1 that the polarization tensor of GWs is parallel-propagated along the null geodesics.
- Both h_+ and $h_\times$ satisfy the same equation that we discussed above for a scalar field.

The conclusion is that, after propagation from the source to the detector, the GW amplitude from an inspiraling binary is still given by eqs. (4.170) and (4.171), but with h_c in eq. (4.172) replaced by

$$h_c(t_s^{\rm ret}) = \frac{4}{a(t_0) r}\left(\frac{G M_c}{c^2}\right)^{5/3}\left(\frac{\pi f_{\rm gw}^{(s)}(t_s^{\rm ret})}{c}\right)^{2/3}\,, \tag{4.184}$$

as long as the geometrical optics approximation is valid. Today this condition is $2\pi f_{\rm gw} \gg t_0^{-1}$, where t_0 is the present age of the Universe, and therefore is satisfied with extreme accuracy by all GWs in which we are interested (in fact, by all GWs whose wavelength is smaller than the present Hubble size of the Universe!). More generally, also the condition $2\pi f_{\rm gw} \gg t_{\rm emis}^{-1}$ is extremely well satisfied, so the geometrical optics approximation is excellent for the whole propagation of the GW from the source to the detector.

In principle eqs. (4.170) and (4.171), together with eq. (4.184), provide the final result. However, it is convenient to express them in terms of the time $t_{\rm obs}$ and the GW frequency $f_{\rm gw}^{\rm (obs)}$ measured by the observer, rather than using the time t_s measured by the source and its associated frequency. Using eqs. (4.150) and (4.151), we see that, in eqs. (4.170) and (4.171),

$$\int^{t_s^{\rm ret}} dt'_s f_{\rm gw}^{(s)}(t'_s) = \int^{t_{\rm obs}^{\rm ret}} dt'_{\rm obs} f_{\rm gw}^{\rm (obs)}(t'_{\rm obs}) \tag{4.185}$$

since the redshift in dt cancels the redshift in f. Writing

$$f_{\rm gw}^{(s)} = (1+z) f_{\rm gw}^{\rm (obs)}\,, \tag{4.186}$$

eq. (4.184) becomes

$$h_c(t_{\rm obs}^{\rm ret}) = \frac{4}{a(t_0)r}\,(1+z)^{2/3}\left(\frac{GM_c}{c^2}\right)^{5/3}\left(\frac{\pi f_{\rm gw}^{(\rm obs)}(t_{\rm obs}^{\rm ret})}{c}\right)^{2/3}$$
$$= \frac{4}{d_L(z)}\,(1+z)^{5/3}\left(\frac{GM_c}{c^2}\right)^{5/3}\left(\frac{\pi f_{\rm gw}^{(\rm obs)}(t_{\rm obs}^{\rm ret})}{c}\right)^{2/3}, \quad (4.187)$$

where in the second line we expressed the result in terms of the luminosity distance, using eq. (4.160). We see that, if we define the quantity

$$\boxed{\mathcal{M}_c \equiv (1+z)M_c = (1+z)\mu^{3/5}m^{2/5}\,,} \quad (4.188)$$

we get

$$h_c(t_{\rm obs}^{\rm ret}) = \frac{4}{d_L}\left(\frac{G\mathcal{M}_c}{c^2}\right)^{5/3}\left(\frac{\pi f_{\rm gw}^{(\rm obs)}(t_{\rm obs}^{\rm ret})}{c}\right)^{2/3}, \quad (4.189)$$

and therefore the GW amplitude takes the same form as in the absence of cosmological expansion, with the replacements $r \to d_L$ and $M_c \to \mathcal{M}_c$. In the general case of non-vanishing redshift, we will reserve the name "chirp mass" for $\mathcal{M}_c$, rather than for M_c. From eqs. (4.151) and (4.173), we find that the dependence of $f_{\rm gw}^{(\rm obs)}$ on $t_{\rm obs}$ is given by

$$f_{\rm gw}^{(\rm obs)}(t_{\rm obs}^{\rm ret}) = \frac{1}{1+z}\,f_{\rm gw}^{(s)}(t_s^{\rm ret})$$
$$= \frac{1}{1+z}\,\frac{1}{\pi}\left(\frac{5}{256}\,\frac{1+z}{\tau_{\rm obs}}\right)^{3/8}\left(\frac{GM_c}{c^3}\right)^{-5/8}$$
$$= \frac{1}{\pi}\left(\frac{5}{256}\,\frac{1}{\tau_{\rm obs}}\right)^{3/8}\left(\frac{G\mathcal{M}_c}{c^3}\right)^{-5/8}, \quad (4.190)$$

where $\tau_{\rm obs} = (1+z)\tau_s$ is the time to coalescence measured by the observer's clock.[20] Then, even the dependence of $f_{\rm gw}^{(\rm obs)}$ on $t_{\rm obs}$ is formally the same as the relation at $z = 0$, once we replace $M_c \to \mathcal{M}_c$. This result is due to the fact that, when $z = 0$, both the GW amplitude and the evolution of the frequency with time are determined by the only time-scale of the problem, which is GM_c/c^3. What we are actually finding is that, in a cosmological context, this time-scale is redshifted, $GM_c/c^3 \to (1+z)GM_c/c^3$. This is a very natural result, which formally amounts to the replacement $M_c \to (1+z)M_c$.

To summarize, the signal received by the observed from a binary inspiral at redshift z, when expressed in terms of the observer time $t_{\rm obs}$, or equivalently in terms of the time to coalescence measured by the observer, $\tau_{\rm obs}$, is given by

$$h_+(\tau_{\rm obs}) = h_c(\tau_{\rm obs})\,\frac{1+\cos^2\iota}{2}\,\cos\left[\Phi(\tau_{\rm obs})\right], \quad (4.191)$$
$$h_\times(\tau_{\rm obs}) = h_c(\tau_{\rm obs})\,\cos\iota\,\sin\left[\Phi(\tau_{\rm obs})\right] \quad (4.192)$$

[20] Since $\tau = t_{\rm coal}^{\rm ret} - t^{\rm ret} = t_{\rm coal} - t$, we have $\tau = \tau^{\rm ret}$, and the result can be written just as a function of the observer's time, rather than of the observer's retarded time.

where (compare with eq. (4.30)),

$$\Phi(\tau_{\rm obs}) = -2\left(\frac{5G\mathcal{M}_c(z)}{c^3}\right)^{-5/8}\tau_{\rm obs}^{5/8} + \Phi_0\,, \quad (4.193)$$

$$h_c(\tau_{\rm obs}) = \frac{4}{d_L(z)}\left(\frac{G\mathcal{M}_c(z)}{c^2}\right)^{5/3}\left(\frac{\pi f_{\rm gw}^{(\rm obs)}(\tau_{\rm obs})}{c}\right)^{2/3}, \quad (4.194)$$

and

$$f_{\rm gw}^{(\rm obs)}(\tau_{\rm obs}) = \frac{1}{\pi}\left(\frac{5}{256}\,\frac{1}{\tau_{\rm obs}}\right)^{3/8}\left(\frac{G\mathcal{M}_c(z)}{c^3}\right)^{-5/8}. \quad (4.195)$$

The latter equation implies also that

$$\dot f_{\rm gw}^{(\rm obs)} = \frac{96}{5}\,\pi^{8/3}\left(\frac{G\mathcal{M}_c(z)}{c^3}\right)^{5/3}[f_{\rm gw}^{(\rm obs)}]^{11/3}. \quad (4.196)$$

In other words, we have the following modifications compared to the case $z = 0$:

- The observed frequency is redshifted with respect to the frequency measured in the source frame, $f^{(\rm obs)} = f^{(s)}/(1+z)$. For instance, we saw below eq. (4.40) that the inspiral of a NS-NS binary system terminates, and the two stars merge, when the intrinsic orbital frequency of the source, in the source frame, is of order 800 Hz. This means that, from the point of view of the observer, the orbital frequency of the source will sweep up to a maximum value of order $800\,{\rm Hz}/(1+z)$. For example, for a NS-NS coalescence at $z \simeq 2$, the maximum value of the source orbital frequency, in the observer frame, is of order 270 Hz, and the quadrupole radiation emitted in the inspiral phase will be cutoff at twice this value.
- The overall factor $1/r$ in the GW amplitude is replaced by $1/d_L(z)$.
- M_c is replaced by $\mathcal{M}_c = (1+z)M_c$.

A very interesting consequence of the above results is the following. Suppose that we can measure the amplitudes of both polarizations $h_+, h_\times$, as well as $\dot f_{\rm gw}^{(\rm obs)}$. The amplitude of h_+ is $h_c(1+\cos^2\iota)/2$, while the amplitude of $h_\times$ is $h_c\cos\iota$. From their ratio, we can therefore obtain the value of $\cos\iota$, that is, the inclination of the orbit with respect to the line of sight. On the other hand, eq. (4.196) shows that, if we measure the value of $\dot f_{\rm gw}^{(\rm obs)}$ corresponding to a given value of $f_{\rm gw}^{(\rm obs)}$, we get the chirp mass $\mathcal{M}_c$. Now in the expression for h_+ and $h_\times$ all parameters have been fixed, except $d_L(z)$.[21] This means that, from the measured value of h_+ (or of $h_\times$) we can now read d_L. If, at the same time, we can measure the redshift z of the source, we have found a gravitational standard candle, and we can use it to measure the Hubble parameter $H(z)$, compare with eq. (4.168). We will discuss in Vol. 2 the rich cosmological information that can be obtained from this type of measurements, as well as the methods proposed to have an associated measure of the redshift (either from optical observations or from GW observations themselves), and the associated experimental uncertainties.

[21] Observe that the ellipticity of the orbit does not enter since, as we discussed in Section 4.1.3, by the time that the stars approach the coalescence stage, angular momentum losses have circularized the orbit to great accuracy. Therefore it is legitimate to use the results for circular orbits, as we have done in this section, and there is no free parameter associated to the ellipticity.

4.2 Radiation from rotating rigid bodies

The production of GWs from a rotating rigid body is of great importance, in particular for application to isolated neutron stars. In Section 4.2.1 we examine the production of GWs in the simplest situation, i.e. the radiation emitted by a rigid body which rotates around one of its principal axes. Then, in Section 4.2.2, we will discuss the more complicated situation where the rotation axis does not coincide with a principal axis, and therefore there is a motion of precession.

Let us first recall, from elementary mechanics (see e.g. Landau and Lifshitz, Vol. I 1976), a few basic notions of kinematics of rigid bodies. A rigid body is characterized by its inertia tensor

$$I^{ij} = \int d^3x\, \rho(\mathbf{x})\, (r^2 \delta^{ij} - x^i x^j)\,. \tag{4.197}$$

where ρ is the mass density. Since any hermitian matrix can be diagonalized by an appropriate rotation, there exists an orthogonal frame where I_{ij} is diagonal. The corresponding axes are called the principal axes of the body, and the eigenvalues I_1, I_2, I_3 are called the principal moments of inertia. We will refer to the frame where I_{ij} is diagonal as the "body frame". Denoting by x'_i the coordinates in the body frame, we have

$$I_1 = \int d^3x'\, \rho(\mathbf{x}')\, ({x'_2}^2 + {x'_3}^2)\,, \tag{4.198}$$

$$I_2 = \int d^3x\, \rho(\mathbf{x}')\, ({x'_1}^2 + {x'_3}^2)\,, \tag{4.199}$$

$$I_3 = \int d^3x\, \rho(\mathbf{x}')\, ({x'_1}^2 + {x'_2}^2)\,. \tag{4.200}$$

From these explicit expressions we see that $I_1 + I_2 \geqslant I_3$. Therefore each principal moment of inertia must be smaller or equal than the sum of the other two. The identity $I_1 + I_2 = I_3$ holds only if $\rho(\mathbf{x}) \sim \delta(x_3)$, that is, for a bidimensional configuration of matter.

A simple geometry is that of an ellipsoid with semiaxes a, b, c, uniform density, and mass m. In this case, eqs. (4.198)–(4.200) give

$$I_1 = \frac{m}{5}\,(b^2 + c^2)\,, \tag{4.201}$$

$$I_2 = \frac{m}{5}\,(a^2 + c^2)\,, \tag{4.202}$$

$$I_3 = \frac{m}{5}\,(a^2 + b^2)\,. \tag{4.203}$$

If the body rotates with angular velocity $\boldsymbol{\omega}$, its angular momentum is

$$J_i = I_{ij}\omega_j\,. \tag{4.204}$$

We denote by (J'_1, J'_2, J'_3) and $(\omega'_1, \omega'_2, \omega'_3)$ the components of the angular momentum and of the angular velocity, respectively, in the body frame. Then $J'_1 = I_1\omega'_1$, $J'_2 = I_2\omega'_2$ and $J'_3 = I_3\omega'_3$. Observe that the direction

of $\boldsymbol{\omega}$ is different from the direction of $\mathbf{J}$ unless either $I_1 = I_2 = I_3$ (which holds only for a spherical object) or the rotation is around one of the principal axes, e.g. when, $\omega'_1 = \omega'_2 = 0$. The rotational kinetic energy is

$$E_{\rm rot} = \frac{1}{2} I_{ij}\omega_i\omega_j\,, \tag{4.205}$$

so in the body frame it is given simply by

$$E_{\rm rot} = \frac{1}{2}(I_1{\omega'_1}^2 + I_2{\omega'_2}^2 + I_3{\omega'_3}^2)\,. \tag{4.206}$$

If we denote by $\hat{\boldsymbol{\omega}}$ the unit vector in the direction of the axis of rotation, so that $\boldsymbol{\omega} = \omega\hat{\boldsymbol{\omega}}$, then $E_{\rm rot} = (1/2)I\omega^2$, where $I = I_{ij}\hat{\omega}_i\hat{\omega}_j$ is called the moment of inertia about the axis of rotation.

4.2.1 GWs from rotation around a principal axis

We first consider the situation in which the body rotates rigidly about one of its principal axes. We denote by (x'_1, x'_2, x'_3) the coordinates in the body frame. This reference frame, by definition, is attached to the body and rotates with it. We take the x'_3 axis as the axis around which the body rotate, and we denote by $\omega_{\rm rot}$ the corresponding angular velocity. We also introduce a fixed reference frame, with coordinates (x_1, x_2, x_3), oriented so that $x'_3 = x_3$, see Fig. 4.13. In both frames, the origin of the axes coincides with the center-of-mass of the body. The two frames are related by a time-dependent rotation matrix $\mathcal{R}_{ij}$,

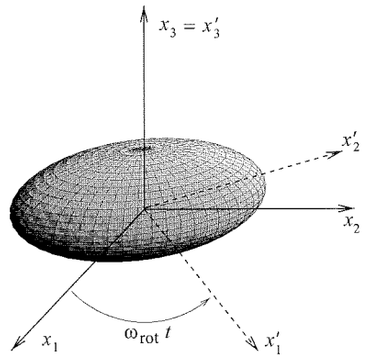

Fig. 4.13 The principal axes (x'_1, x'_2, x'_3), which rotate with the rigid body, and the fixed axes (x_1, x_2, x_3).

$$x'_i = \mathcal{R}_{ij}x_j\,, \tag{4.207}$$

with

$$\mathcal{R}_{ij} = \begin{pmatrix} \cos\omega_{\rm rot}t & \sin\omega_{\rm rot}t & 0 \\ -\sin\omega_{\rm rot}t & \cos\omega_{\rm rot}t & 0 \\ 0 & 0 & 1 \end{pmatrix}_{ij}\,. \tag{4.208}$$

We denote by $I'_{ij} = {\rm diag}(I_1, I_2, I_3)$ the inertia tensor in the (x'_1, x'_2, x'_3) coordinate system, and by I_{ij} its components in the (x_1, x_2, x_3) frame. Thus, I'_{ij} is a constant matrix, while I_{ij} is time-dependent. The fact that the moment of inertia is a tensor implies that

$$\begin{aligned} I'_{ij} &= \mathcal{R}_{ik}\mathcal{R}_{jl}I_{kl} \\ &= (\mathcal{R}I\mathcal{R}^T)_{ij}\,, \end{aligned} \tag{4.209}$$

where $\mathcal{R}^T$ is the transpose matrix, and therefore

$$I = \mathcal{R}^T I'\mathcal{R}\,. \tag{4.210}$$

This gives

$$\begin{aligned} I_{11} &= I_1\cos^2\omega_{\rm rot}t + I_2\sin^2\omega_{\rm rot}t \\ &= 1 + \frac{I_1 - I_2}{2}\cos 2\omega_{\rm rot}t\,, \end{aligned} \tag{4.211}$$

$$I_{12} = \frac{I_1 - I_2}{2} \sin 2\omega_{\rm rot} t \,, \tag{4.212}$$

$$I_{22} = I_1 \sin^2 \omega_{\rm rot} t + I_2 \cos^2 \omega_{\rm rot} t$$
$$= 1 - \frac{I_1 - I_2}{2} \cos 2\omega_{\rm rot} t \,, \tag{4.213}$$

$$I_{33} = I_3 \,, \tag{4.214}$$

while $I_{13} = I_{23} = 0$. Recall that in the quadrupole approximation the GW amplitude depends on the second moment of the mass density M^{ij}. From eq. (4.197) we see that M^{ij} differ from I^{ij} by an overall minus sign, and for the absence of the trace term.[22] However, the trace of a tensor is invariant under rotation; in fact, from eq. (4.209), using the cyclic property of the trace and the property of the orthogonal matrices that $\mathcal{R}\mathcal{R}^T$ is equal to the identity matrix, we have $\mathrm{Tr}\, I = \mathrm{Tr}\,[\mathcal{R}^T I' \mathcal{R}] = \mathrm{Tr}\,[I' \mathcal{R}\mathcal{R}^T] = \mathrm{Tr}\, I'$. Since $\mathrm{Tr}\, I' = I_1 + I_2 + I_3$ is a constant, we have

$$M_{ij} = -I_{ij} + c_{ij} \,, \tag{4.215}$$

where c_{ij} are constants. In the computation of the GW amplitude only the second time derivative of M_{ij} enters and therefore the explicit value of the constants is irrelevant, and we can write

$$M_{11} = -\frac{I_1 - I_2}{2} \cos 2\omega_{\rm rot} t + \text{constant} \,, \tag{4.216}$$

$$M_{12} = -\frac{I_1 - I_2}{2} \sin 2\omega_{\rm rot} t + \text{constant} \,, \tag{4.217}$$

$$M_{22} = +\frac{I_1 - I_2}{2} \cos 2\omega_{\rm rot} t + \text{constant} \,, \tag{4.218}$$

while M_{13}, M_{23} and M_{33} are constant. We observe that, in our setting in which the body rotates around its principal axis x_3', there is a time-varying second mass moment only if $I_1 \neq I_2$, which is quite clear geometrically. We also see that M_{ij} is a periodic function of $2\omega_{\rm rot} t$, so we already understand that we have production of GWs with a frequency $\omega_{\rm gw} = 2\omega_{\rm rot}$.

We can now compute the GW amplitude received by an observer at a distance r, whose line-of-sight makes an angle ι with the direction of the spin of the star, i.e. with the x_3 axis, see Fig. 4.14. We use eq. (3.72), setting with $\theta = \iota$ and, without loss of generality, we orient the fixed frame (x_1, x_2, x_3) so that the observer is at $\phi = 0$.

Inserting the expressions (4.216)–(4.218) for M_{ij} and taking into account that $\ddot{M}_{13} = \ddot{M}_{23} = \ddot{M}_{33} = 0$, eq. (3.72) gives

$$h_+ = \frac{1}{r} \frac{4G\omega_{\rm rot}^2}{c^4} (I_1 - I_2) \frac{1 + \cos^2 \iota}{2} \cos(2\omega_{\rm rot} t) \,, \tag{4.219}$$

$$h_\times = \frac{1}{r} \frac{4G\omega_{\rm rot}^2}{c^4} (I_1 - I_2) \cos\iota \sin(2\omega_{\rm rot} t) \,. \tag{4.220}$$

We therefore have a periodic GW, with $\omega_{\rm gw} = 2\omega_{\rm rot}$. The fact that h_+ is proportional to $(1+\cos^2\iota)/2$, while $h_\times$ to $\cos\iota$, is the same result that we found for the GW amplitude of a binary system in a circular orbit,

[22] Actually, for a relativistic source (and in the approximation that the internal gravitational fields are not strong) M^{ij} is really the second moment of T^{00}/c^2, i.e. the energy density over c^2. For non-relativistic internal motions, T^{00}/c^2 becomes equal to the mass density ρ. Otherwise, all the arguments below go through if, in the definition of I^{ij}, we define ρ to be T^{00}/c^2.

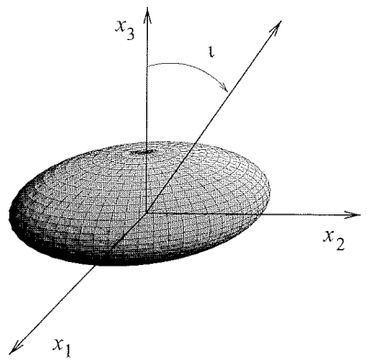

Fig. 4.14 The rigid body rotating around the x_3 axis; ι is the angle between the line-of-sight and the x_3 axis.

see eq. (3.332). In fact, this is a generic property of eq. (3.72) whenever $\ddot{M}_{11} = -\ddot{M}_{22}$ and $\ddot{M}_{13} = \ddot{M}_{23} = \ddot{M}_{33} = 0$.

It is useful to define the ellipticity ϵ by

$$\epsilon \equiv \frac{I_1 - I_2}{I_3} \,. \tag{4.221}$$

For instance, for a homogeneous ellipsoid with semiaxes a, b and c, in the limit of small asymmetry, i.e. $a \simeq b$, eqs. (4.198)–(4.200) give

$$\epsilon \simeq \frac{b - a}{a} + O(\epsilon^2) \,. \tag{4.222}$$

We write the angular velocity of the source as $\omega_{\rm rot} = 2\pi f_{\rm rot}$ and we introduce $f_{\rm gw} = 2 f_{\rm rot}$, which is the frequency of the GW. In terms of $f_{\rm gw}$ and of ϵ, the result for the GW amplitude found above can be rewritten as

$$\boxed{\begin{aligned} h_+ &= h_0 \frac{1 + \cos^2 \iota}{2} \cos(2\pi f_{\rm gw} t) \,, \\ h_\times &= h_0 \cos\iota \sin(2\pi f_{\rm gw} t) \,, \end{aligned}} \tag{4.223}$$

where

$$\boxed{h_0 = \frac{4\pi^2 G}{c^4} \frac{I_3 f_{\rm gw}^2}{r} \epsilon \,.} \tag{4.224}$$

Neutron stars typically have a mass $m \simeq 1.4 M_\odot$ and a radius $a \simeq 10$ km, which gives $I_3 \simeq (2/5) m a^2 \simeq 1 \times 10^{38}\,\mathrm{kg\,m^2}$. The value of the ellipticity depends on the neutron star properties, and in particular on the maximum strain that can be supported by its crust. This is quite uncertain but, as we will discuss in Vol. 2, plausible values are in the range $\epsilon \leqslant 10^{-6}$, although values as large as $\epsilon \simeq 10^{-5}$ can be considered. Inserting these numerical reference values, and taking a typical galactic distance $r = 10$ kpc, eq. (4.224) gives

$$h_0 \simeq 1.06 \times 10^{-25} \left(\frac{\epsilon}{10^{-6}}\right) \left(\frac{I_3}{10^{38}\,\mathrm{kg\,m^2}}\right) \left(\frac{10\,\mathrm{kpc}}{r}\right) \left(\frac{f_{\rm gw}}{1\,\mathrm{kHz}}\right)^2 . \tag{4.225}$$

Observe that neutron stars that rotate more rapidly produce a stronger GW signal, since $h_0 \sim f_{\rm gw}^2$.

We next compute the power P radiated in GWs, plugging eqs. (4.216)–(4.218) into the quadrupole formula (3.76). Observing that $\dddot{M}_{11} = -\dddot{M}_{22}$, this gives

$$P = \frac{2G}{5c^5} \langle \dddot{M}_{11}^2 + \dddot{M}_{12}^2 \rangle$$
$$= \frac{32G}{5c^5} \epsilon^2 I_3^2 \omega_{\rm rot}^6 \,, \tag{4.226}$$

and therefore the rotational energy of the star decreases, because of GW emission, as

$$\frac{dE_{\rm rot}}{dt} = -\frac{32G}{5c^5} \epsilon^2 I_3^2 \omega_{\rm rot}^6 \,. \tag{4.227}$$

Since the rotational energy of a star rotating around its principal axis x_3 is $E_{\rm rot} = (1/2) I_3 \omega_{\rm rot}^2$ (see eq. (4.206)), if GW emission were the dominant mechanism for the loss of rotational energy, the rotational frequency of a neutron star should decrease as

$$\dot{\omega}_{\rm rot} = -\frac{32G}{5c^5}\,\epsilon^2 I_3 \omega_{\rm rot}^5 \,. \tag{4.228}$$

Experimentally, from the electromagnetic signal emitted by neutron stars observed as pulsars (see Chapter 6), one rather finds $\dot{\omega}_{\rm rot} \sim -\omega_{\rm rot}^n$ where n, called the braking index, depends on the specific pulsar but typically ranges between 2 and 3, rather than $n = 5$. This means that GW emission is not the main energy loss mechanism for a rotating pulsar, and other mechanisms, of electromagnetic nature, dominate.

4.2.2 GWs from freely precessing rigid bodies

In general, in astronomical objects the rotation axis does not coincide with a principal axis and, as a consequence, the motion of the rigid body is a combination of rotation around a principal axis and precession. As we will see in this section, the precession motion introduces qualitatively new features in the GWs radiated.

To compute the GW production we proceed as in eqs. (4.207)–(4.209). We first introduce a fixed reference frame, with axes (x_1, x_2, x_3). In this inertial frame the angular momentum $\mathbf{J}$ of the rigid body is conserved, and we choose the x_3 axis in the direction of $\mathbf{J}$. Next we introduce the body frame, i.e. a reference frame attached to the rotating body, with coordinates (x_1', x_2', x_3'), whose axes coincide with the principal axes of the body. The relation between the two frames is given by the Euler angles (α, β, γ) defined in Fig. 4.15.[23]

To pass from the fixed frame to the body frame we first perform a counterclockwise rotation by an angle β around the x_3 axis. This brings the x_1 axis onto an axis which is called the line of nodes (which is the intersection of the (x_1, x_2) plane with the (x_1', x_2') plane). Next we perform a counterclockwise rotation by an angle α around the line of nodes. This brings the x_3 axis onto the x_3' axis. Finally, we perform a counterclockwise rotation by an angle γ around the x_3' axis, which brings the line of nodes onto the x_1' axis. Therefore we have $x_i' = \mathcal{R}_{ij} x_j$, as in eq. (4.207), but now the rotation matrix is more complicated,

$$\mathcal{R} = \begin{pmatrix} \cos\gamma & \sin\gamma & 0 \\ -\sin\gamma & \cos\gamma & 0 \\ 0 & 0 & 1 \end{pmatrix} \begin{pmatrix} 1 & 0 & 0 \\ 0 & \cos\alpha & \sin\alpha \\ 0 & -\sin\alpha & \cos\alpha \end{pmatrix} \begin{pmatrix} \cos\beta & \sin\beta & 0 \\ -\sin\beta & \cos\beta & 0 \\ 0 & 0 & 1 \end{pmatrix} . \tag{4.229}$$

The motion of the rigid body is specified once we know how α, β and γ evolve with time. Let us recall, from elementary mechanics (see again Landau and Lifshitz, Vol. I 1976), how this can be obtained. In the (x_1, x_2, x_3) frame, the angular momentum $\mathbf{J}$ is conserved (this, of course,

[23] In the literature, (α, β, γ) are usually denote by (θ, ϕ, ψ), respectively. However, here we prefer to reserve the notation (θ, ϕ) to denote the angles that describe the angular distribution of the gravitational radiation.

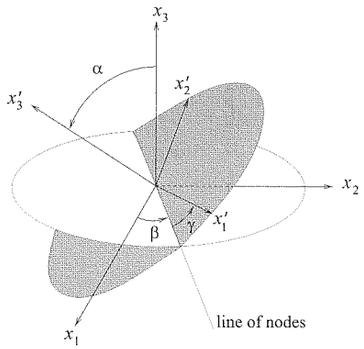

Fig. 4.15 The definition of the Euler angles (α, β, γ).

is not the case in the body frame, which is non-inertial, since it is rotating), and we oriented the x_3 axis so that $\mathbf{J} = (0, 0, J)$. In the (x_1', x_2', x_3') frame, instead, we denote the components of the angular momentum by (J_1', J_2', J_3'). From Fig. 4.15 we see that

$$\begin{aligned} J_1' &= J \sin\alpha \sin\gamma \,, \\ J_2' &= J \sin\alpha \cos\gamma \,, \\ J_3' &= J \cos\alpha \,. \end{aligned} \tag{4.230}$$

On the other hand, we can write (J_1', J_2', J_3') in terms of $\dot{\alpha}, \dot{\beta}$ and $\dot{\gamma}$ using again Fig. 4.15 and observing that, as a vector, the angular velocity $d\boldsymbol{\alpha}/dt$ is directed along the line of nodes, so its components in the body frame are

$$\frac{d\boldsymbol{\alpha}}{dt} = (\dot{\alpha}\cos\gamma, -\dot{\alpha}\sin\gamma, 0) \,. \tag{4.231}$$

Similarly, $d\boldsymbol{\beta}/dt$ is directed along the x_3 axis, so its components in the body frame are

$$\frac{d\boldsymbol{\beta}}{dt} = (\dot{\beta}\sin\alpha\sin\gamma, \dot{\beta}\sin\alpha\cos\gamma, \dot{\beta}\cos\alpha) \,, \tag{4.232}$$

while $d\boldsymbol{\gamma}/dt$ is along the x_3' axis, so in the body frame $d\boldsymbol{\gamma}/dt = (0, 0, \dot{\gamma})$. The total angular velocity $\boldsymbol{\omega}$ is the vector sum of these angular velocities, $\boldsymbol{\omega} = d\boldsymbol{\alpha}/dt + d\boldsymbol{\beta}/dt + d\boldsymbol{\gamma}/dt$, so its components ω_i' in the body frame are

$$\begin{aligned} \omega_1' &= \dot{\alpha}\cos\gamma + \dot{\beta}\sin\alpha\sin\gamma \,, \\ \omega_2' &= -\dot{\alpha}\sin\gamma + \dot{\beta}\sin\alpha\cos\gamma \,, \\ \omega_3' &= \dot{\gamma} + \dot{\beta}\cos\alpha \,. \end{aligned} \tag{4.233}$$

In the body frame the inertia tensor is diagonal, with eigenvalues I_1, I_2 and I_3, so $J_1' = I_1\omega_1'$, $J_2' = I_2\omega_2'$ and $J_3' = I_3\omega_3'$. Comparing eqs. (4.230) and (4.233) we therefore get

$$I_1(\dot{\alpha}\cos\gamma + \dot{\beta}\sin\alpha\sin\gamma) = J\sin\alpha\sin\gamma \,, \tag{4.234}$$

$$I_2(-\dot{\alpha}\sin\gamma + \dot{\beta}\sin\alpha\cos\gamma) = J\sin\alpha\cos\gamma \,, \tag{4.235}$$

$$I_3(\dot{\gamma} + \dot{\beta}\cos\alpha) = J\cos\alpha \,. \tag{4.236}$$

These are first order equations in the variables (α, β, γ), and are the first integral of the equations of motion provided by the conservation of angular momentum.[24] One can now integrate these equations and obtain $\alpha(t), \beta(t)$ and $\gamma(t)$. In the most general case, the result can be written in terms of elliptic functions, and we will get back to it later in this section. However, we first limit ourselves to the simpler case of an axisymmetric body with $I_1 = I_2$.

"Wobble" radiation from an axisymmetric rigid body

We consider an axisymmetric body, whose longitudinal axis x_3' makes an angle α with the angular momentum axis x_3. The angle α is often

[24] They are in fact the first integral of the Euler equations for rigid bodies in the absence of external torques,

$$\begin{aligned} I_1\dot{\omega}_1' &= \omega_2'\omega_3'(I_2 - I_3) \\ I_2\dot{\omega}_2' &= \omega_1'\omega_3'(I_3 - I_1) \\ I_3\dot{\omega}_3' &= \omega_1'\omega_2'(I_1 - I_2) \end{aligned}$$

as we easily verify taking the first derivative of eqs. (4.234)–(4.236) and using eq. (4.233).

called the "wobble" angle, and the corresponding GW emission is called "wobble radiation".

When $I_1 = I_2$, the analytic solution of eqs. (4.234)–(4.236) is very simple. Multiplying the first equation by $\cos\gamma$ and the second by $\sin\gamma$ and subtracting them, we get

$$\dot{\alpha} = 0\,. \tag{4.237}$$

This shows that the inclination of the x_3' axis with respect to the angular momentum $\mathbf{J}$ is constant. Multiplying the first equation by $\sin\gamma$ and the second by $\cos\gamma$ and summing them, we get

$$I_1\dot{\beta}\sin\alpha = J\sin\alpha\,. \tag{4.238}$$

This shows that, if $\alpha \neq 0$, the x_3' axis rotates with a constant angular velocity $\dot{\beta} = J/I_1$ about the direction of $\mathbf{J}$. We define

$$\Omega \equiv \dot{\beta} = \frac{J}{I_1}\,. \tag{4.239}$$

Finally, having found that both $\cos\alpha$ and $\dot{\beta}$ are constants, eq. (4.236) shows that even $\dot{\gamma}$ is constant. Equation (4.236), together with $J = I_1\dot{\beta}$, gives

$$\omega_{\rm p} \equiv -\dot{\gamma} = \frac{I_3 - I_1}{I_3}\,\Omega\cos\alpha\,. \tag{4.240}$$

The minus sign in the definition $\omega_{\rm p} = -\dot{\gamma}$ is chosen so that, for an oblate body ($I_3 > I_1$), which is the normal shape of astrophysical objects, $\omega_{\rm p} > 0$.[25] Using eq. (4.233) we see that the components of the angular velocity in the body frame evolve as[26]

$$\begin{aligned}
\omega_1' &= a\cos(\omega_{\rm p}t)\,,\\
\omega_2' &= a\sin(\omega_{\rm p}t)\,,\\
\omega_3' &= b\,,
\end{aligned} \tag{4.242}$$

where $a = \Omega\sin\alpha$ and $b = -\omega_{\rm p} + \Omega\cos\alpha$ are constants. This shows that, in the body frame, the angular velocity rotates in the (x_1', x_2') plane, i.e. *precesses* around the x_3' axis, with angular velocity $\omega_{\rm p}$. This precession is counterclockwise if $\omega_{\rm p} > 0$ (which justifies the notation $\omega_{\rm p}$ for $-\dot{\gamma}$). Observe that $|I_3 - I_1| \ll I_3$ (in a NS, a possible value could be $|I_3 - I_1|/I_3 \sim 10^{-7}$), and therefore $|\omega_{\rm p}| \ll \Omega$. This motion is called free precession, since it takes place in the absence of external torques, just as a consequence of the deviation of the rigid body from spherical symmetry.

We can now compute how the inertia tensor of the rigid body evolves with time, in the fixed frame with coordinates (x_1, x_2, x_3). As before we denote by I' the inertia tensor in the body frame, so $I' = \mathrm{diag}\,(I_1, I_1, I_3)$ is a constant matrix, while we denote by I_{ij} the inertia tensor in the fixed frame. Then, as in eq. (4.210), $I_{ij} = (\mathcal{R}^T I'\mathcal{R})_{ij}$, but now $\mathcal{R}$ is given by eq. (4.229).

[25] Using the expression for $\dot{\gamma}$ given in eq. (4.240), we have

$$\begin{aligned}
\omega_3' &= \dot{\gamma} + \dot{\beta}\cos\alpha\\
&= (I_1/I_3)\Omega\cos\alpha\,,
\end{aligned}$$

and therefore we can also write

$$\omega_{\rm p} = \frac{I_3 - I_1}{I_1}\omega_3'\,. \tag{4.241}$$

[26] Observe that, for an axisymmetric body, the orientation of the principal axes in the (x_1', x_2') plane is arbitrary. We choose the origin of time so that $\beta(t = 0) = 0$, and then we choose the orientation of the (x_1', x_2') axes so that, at $t = 0$, $\gamma(0) = \pi/2$. Therefore eq. (4.240) gives $\gamma(t) = (\pi/2) - \omega_{\rm p}t$.

The explicit computation is simplified observing that, if we write the rotation matrix (4.229) as $\mathcal{R} = A(\gamma)B(\alpha)C(\beta)$, we see that

$$\begin{aligned}
\mathcal{R}^T I'\mathcal{R} &= (C^T B^T A^T) I' (ABC)\\
&= (C^T B^T) I' (BC)
\end{aligned} \tag{4.243}$$

because, when $I_1 = I_2$, the matrix A commutes with the matrix I', and $A^T A = 1$ because it is an orthogonal matrix. Therefore, the angle γ drops out from I_{ij}, and the remaining matrix multiplication gives

$$\begin{aligned}
I_{11} &= I_1(\cos^2\beta + \cos^2\alpha\sin^2\beta) + I_3\sin^2\alpha\sin^2\beta\\
&= \frac{1}{2}(I_1 - I_3)\sin^2\alpha\cos 2\beta + \text{constant}\,,\\
I_{12} &= \frac{1}{2}(I_1 - I_3)\sin^2\alpha\sin 2\beta\,,\\
I_{22} &= I_1(\sin^2\beta + \cos^2\alpha\cos^2\beta) + I_3\sin^2\alpha\cos^2\beta\\
&= -\frac{1}{2}(I_1 - I_3)\sin^2\alpha\cos 2\beta + \text{constant}\,,\\
I_{13} &= -(I_1 - I_3)\sin\alpha\cos\alpha\sin\beta\,,\\
I_{23} &= (I_1 - I_3)\sin\alpha\cos\alpha\cos\beta\,,\\
I_{33} &= I_1\sin^2\alpha + I_3\cos^2\alpha = \text{constant}\,.
\end{aligned} \tag{4.244}$$

Observe that, since γ dropped out and α is constant, the time dependence of these expressions comes uniquely from β which, from eq. (4.239), is $\beta(t) = \Omega t$ (recall that we have chosen the origin of time so that $\beta = 0$ at $t = 0$, see Note 26). As in eq. (4.215), $M_{ij} = -I_{ij}$, plus constant terms that give zero upon derivation. Therefore, we get

$$\begin{aligned}
\ddot{M}_{11} &= 2(I_1 - I_3)\Omega^2\sin^2\alpha\cos(2\Omega t)\,,\\
\ddot{M}_{12} &= 2(I_1 - I_3)\Omega^2\sin^2\alpha\sin(2\Omega t)\,,\\
\ddot{M}_{22} &= -2(I_1 - I_3)\Omega^2\sin^2\alpha\cos(2\Omega t)\,,\\
\ddot{M}_{13} &= -(I_1 - I_3)\Omega^2\sin\alpha\cos\alpha\sin(\Omega t)\,,\\
\ddot{M}_{23} &= (I_1 - I_3)\Omega^2\sin\alpha\cos\alpha\cos(\Omega t)\,,\\
\ddot{M}_{33} &= 0\,.
\end{aligned} \tag{4.245}$$

We see that some matrix elements of $\ddot{M}_{ij}$ oscillate as $\sin(2\Omega t)$ or $\cos(2\Omega t)$, while others as $\sin(\Omega t)$ or $\cos(\Omega t)$. From this, we already understand that we will have GW emission at two frequencies, $\omega_{\rm gw} = 2\Omega$ and $\omega_{\rm gw} = \Omega$. The origin of these factors is easily traced back: since the only time dependence comes from $\beta(t)$, and β describes a rotation in the (x_1, x_2) plane, the time-dependent part of I_{ij} has a factor $\sin(\Omega t)$ or $\cos(\Omega t)$ for each index i or j that take the value 1 or 2, while the index 3 produces no further time dependence. Then, as far as the time-dependent part is concerned, we have $I_{11} \sim \sin^2\Omega t \sim \cos(2\Omega t)$, $I_{22} \sim \cos^2\Omega t \sim \cos(2\Omega t)$, $I_{12} \sim \sin(\Omega t)\cos(\Omega t) \sim \sin(2\Omega t)$, while $I_{13} \sim \sin(\Omega t)$ and $I_{23} \sim \cos(\Omega t)$. Thus, the fact that, beside the expected radiation at $\omega_{\rm gw} = 2\Omega$, we also have radiation at $\omega_{\rm gw} = \Omega$, is a consequence of the fact that the motion of precession produces, together

with a time-varying value of I_{ij} with $i, j = 1, 2$, also a variation in I_{23} and I_{13}.

The computation of the GW amplitude radiated in a direction corresponding to polar angles $(\theta = \iota, \phi = 0)$ is now performed using eq. (3.72). We get

$$\begin{aligned} h_+ &= \frac{1}{r}\frac{G}{c^4}\left[\ddot{M}_{11} - \ddot{M}_{22}\cos^2\iota + \ddot{M}_{23}\sin 2\iota - \ddot{M}_{33}\sin^2\iota\right] \\ &= A_{+,1}\cos(\Omega t) + A_{+,2}\cos(2\Omega t) \qquad (4.246) \\ h_\times &= \frac{2}{r}\frac{G}{c^4}\left[\ddot{M}_{12}\cos\iota - \ddot{M}_{13}\sin\iota\right] \\ &= A_{\times,1}\sin(\Omega t) + A_{\times,2}\sin(2\Omega t)\,, \qquad (4.247) \end{aligned}$$

where

$$A_{+,1} = h_0' \sin 2\alpha \,\sin\iota\cos\iota\,, \qquad (4.248)$$
$$A_{+,2} = 2h_0' \sin^2\alpha\,(1+\cos^2\iota)\,, \qquad (4.249)$$
$$A_{\times,1} = h_0' \sin 2\alpha \sin\iota\,, \qquad (4.250)$$
$$A_{\times,2} = 4h_0' \sin^2\alpha\,\cos\iota\,. \qquad (4.251)$$

and[27]

$$h_0' = -\frac{G}{c^4}\frac{(I_3 - I_1)\Omega^2}{r}\,. \qquad (4.252)$$

[27] Observe that the overall sign of the amplitude depends on the choice of the origin of time, and on the definition of the axes $(\hat{\mathbf{u}}, \hat{\mathbf{v}})$ in the plane transverse to the propagation direction, with respect to which the polarizations are defined. With our definition, when $\iota = 0$ these axes are $\hat{\mathbf{u}} = \hat{\mathbf{x}}$ and $\hat{\mathbf{v}} = \hat{\mathbf{y}}$, see page 111 and Fig. 3.2. In the literature, this computation has been performed choosing $\hat{\mathbf{u}}$ and $\hat{\mathbf{v}}$ so that, when $\iota = 0$, $\hat{\mathbf{u}} = \hat{\mathbf{y}}$ and $\hat{\mathbf{v}} = -\hat{\mathbf{x}}$. This is related to our convention by a rotation of the $(\hat{\mathbf{u}}, \hat{\mathbf{v}})$ axes in the transverse plane, by an angle $\psi = \pi/2$. Under this rotation $h_+ \to -h_+$ and $h_\times \to -h_\times$, see eq. (2.194), so $h_0' \to -h_0'$.

Of course it is understood that, on the right-hand side of eqs. (4.246) and (4.247), t is actually the retarded time. As we already anticipated, we have radiation at both $\omega_{\rm gw} = \Omega$ and at $\omega_{\rm gw} = 2\Omega$.

Observe that $A_{+,1}/A_{\times,1} = \cos\iota$. Therefore from this ratio (or, equivalently, from $A_{+,2}/A_{\times,2}$) we get the inclination angle ι (which, by definition, is in the range $0 \leqslant i \leqslant \pi$). Given ι, the ratio $A_{+,1}/A_{+,2}$ determines the angle α. The overall value of the amplitude then fixes $|h_0'|$. If the distance to the source is known by other means, we therefore get a measure of $|I_1 - I_3|$.

It is now straightforward to compute the total power radiated. Using eq. (3.76) and observing, from eq. (4.245), that $\dddot{M}_{33} = 0$ and $\sum_k \dddot{M}_{kk} = 0$, we get

$$\begin{aligned} P_{\rm quad} &= \frac{G}{5c^5}\langle \dddot{M}_{11}^2 + \dddot{M}_{22}^2 + 2\dddot{M}_{12}^2 + 2\dddot{M}_{13}^2 + 2\dddot{M}_{23}^2\rangle \\ &= \frac{2G}{5c^5}(I_1 - I_3)^2\Omega^6\,\sin^2\alpha(\cos^2\alpha + 16\sin^2\alpha)\,, \qquad (4.253) \end{aligned}$$

where the term $\sin^2\alpha\cos^2\alpha$ is from the radiation at $\omega_{\rm gw} = \Omega$ and the term $16\sin^4\alpha$ is from the radiation at $\omega_{\rm gw} = 2\Omega$. Observe that, in the limit of small α, the power radiated at $\omega_{\rm gw} = \Omega$ is $O(\alpha^2)$ while the power radiated at $\omega_{\rm gw} = 2\Omega$ is $O(\alpha^4)$, so for sufficiently small α the radiation at $\omega_{\rm gw} = \Omega$ is dominant. The two contributions become equal when $\cos^2\alpha = 16\sin^2\alpha$, i.e. for $\alpha \simeq 0.245\,{\rm rad} \simeq 14°$.

The back-reaction of GWs

We can now compute how the emission of GWs back-reacts on the motion of the rigid body. The energy radiated in GWs is supplied by the rotational energy $E_{\rm rot}$ of the rigid body, so

$$\frac{dE_{\rm rot}}{dt} = -\frac{2G}{5c^5}(I_1 - I_3)^2\Omega^6\,\sin^2\alpha(\cos^2\alpha + 16\sin^2\alpha)\,. \qquad (4.254)$$

The angular momentum radiated (in the quadrupole approximation that we are using) is computed from eq. (3.97), and is supplied by the angular momentum $\mathbf{J} = (0, 0, J)$ of the rigid body. Setting $i = 3$ into eq. (3.97), we have

$$\begin{aligned} \frac{dJ}{dt} &= -\frac{2G}{5c^5}\langle \ddot{M}_{1a}\dddot{M}_{2a} - \ddot{M}_{2a}\dddot{M}_{1a}\rangle \\ &= -\frac{4G}{5c^5}\langle \ddot{M}_{1a}\dddot{M}_{2a}\rangle\,, \qquad (4.255) \end{aligned}$$

where we observed that we can replace Q_{ka} by M_{ka} since $\epsilon^{3kl}\delta_{ka}Q_{la} = \epsilon^{3kl}Q_{kl} = 0$, and similarly $Q_{la} \to M_{la}$, and in the last line we integrated by part a time derivative, inside the temporal average. Inserting the explicit expressions (4.245), we get

$$\frac{dJ}{dt} = -\frac{2G}{5c^5}(I_1 - I_3)^2\Omega^5\,\sin^2\alpha(\cos^2\alpha + 16\sin^2\alpha)\,. \qquad (4.256)$$

Comparing this result with eq. (4.254), we see that $dE_{\rm rot}/dt = \Omega dJ/dt$. Since $\Omega = \dot\beta$ and $J = I_1\dot\beta$ (see eq. (4.239)), the above equation gives

$$\ddot\beta = -\frac{2G}{5c^5}\frac{(I_1 - I_3)^2}{I_1}\,\dot\beta^5\,\sin^2\alpha(\cos^2\alpha + 16\sin^2\alpha)\,. \qquad (4.257)$$

The equation governing the evolution of α can instead be obtained writing the rotational kinetic energy as in eq. (4.206), and using $\omega_1' = J_1'/I_1 = (J/I_1)\sin\alpha\sin\gamma$, $\omega_2' = J_2'/I_1 = (J/I_1)\sin\alpha\cos\gamma$, and $\omega_3' = J_3'/I_3 = (J/I_3)\cos\alpha$, see eq. (4.230). This gives

$$E_{\rm rot} = \frac{J^2}{2}\left(\frac{\sin^2\alpha}{I_1} + \frac{\cos^2\alpha}{I_3}\right)\,. \qquad (4.258)$$

Taking the time derivative and making use of eq. (4.256) and of $J = I_1\dot\beta$ on the right-hand side, and of eq. (4.254) on the left-hand side, we get

$$\dot\alpha = -\frac{2G}{5c^5}\frac{(I_1 - I_3)^2}{I_1}\,\dot\beta^4\,\sin\alpha\cos\alpha(\cos^2\alpha + 16\sin^2\alpha)\,. \qquad (4.259)$$

Equations (4.257) and (4.259) determine the evolution of the angles α and β. We see that, because of the back-reaction of GWs, both the inclination angle α, and the angular velocity $\dot\beta$ decrease. However, using eqs. (4.256) and (4.259), we see that

$$\frac{d}{dt}(J\cos\alpha) = 0\,. \qquad (4.260)$$

Therefore J decreases and α decreases (i.e. $\cos\alpha$ increases) in such a way that $J\cos\alpha$ stays constant. Since $J\cos\alpha$ is the projection of the angular momentum over the x_3' axis of the body (see eq. (4.230)), we find that the rigid body rotates around its longitudinal axis with a constant angular velocity $\omega_3' = (J/I_3)\cos\alpha$. The rotation of the body around its longitudinal axis is not affected by the GW back-reaction.

To study in more detail the coupled system of equations (4.257) and (4.259), we introduce the dimensionless function

$$u(t) = \dot\beta(t)/\dot\beta_0\,, \tag{4.261}$$

where $\dot\beta_0$ is the value of $\dot\beta(t)$ at some initial value $t = 0$, and we also introduce the time-scale

$$\tau_0 \equiv \left[\frac{2G}{5c^5}\,\frac{(I_1-I_3)^2}{I_1}\,\dot\beta_0^4\right]^{-1} \tag{4.262}$$
$$\simeq 1.8\times 10^6\,\mathrm{yr}\left(\frac{10^{-7}}{(I_1-I_3)/I_3}\right)^2\left(\frac{1\,\mathrm{kHz}}{f_0}\right)^4\left(\frac{10^{38}\,\mathrm{kg\,m^2}}{I_1}\right),$$

where $f_0 = \dot\beta_0/(2\pi)$, and we used as reference for $(I_1 - I_3)/I_3$ and for I_3, values that can be typical for neutron stars. Then eqs. (4.257) and (4.259) become

$$\dot u = -\frac{1}{\tau_0}\,u^5\sin^2\alpha(\cos^2\alpha + 16\sin^2\alpha)\,, \tag{4.263}$$

$$\dot\alpha = -\frac{1}{\tau_0}\,u^4\sin\alpha\cos\alpha(\cos^2\alpha + 16\sin^2\alpha)\,, \tag{4.264}$$

with initial conditions $u(0) = 1$ and $\alpha(0) = \alpha_0$. In this form, it is clear that τ_0 is the characteristic time-scale of the problem, and the equations could be recast in a completely dimensionless form introducing a dimensionless variable $x = t/\tau_0$, so that $\tau_0\dot u = du/dx$ and $\tau_0\dot\alpha = d\alpha/dx$.

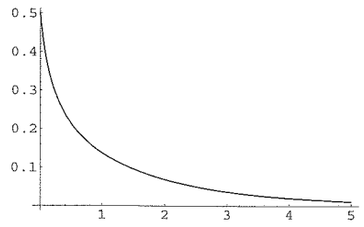

Fig. 4.16 The inclination angle $\alpha(t)$, plotted as a function of t/τ_0, with initial conditions $\alpha(0) = 0.5, u(0) = 1$.

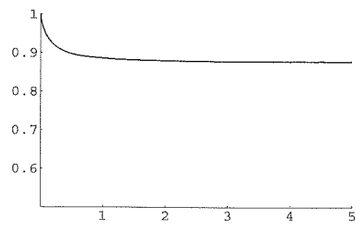

Fig. 4.17 The function $u(t) = \dot\beta/\dot\beta_0$, plotted against t/τ_0, with initial conditions $\alpha(0) = 0.5, u(0) = 1$.

The asymptotic behavior of the solution can be easily read from eqs. (4.263) and (4.264), making use also of the fact that, as we shown above, $J\cos\alpha$ is a constant of motion. Since $J = I_1\dot\beta$, this means that $\dot\beta_\infty\cos\alpha_\infty = \dot\beta_0\cos\alpha_0$, where the subscripts ∞ denotes the value at $t = \infty$. In terms of u, this means

$$u_\infty\cos\alpha_\infty = \cos\alpha_0\,. \tag{4.265}$$

Equating to zero the right-hand sides of eqs. (4.263) and (4.264), we see that the possible fixed points of the evolution are either $u = 0$ or $\alpha = 0, \pi$. However, the value $u_\infty = 0$ is not consistent with eq. (4.265) (unless $\alpha_0 = \pi/2$; clearly, this is an unstable fixed point, in which an infinitesimal perturbation drives the evolution either toward $\alpha = 0$ or $\alpha = \pi$). Therefore the only asymptotic solution, for $\alpha_0 < \pi/2$, has $\alpha_\infty = 0$. Then, eq. (4.265) shows that $u_\infty = \cos\alpha_0$. Once we realize that u approaches a finite constant u_∞ and that $\alpha \to 0$, from eq. (4.264) we see that at large times $\dot\alpha \simeq -\alpha/\tau_\infty$, and therefore $\alpha(t)$ approaches zero exponentially, with a time-scale $\tau_\infty = \tau_0/u_\infty^4$, which is obtained simply replacing $\dot\beta_0$ with $\dot\beta_\infty$ in eq. (4.262).

The numerical integration of eqs. (4.263) and (4.264) is straightforward, and we show in Figs. 4.16 and 4.17 the solution for the initial condition $\alpha_0 = 0.5$, which confirms the asymptotic behavior found analytically.

In conclusion, on a time-scale given by eq. (4.262), the rigid body aligns its rotation axis with the direction of the angular momentum ($\alpha \to 0$), while the rotational angular velocity $\dot\beta = \Omega$ around the x_3 axis decreases toward the constant value $\Omega_0\cos\alpha_0$, and the rotational velocity around its principal axis $\omega_3' = \Omega\cos\alpha$ stays constant.

Finally, it is interesting to compare the frequency $\omega_{\rm em}$ of the electromagnetic pulses of a pulsar, idealized as a rotating rigid body,[28] with the frequency of the GWs that it emits. If a pulsar rotates around its principal axis with frequency Ω, and has $I_1 \neq I_2$, which is the case discussed in Section 4.2.1, then $\omega_{\rm em} = \Omega$, so we can determine Ω very precisely by electromagnetic observations, and GW emission is at $\omega_{\rm gw} = 2\Omega$. In this case, therefore, we have an accurate prediction of the frequency at which we expect GW emission.

Instead, in the case of "wobble" radiation discussed in this subsection, in the limit of small α, the axes x_3 and x_3' almost coincide. If the source of the electromagnetic radiation is some "hot spot" fixed on the star surface then, for a far observer, the hot spot is basically rotating around the x_3 axis with a total angular velocity $\omega_{\rm rot} = \dot\beta + \dot\gamma = \Omega - \omega_{\rm p}$, see Fig. 4.15, so

$$\Omega = \omega_{\rm rot} + \omega_{\rm p}\,. \tag{4.266}$$

The mean frequency $\omega_{\rm em}$ of repetition of the electromagnetic pulses will be equal to $\omega_{\rm rot}$, so $\omega_{\rm em} = \Omega - \omega_{\rm p}$. Instead, we saw that wobble gravitational radiation is emitted at $\omega_{\rm gw} = \Omega$ and at $\omega_{\rm gw} = 2\Omega$, so these two lines are shifted, with respect to $\omega_{\rm em}$ and to $2\omega_{\rm em}$, by the unknown quantities $\omega_{\rm p}$ and $2\omega_{\rm p}$, respectively. Using eq. (4.240), for the line at $\omega_{\rm gw} = \Omega$, we have

$$\omega_{\rm gw} \simeq \left(1 + \frac{I_3 - I_1}{I_3}\cos\alpha\right)\omega_{\rm em}\,. \tag{4.267}$$

Since $|I_1 - I_3|/I_3$ is in general very small, e.g. could be of order 10^{-7} in a neutron star, the difference between the actual GW frequency and the value suggested by electromagnetic observation is small. An axisymmetric astrophysical object is normally expected to be oblate ($I_3 > I_1$), and in this case $\omega_{\rm gw} > \omega_{\rm em}$. For a prolate body ($I_3 < I_1$), instead, we have $\omega_{\rm gw} < \omega_{\rm em}$.

[28] The discussion below is really specific to our crude modelization of neutron stars as rigid bodies. Real neutron stars are rather mostly fluid in their interior. See the Further Reading section for the results with a more realistic modelization of neutron stars.

Rotating and precessing triaxial bodies

We now study the radiation emitted by a generic triaxial body. We choose the axes of the body frame so that $I_1 < I_2 < I_3$. The time-dependent moment of inertia I_{ij} in the fixed frame is again computed

from $I_{ij} = (\mathcal{R}^T I' \mathcal{R})_{ij}$, with $\mathcal{R}$ given by eq. (4.229), but now the dependence on γ does not cancel, contrary to the case $I_1 = I_2$ discussed above, compare with eq. (4.243).

Once expressed I_{ij} in terms of α, β, γ, to compute the waveform we need the time-dependence of the Euler angles, which can be found for instance in Landau and Lifshitz, Vol. I (1976). The evolution of the components of the angular velocity in the body frame is[29]

$$\begin{aligned} \omega_1' &= a\,\mathrm{cn}(\tau, m)\,, \\ \omega_2' &= a \left[\frac{I_1(I_3 - I_1)}{I_2(I_3 - I_2)}\right]^{1/2} \mathrm{sn}(\tau, m)\,, \\ \omega_3' &= b\,\mathrm{dn}(\tau, m)\,, \end{aligned} \tag{4.268}$$

[29] We assume for definiteness $J^2 > 2EI_2$; in this case, in the body frame, the apparent precession of $\mathbf{J}$ is around the x_3' axis; if instead $J^2 < 2EI_2$, it is around the x_1' axis.

where cn, sn and dn are elliptic functions,[30] and τ is a rescaled time variable,

$$\tau = bt \left[\frac{(I_3 - I_2)(I_3 - I_1)}{I_1 I_2}\right]^{1/2} . \tag{4.269}$$

[30] For the elliptic functions cn, sn and dn and for the Jacobi theta functions that will appear below, we follow the notation and conventions of Abramowitz and Stegun (1972).

The parameter m of the elliptic functions is given by

$$m = \frac{(I_2 - I_1) I_1 a^2}{(I_3 - I_2) I_3 b^2}\,, \tag{4.270}$$

and a, b are the initial values of ω_1' and ω_3',

$$a = \omega_1'(0)\,, \qquad b = \omega_3'(0)\,. \tag{4.271}$$

Observe that we have chosen the origin of time so that $\omega_2'(0) = 0$. In the limit $I_1 = I_2$ we have $m = 0$; since $\mathrm{cn}(\tau, 0) = \cos\tau$, $\mathrm{sn}(\tau, 0) = \sin\tau$, and $\mathrm{dn}(\tau, 0) = 1$, in this limit we recover the result (4.242). The elliptic functions are periodic functions of τ, with periodicity $4K(m)$, where $K(m)$ it the complete elliptic integral of the first kind. The components of the angular velocity in the body frame are therefore periodic in t, with period

$$T = \frac{4K(m)}{b} \left[\frac{I_1 I_2}{(I_3 - I_2)(I_3 - I_1)}\right]^{1/2} . \tag{4.272}$$

To compute I_{ij}, we need explicitly the time-dependence of the Euler angles. The solution for α and γ is

$$\cos\alpha(t) = \frac{I_3 b}{J}\,\mathrm{dn}(\tau, m)\,, \tag{4.273}$$

$$\tan\gamma(t) = \left[\frac{I_1(I_3 - I_2)}{I_2(I_3 - I_1)}\right]^{1/2} \frac{\mathrm{cn}(\tau, m)}{\mathrm{sn}(\tau, m)}\,, \tag{4.274}$$

so they are both periodic with period T. The solution for β is instead

$$\beta(t) = \frac{2\pi}{T'}\,t + \beta_1(t)\,, \tag{4.275}$$

where

$$\begin{aligned} \frac{2\pi}{T'} &= \frac{J}{I_1} - \frac{2i}{T}\frac{\vartheta_4'(i\pi c_1)}{\vartheta_4(i\pi c_1)} \\ &= \frac{J}{I_1} + \frac{2b}{K(m)} \left[\frac{(I_3 - I_2)(I_3 - I_1)}{I_1 I_2}\right]^{1/2} \sum_{n=1}^{\infty} \frac{q^n}{1 - q^{2n}} \sinh(2\pi n c_1)\,. \end{aligned} \tag{4.276}$$

Here ϑ_4 is a Jacobi theta function, c_1 is defined to be any[31] solution of the equation $\mathrm{sn}[2ic_1 K(m), m] = iI_3 b/(I_1 a)$, and

$$q = \exp\{-\pi K(1 - m)/K(m)\}\,. \tag{4.277}$$

[31] Since the elliptic functions and the theta functions have the same periodicity, all solutions for c_1 are equivalent.

The function $\beta_1(t)$ can be written as a ratio of theta functions,

$$\beta_1(t) = \frac{\vartheta_4(\frac{2\pi t}{T} - i\pi c_1)}{\vartheta_4(\frac{2\pi t}{T} + i\pi c_1)}\,, \tag{4.278}$$

and admits the series expansion

$$\beta_1(t) = \sum_{n=1}^{\infty} \left[\frac{-2q^n}{n(1 - q^{2n})}\right] \sin\left(\frac{4\pi n t}{T}\right) . \tag{4.279}$$

Observe that $\beta_1(t)$ is periodic with period $T/2$. In the problem there are therefore two distinct periodicities, T and T', and we can expect that the frequency spectrum of the gravitational radiation will have two sets of lines. The fact that γ is periodic with period T identifies $2\pi/T$ as the angular frequency associated to precession, so we define

$$\begin{aligned} \omega_{\mathrm{p}} &= \frac{2\pi}{T} \\ &= \frac{\pi b}{2K(m)} \left[\frac{(I_3 - I_2)(I_3 - I_1)}{I_1 I_2}\right]^{1/2} . \end{aligned} \tag{4.280}$$

The angular frequency associated to rotation around the x_3 axis is instead[32]

$$\omega_{\mathrm{rot}} = \frac{2\pi}{T'} - \frac{2\pi}{T}\,. \tag{4.281}$$

[32] One can also check this result observing that, in the limit of small wobble angle, it gives $\omega_{\mathrm{rot}} = \dot\beta - \omega_{\mathrm{p}}$. Since $\dot\gamma = -\omega_{\mathrm{p}}$, seeeq. (4.240), we get $\omega_{\mathrm{rot}} = \dot\beta + \dot\gamma$, in agreement with the discussion above eq. (4.266).

Given these complicated but explicit solutions for $\alpha(t)$, $\beta(t)$ and $\gamma(t)$, one could in principle plug them into the rotation matrix $\mathcal{R}_{ij}$ and grind, to obtain the moment of inertia in the fixed frame, and hence the waveform. However, the discrete nature of the spectrum becomes more evident if, rather than working with the exact expressions, we perform a series expansion for small wobble angle (which is equivalent to expanding in powers of m) and small deviations from axisymmetry.[33] The result, up to second order in m, is

$$\begin{aligned} h_+ &= A_{+,0}\cos(2\omega_{\mathrm{rot}} t) \\ &\quad + A_{+,1}\cos[(\omega_{\mathrm{rot}} + \omega_{\mathrm{p}})t] + A_{+,2}\cos[2(\omega_{\mathrm{rot}} + \omega_{\mathrm{p}})t]\,, \end{aligned} \tag{4.282}$$

$$\begin{aligned} h_\times &= A_{\times,0}\sin(2\omega_{\mathrm{rot}} t) \\ &\quad + A_{\times,1}\sin[(\omega_{\mathrm{rot}} + \omega_{\mathrm{p}})t] + A_{\times,2}\sin[2(\omega_{\mathrm{rot}} + \omega_{\mathrm{p}})t]\,, \end{aligned} \tag{4.283}$$

[33] This computation is performed in Zimmermann (1980) and Van Den Broeck (2005), see the Further Reading.

where

$$\begin{aligned} A_{+,0} &= h_0\,(1/2)(1+\cos^2\iota)\,, \\ A_{+,1} &= 2h_0' g(\alpha_0)\,\sin\iota\cos\iota\,, \\ A_{+,2} &= 2h_0' g^2(\alpha_0)\,(1+\cos^2\iota)\,, \\ A_{\times,0} &= h_0\,\cos\iota\,, \\ A_{\times,1} &= 2h_0' g(\alpha_0)\,\sin\iota\,, \\ A_{\times,2} &= 4h_0'\,g^2(\alpha_0)\cos\iota\,. \end{aligned} \tag{4.284}$$

The amplitudes h_0 and h_0' are defined as

$$h_0 = -\frac{1}{r}\,\frac{4G\omega_{\rm rot}^2}{c^4}\,(I_1 - I_2)\,, \tag{4.285}$$

$$h_0' = -\frac{1}{r}\,\frac{G(\omega_{\rm rot}+\omega_{\rm p})^2}{c^4}\left(I_3 - \frac{I_1+I_2}{2}\right)\,, \tag{4.286}$$

and

$$g(\alpha_0) \equiv \frac{I_1 a}{I_3 b}\,. \tag{4.287}$$

Using eqs. (4.234) and (4.236), and recalling that we have chosen the origin of time so that $\gamma(0) = \pi/2$, we see that $I_1 a/(I_3 b) = \tan\alpha_0$, where $\alpha_0 = \alpha(t=0)$. Therefore, in the limit of small wobble angle α_0, we have $g(\alpha_0) \simeq \alpha_0$.

From these expressions we see that, setting $\alpha_0 = 0$ (and therefore $g(\alpha_0) = 0$) we recover the correct limit of rotation around a principal axis, given in eqs. (4.219), (4.220) and (4.224).[34]

Instead, setting $I_1 = I_2$ (and recalling, from eq. (4.281) and Note 32, that $\Omega = \omega_{\rm rot} + \omega_{\rm p}$), we recover the correct limit of precession of an axisymmetric body when α is small, given in eqs. (4.246)–(4.252)

We see that, to zeroth-order in $g(\alpha_0)$, we find the line at $\omega_{\rm gw} = 2\omega_{\rm rot}$ due to rotation around a principal axis. To order $g(\alpha_0)$ emerges a line at $\omega_{\rm gw} = \omega_{\rm rot} + \omega_{\rm p}$, and to order $g^2(\alpha_0)$ we get a further line at $\omega_{\rm gw} = 2\omega_{\rm rot} + 2\omega_{\rm p}$. If we expand to higher order in $g(\alpha_0)$, we find two sets of lines at frequencies, respectively,

$$\omega_{\rm gw} = 2\omega_{\rm rot} + 2k\omega_{\rm p}\,, \tag{4.288}$$

and

$$\omega_{\rm gw} = \omega_{\rm rot} + (2k+1)\omega_{\rm p}\,, \tag{4.289}$$

with $k = 0, 1, 2, \ldots$, whose intensity is suppressed by increasing powers of $g(\alpha_0)$.

To conclude this section, we should stress that all results discussed above have been obtained for rigid bodies. For application to neutron stars, a more realistic modeling of the neutron star interior (e.g. a fluid body with an elastic crust) is necessary. We will come back to realistic neutron stars in Vol. 2.

[34] Observe that in Section 4.2.1 we choose the origin of time so that, at $t = 0$, the axis x_1' is aligned with the axis x_1, i.e. $\gamma(0) = 0$, while here we have chosen $\gamma(0) = \pi/2$. This is the origin of the overall minus sign between eq. (4.224) and eq. (4.285). As discussed in Note 27, we can reabsorb the minus sign in both h_0 and h_0' rotating by an angle $\pi/2$ in the transverse plane the axes $(\hat{\mathbf{u}}, \hat{\mathbf{v}})$ used to define the plus and cross polarizations.

4.3 Radial infall into a black hole

In this section we compute the GWs produced when an object falls radially into a black hole. We will start from the simple case of the infall of a point-like particle. In principle, in a full computation we should treat GWs as perturbations over the curved black hole space-time, rather than using the expansion over flat space-time of the linearized theory that we have discussed until now. As we will see, however, the low-frequency part of the spectrum can be computed within our formalism, and the frequency at which the approach breaks down can be estimated. This allows us to perform, in a rather simple setting, this instructive computation. Next we will consider what happens when a real star, rather than a point-like object, falls into a black hole. We will see that the star can be disrupted by the tidal force of the black hole, and as a result the radiation emitted by the various parts of the body adds up incoherently. Beside its intrinsic interest, this problem will then allow us to appreciate the difference between coherent and incoherent emission of gravitational radiation.

4.3.1 Radiation from an infalling point-like mass

We then begin by computing the radiation generated by a point-like particle of mass m which falls radially into a black hole of mass M, with $m \ll M$. We make a number of simplifying assumptions. First of all, we compute the GW production using the equations of linearized theory. In principle this is not correct, since in linearized theory we expand around the flat-space metric, while here we should rather expand around the Schwarzschild metric. Second, we use the Newtonian equation of motion, rather than the geodesics of general relativity in the Schwarzschild metric. Thus, if the particle comes from the positive direction of the z axis, starting with zero velocity at infinity, we write

$$\frac{1}{2}m\dot{z}^2 - \frac{GmM}{z} = 0 \tag{4.290}$$

and therefore

$$\dot{z} = -c\left(\frac{R_S}{z}\right)^{1/2}\,, \tag{4.291}$$

where $R_S = 2GM/c^2$ is the Schwarzschild radius of the black hole. Third, we assume that most of the radiation is emitted when the particle is non-relativistic, and therefore we use the quadrupole formula.

In the last part of the trajectory, close to the black hole horizon, all these assumptions break down. In particular, eq. (4.291) is certainly not valid close to the horizon, and it is also incompatible with the non-relativistic assumption, since it formally gives $\dot{z} = -c$ at $z = R_S$. However, at sufficiently large distances the flat-space Newtonian approximation is correct, and these approximations become legitimate. Thus, we first compute the radiation emitted from $z = +\infty$ until a value $z = R$.

As long as $R \gg R_S$ our approximations are justified. We will then discuss the extrapolation $R \to R_S$.

We first compute the total radiated power, using eq. (3.76) and observing that, in our problem, we have only one non-vanishing component of M_{ij}, $M_{33} = mz^2(t)$. Then

$$P_{\rm quad} = \frac{2}{15}\frac{G}{c^5}\langle \dddot{M}_{33}^2 \rangle = \frac{2}{15}\frac{Gm^2}{c^5}\langle (6\dot{z}\ddot{z} + 2z\dddot{z})^2 \rangle \,. \tag{4.292}$$

The total radiated energy, in the quadrupole approximation, is therefore

$$E = \frac{2}{15}\frac{Gm^2}{c^5}\int_{-\infty}^{t_{\rm max}} dt\,(6\dot{z}\ddot{z} + 2z\dddot{z})^2 \,, \tag{4.293}$$

where the integration over t make superfluous the time average[35] $\langle \ldots \rangle$, and $t_{\rm max}$ is defined by $z(t_{\rm max}) = R$. We write $dt = dz/\dot{z}$ and, using eq. (4.291), $\ddot{z} = -c^2 R_S/(2z^2)$ and $\dddot{z} = -(c^3/R_S^2)(R_S/z)^{7/2}$. Then, setting $u = z/R_S$, we get

$$E = \frac{2}{15}\frac{Gm^2}{R_S}\int_{R/R_S}^{\infty} du\, u^{-9/2} = \frac{4}{105}\frac{Gm^2}{R_S}\left(\frac{R_S}{R}\right)^{7/2} \,. \tag{4.294}$$

Of course, the radiation increases if R decreases. If we extrapolate the result down to $R = R_S = 2GM/c^2$ we get

$$E = \frac{2}{105}\,mc^2\left(\frac{m}{M}\right) \simeq 0.019\,mc^2\left(\frac{m}{M}\right) \,. \tag{4.295}$$

This extrapolation turns out to be remarkably close to the result obtained with the expansion over the Schwarzschild metric, using the general relativistic equations of motion and performing the full relativistic computation of GW production rather than using the quadrupole formula. The result of this calculation[36] is in fact

$$E \simeq 0.010\,mc^2\left(\frac{m}{M}\right) \,. \tag{4.296}$$

Observe that the energy radiated in GWs is smaller than the rest energy mc^2 of the particle, by a factor m/M.

The fact that the quadrupole approximation works quite well means that, despite the fact that in the last part of the trajectory the particle becomes relativistic, still the total power is dominated by the quadrupole and in general by the lowest multipoles. Since the radiation emitted at high multipoles is beamed into a narrow forward cone, while at low multipoles it is distributed on a large solid angle, the fact that the low multipoles dominate means that, in the radial infall into a black hole, there is no beaming of gravitational radiation. We will see a similar phenomenon when we study the gravitational radiation emitted by an accelerated particle, in Section 4.4. This is in sharp contrast with the electromagnetic case where instead, when the source reaches relativistic velocities, the high multipoles dominate, and the radiation is beamed.

[35] As we will see below, the frequency spectrum is peaked at $\omega = O(c/R_S)$, so the typical period of the GW is of the order of the light travel time across the Schwarzschild radius R_S. Therefore the integral over time from $-\infty$ to $t_{\rm max}$ is actually an integration over many periods of the typical gravitational radiation.

[36] See Davies, Ruffini, Press and Price (1971). We will discuss this computation in Vol. 2.

We can also use eq. (4.296) to give an estimate of the energy radiated in GWs in the head-on collision of two black holes of equal mass M. In this case, we substitute m with the reduced mass $M/2$ and we get $E \sim 2.5 \times 10^{-3} Mc^2$, which is quite close to the result $E \simeq (1-2)\times 10^{-3} Mc^2$ obtained from numerical simulations.

We now wish to compute the frequency spectrum of the radiation emitted. In principle, in order to compute the Fourier transform of a function of time $F(t)$, we need to know $F(t)$ on the whole interval $-\infty < t < \infty$. However, our Newtonian trajectory (4.291) is a good approximation to the exact general relativistic geodesic only up to a maximum value of time $t_{\rm max}$ such that $z(t_{\rm max}) \equiv R \gg R_S$; beyond $t_{\rm max}$ it becomes at first a poor approximation to the correct result and finally it even becomes completely meaningless physically, since it formally gives $|\dot{z}| > 1$ and $z < R_S$. Therefore, within our non-relativistic Newtonian approximation, we cannot compute the full form of the spectrum. However, we know that a system with typical size d and typical velocity v radiates GWs with a reduced wavelength $\lambda\!\!\!^{-} \sim d(c/v)$, see eq. (3.24). When the particle approaches the horizon, the size of the relevant length-scale of the particle–black hole system, for computing the time-varying part of the mass moment, is of order R_S, and $v \sim c$, and therefore $\lambda\!\!\!^{-} \sim R_S$. On the other hand, when the particle is at $R \gg R_S$, the length-scale which enters in the time-varying quadrupole moment is of order R, and $v \ll c$, so the system radiates at $\lambda\!\!\!^{-} \sim R(c/v) \gg R \gg R_S$.

This means that, with the Newtonian part of the trajectory, we can reliably compute the part of the spectrum with $\lambda\!\!\!^{-} \gg R_S$, or $\omega R_S \ll c$, since this radiation is generated when the particle is at large distance from the black hole. The complete spectrum will be peaked at $\omega R_S \sim c$, but the radiation at these frequencies is generated close to the horizon where a full general-relativistic computation is necessary. Finally, the spectrum will be necessarily cutoff exponentially for $\omega R_S \gg c$, since there is no length-scale smaller than R_S in the problem.

To compute the spectrum at $\omega R_S \ll c$ we can therefore use eq. (4.291). The solution of this equation of motion is

$$z^{3/2}(t) - z^{3/2}(t_0) = \frac{3}{2}R_S^{1/2}c(t_0 - t) \,. \tag{4.297}$$

Defining $\bar{t}$ from $(3/2)R_S^{1/2}c\bar{t} \equiv z^{3/2}(t_0) + (3/2)R_S^{1/2}ct_0$, eq. (4.297) becomes $z^{3/2}(t) = (3/2)R_S^{1/2}c(\bar{t} - t)$. At $t = -\infty$ we have $z(t) = +\infty$, while the minimum value $z(t) = R$ is reached at a finite time

$$t_{\rm max} = \bar{t} - \frac{2R^{3/2}}{3cR_S^{1/2}} \,. \tag{4.298}$$

We further introduce the variable $\tau = \bar{t} - t$, so

$$z(\tau) = \left(\frac{3}{2}R_S^{1/2}c\tau\right)^{2/3} \,, \tag{4.299}$$

and $c\tau$ ranges over the interval $2R^{3/2}/(3R_S^{1/2}) < c\tau < \infty$. Equation (4.292) gives

$$E = \frac{2G}{15c^5}\int_{-\infty}^{t_{\max}} dt\, \dddot{M}_{33}^2 \,. \tag{4.300}$$

Writing $M_{33}(t)$ in Fourier transform one obtains

$$E = \frac{2G}{15c^5}\, 2\int_0^{\omega_{\max}} \frac{d\omega}{2\pi}\, \omega^6 |\tilde{M}_{33}(\omega)|^2 \,, \tag{4.301}$$

where, as discussed above, $\omega_{\max} \ll c/R_S$ is the frequency for which our ignorance of the trajectory beyond $t_{\max}$ becomes important.[37] However, here we must be careful because

$$\tilde{M}_{33}(\omega) = m\int_{-\infty}^{t_{\max}} dt\, z^2(t) e^{i\omega t} \tag{4.302}$$

diverges, since as $t \to -\infty$ we have $z(t) \to +\infty$. Fortunately, this divergence is harmless: it simply reflects the fact that the size of the particle-black hole system, and therefore its quadrupole moment, goes to infinity. However this divergent part of the quadrupole moment is static since, from eq. (4.291), as $z \to \infty$ we have $\dot{z} \to 0$, and therefore it does not contribute to GW production. To dispose of this divergence, the simplest way is to consider the Fourier transform of $\ddot{M}_{33}(t)$ rather than of $M_{33}(t)$, since in $\ddot{M}_{33}(t)$ the static term has been eliminated. Therefore, instead of eq. (4.301), we write

$$E = \frac{4G}{15c^5}\int_0^{\omega_{\max}} \frac{d\omega}{2\pi}\, \omega^2 |\tilde{\ddot{M}}_{33}(\omega)|^2 \,. \tag{4.303}$$

Using eq. (4.299) we find

$$\begin{aligned} \ddot{M}_{33}(t) &= 2m(z\ddot{z} + \dot{z}^2) \\ &= m\left(\frac{2R_S c^2}{3\tau}\right)^{2/3} , \end{aligned} \tag{4.304}$$

and, recalling that $-\infty < t < t_{\max}$ corresponds to $\tau_{\min} < \tau < \infty$ with $\tau_{\min} \equiv 2R^{3/2}/(3cR_S^{1/2})$,

$$\tilde{\ddot{M}}_{33}(\omega) = m\left(\frac{2R_S c^2}{3}\right)^{2/3}\int_{\tau_{\min}}^{\infty} d\tau\, \tau^{-2/3} e^{-i\omega\tau} \,. \tag{4.305}$$

Defining $u = \omega\tau$,

$$\tilde{\ddot{M}}_{33}(\omega) = m\omega^{-1/3}\left(\frac{2R_S c^2}{3}\right)^{2/3}\int_{\omega\tau_{\min}}^{\infty} du\, u^{-2/3} e^{-iu} \,. \tag{4.306}$$

The computation is valid down to R of order a few times R_S, so $\tau_{\min} = O(R_S/c)$ and, in the limit $\omega R_S \ll c$, which is the limit in which our computation is justified, the leading term is obtained approximating the

[37] The contribution from negative frequencies gives the factor of 2 in front of the integral.

lower limit of the above integral with zero. Then we get an Euler Gamma function

$$\int_0^{\infty} du\, u^{-2/3} e^{-iu} = e^{-i\pi/6}\,\Gamma(1/3) \,, \tag{4.307}$$

as one can see rotating the contour to the negative imaginary semiaxis of the complex u-plane, and eq. (4.303) gives

$$\begin{aligned} \frac{dE}{d\omega} &= \frac{2G}{15\pi c^5}\omega^2 |\tilde{\ddot{M}}_{33}(\omega)|^2 \\ &= \left(\frac{2}{3}\right)^{7/3}\frac{\Gamma^2(1/3)}{5\pi}\,\frac{Gm^2}{c}\left(\frac{\omega R_S}{c}\right)^{4/3} \\ &\simeq 0.177\,\frac{Gm^2}{c}\left(\frac{\omega R_S}{c}\right)^{4/3} , \qquad (\omega R_S \ll c) \,. \end{aligned} \tag{4.308}$$

To study the spectrum when $\omega R_S/c$ is not small we need the full general-relativistic computation, but we expect from the physical arguments presented above that it must reach a maximum at $\omega R_S/c = O(1)$, and will be cutoff exponentially when $\omega R_S/c \gg 1$. Indeed, the numerical results of Davies, Ruffini, Press and Price (1971) show that the spectrum reaches a maximum at $\omega R_S/c \simeq 0.64$ and then is cutoff exponentially, with an empirical law $dE/d\omega \sim \exp\{-\kappa\,\omega R_S/c\}$ with $\kappa \simeq 5$.

4.3.2 Tidal disruption of a real star falling into a black hole. Coherent and incoherent radiation

We have seen in the previous subsection that, within the non-relativistic Newtonian approximation, we can correctly reproduce the order of magnitude of the power radiated in the radial infall of a point-like particle into a BH, and we can compute the spectrum for $\omega R_S \ll 1$. The inclusion of the full non-linearities of general relativity amounts only to a correction of about a factor of two in the total power, compare eqs. (4.295) and (4.296).

A point-like particle is however an idealization, and in astrophysical applications we are rather interested in the infall of an extended object like a main sequence star, a white dwarf or a neutron star. We will see in this subsection that in this case, because of the tidal disruption of the star as it falls into the BH, the radiation can be emitted incoherently, and this can reduce the production of GWs by many orders of magnitudes.

To understand qualitatively the difference between coherent and incoherent radiation, observe that in eq. (4.295) we found a radiated energy $E \sim m^2/M$, where M is the BH mass and m is the mass of the infalling particle (or, more precisely, the reduced mass of the particle–BH system, but we are assuming $m \ll M$). If we describe an extended object of mass m as a collection of N particles of mass δm and $m = N\delta m$, we therefore find that, if the N constituents radiate coherently as a single object of mass m, the radiated energy is

$$E^{(\text{coherent})} \sim \frac{m^2}{M} = N^2\frac{(\delta m)^2}{M} \,. \tag{4.309}$$

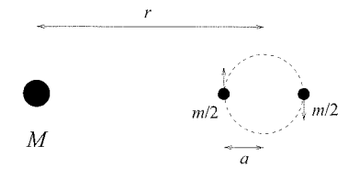

Fig. 4.18 The estimate of the tidal radius discussed in the text.

This N^2 dependence can also be understood observing that the total amplitude of the GW is the sum of the separate amplitudes, so $h_{\rm tot} = \sum_{i=1}^{N} h_i$, where i labels the elementary constituents. For coherent radiation the various terms in this sum have the same phase, so $h^{\rm tot} = O(N)$ and the radiated energy $E \sim \dot{h}^2_{\rm tot}$ is $O(N^2)$. For incoherent radiation, the mixed terms in $(\sum_i \dot{h}_i)^2$ interfere destructively and we are only left with the diagonal terms $\sum_i \dot{h}_i^2$. Therefore in this case the energy is N times the energy radiated by a single constituent,

$$E^{\rm (incoherent)} \sim N \frac{(\delta m)^2}{M} = \frac{1}{N}\,\frac{m^2}{M}\,, \tag{4.310}$$

and the incoherent radiation is smaller by a factor N with respect to coherent radiation. Observe that, in the limit $N \to \infty$ with m fixed, the incoherent radiation even goes to zero.

Whether a distribution of sources radiates coherently or incoherently depends on the wavelength of the GW that we consider and on the linear size a of the system. If $a \ll \lambda\!\!\!^{-}$, the phase of the GW does not change appreciably over the whole source and the radiation is coherent, while if $a \gg \lambda\!\!\!^{-}$ the phases from the single constituents oscillate strongly over the system and the mixed terms in $(\sum_i \dot{h}_i)^2$ average to zero, so the radiation is incoherent. The transition between these two regimes is governed by a form factor which, for the problem of the infall of a star into a black hole (BH), will be computed below.

To perform this computation, we need first of all to understand how the shape of an infalling star is distorted by the tidal gravitational field of the black hole. A star is an object held together by self-gravity. A first crude estimate of the tidal radius $r_{\rm tidal}$, i.e. of the star–BH distance where the tidal force exerted by the BH is strong enough to disrupt the star, can be obtained as follows. We model a star of mass m as two particle of mass $m/2$, orbiting each other in a circular orbit of radius a, and we consider a BH of mass M at a distance r from the center of the star, see Fig. 4.18. Then the tidal force which tends to disrupt the star is

$$\begin{aligned} F_{\rm tidal} &= \frac{GM(m/2)}{(r-a)^2} - \frac{GM(m/2)}{(r+a)^2} \\ &\simeq 2GMm\frac{a}{r^3}\,. \end{aligned} \tag{4.311}$$

The system is broken apart if this force is larger than the gravitational attraction between the two bodies of mass $m/2$, so if

$$2GMm\frac{a}{r^3} > \frac{G(m/2)^2}{(2a)^2}\,, \tag{4.312}$$

which gives $r < r_{\rm tidal} \simeq 3.2(M/m)^{1/3}a$. The numerical coefficient depends of course on our crude schematization of the extended object. If we rather model the star as an incompressible spheroid of mass m, mean radius a and constant density, the tidal radius becomes (see Chandrasekhar 1969, Section 56)

$$r_{\rm tidal} \simeq 2.2\,(M/m)^{1/3}a\,. \tag{4.313}$$

We denote by a the radius of the star when it is far from the BH, and by a_h the value of its radial size by the time that the star is close to the BH horizon. We can estimate the order of magnitude of a_h, using the Newtonian trajectory (4.297) for a particle falling radially along the z axis,

$$z(t) = \left[z_0^{3/2} + \frac{3}{2}R_S^{1/2}c(t_0 - t)\right]^{2/3}\,. \tag{4.314}$$

Taking the variation with respect to z_0 we see from this equation that two points that at time t_0 are separated by a radial distance δz_0, at time t are separated by $\delta z(t) = [z_0/z(t)]^{1/2}\delta z_0$. We take as t_0 the time when the star crosses the tidal radius, and is therefore still undeformed. Then near the horizon the star is an ellipsoid with semimajor axis a_h given by

$$a_h = \left(\frac{r_{\rm tidal}}{R_S}\right)^{1/2} a\,. \tag{4.315}$$

The evolution of the shape of the star as it plunges toward the BH is shown in Fig. 4.19. The effect of the tidal distortion can be quite dramatic. For instance, a main sequence star of $1M_\odot$ has a radius $a \simeq 7 \times 10^5$ km. If it falls into a BH with a mass $10M_\odot$ and therefore $R_S \simeq 30$ km, eq. (4.313) gives $r_{\rm tidal} \simeq 4.7a$ and $(r_{\rm tidal}/R_S)^{1/2} \sim 300$.

We know from the previous subsection that most of the radiation is emitted when the star is close to the horizon and therefore when it has a size a_h in the radial direction. From the discussion at the beginning of this subsection we know that a source whose larger dimension is of order a_h will radiate coherently only the wavelengths which satisfy $\lambda\!\!\!^{-} \gg a_h$, or $\omega \ll c/a_h$. Therefore the parameter which governs the loss of coherence is

$$A(\omega) \equiv \frac{\omega a_h}{c} = \frac{\omega a}{c}\left(\frac{r_{\rm tidal}}{R_S}\right)^{1/2}\,. \tag{4.316}$$

For frequencies such that $A(\omega) \gg 1$ we have incoherent radiation while for frequencies that satisfy $A(\omega) \ll 1$ the radiation is coherent. In the formal limit $a \to 0$ we have $A(\omega) \to 0$ and we get back the point-like result.

As we mentioned in the previous subsection, the point-like spectrum is peaked at $\omega = \bar{\omega} \simeq 0.64c/R_S$. Therefore, when $0.64/R_S \ll 1/a_h$, only the high-frequency tails of the point-like spectrum are suppressed because of incoherent emission. These high frequency tails contributed anyway negligibly to the total power even in the point-like case, since we saw that they were already exponentially suppressed. Therefore, when $0.64/R_S \ll 1/a_h$ the total power is practically the same as in the point-like case. On the contrary, if $0.64/R_S \gg 1/a_h$, incoherent emission suppresses the radiation in the region which includes the peak, and where most of the power is concentrated, and the total radiated power becomes a negligible fraction of the point-like case. Defining $\bar{A} =$

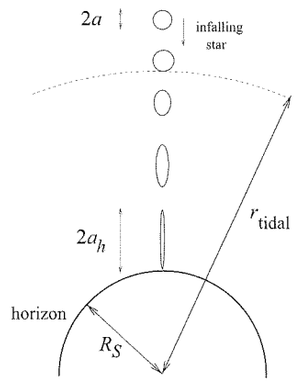

Fig. 4.19 An infalling star of radius a is tidally deformed by the black hole when it enters within the tidal radius $r_{\rm tidal}$. By the time the horizon is approached, the the star is an ellipsoid with semimajor axis a_h.

Table 4.1 Suppression of gravitational radiation for stars falling radially into a black hole, for different values of the mass M of the black hole. In all cases the mass of the star is taken to be $m = 1\,M_\odot$. Adapted from Table 1 of Haugan, Shapiro and Wasserman (1982).

Stellar type	a(km)	$M/M_\odot$	$(r_{\rm tidal}/R_S)^{1/2}$	$\bar{A}$
Main sequence	7×10^5	10	300	3×10^5
		10^3	70	500
		10^6	7	1
White dwarf	10^4	10	40	430
		10^3	8	7
		10^6	1	0.01
Neutron star	10	10	1.3	0.4
		10^3	1	7×10^{-3}
		10^6	1	10^{-5}

$\bar{\omega}a_h/c = 0.64\,a_h/R_S$ and using eqs. (4.315) and (4.313), we find

$$\bar{A} \simeq \frac{a}{R_S}\left(\frac{M}{m}\right)^{1/9}\,, \tag{4.317}$$

and, if $\bar{A} \gtrsim 1$, we have a strong suppression of the total radiated power. In Table 4.1 we show the dilatation factor $(r_{\rm tidal}/R_S)^{1/2}$ and the parameter $\bar{A}$ for a range of different stars. Observe, from eq. (4.317), that for a given mass m the suppression is more important for stars with large radius a, since they are less compact and have less self-gravity to resist the tidal force of the black hole, and also it is more important for lower BH masses, because the smaller gravitational attraction at a fixed distance is overcompensated by the decrease in Schwarzschild radius, so tidal stripping takes place at shorter radial distances, where the gravitational field is stronger.

From eq. (4.317) and Table 4.1 we see for instance that a $1M_\odot$ main sequence star produces significant GWs only if it falls into a supermassive BH with mass $M > O(10^6)M_\odot$. For a white dwarf we need $M > O(10^4)M_\odot$, while for a neutron star our equation suggest that it is needed $M > O(3)M_\odot$. Actually, a neutron star is so compact and has such a large rigidity that we certainly cannot treat it as a dust ball. We will examine in more detail black hole–neutron star coalescences in Vol. 2.

Having understood the physics with relatively simple arguments, we can now be more quantitative and compute the form factor. We found below eq. (4.297) that the solution of the Newtonian equation of motion, for a particle falling along the z axis which at $t = t_0$ has $z(t) = z_i$, can be written as

$$z^{3/2}(t;\bar{t}_i) = \frac{3}{2}R_S^{1/2}c(\bar{t}_i - t)\,, \tag{4.318}$$

with $\bar{t}_i$ defined by

$$\bar{t}_i = t_0 + \frac{2z_i^{3/2}}{3cR_S^{1/2}}\,. \tag{4.319}$$

Therefore, for a swarm of N particles of equal mass δm, eq. (4.302) gives

$$\tilde{M}_{33}(\omega) = \delta m \sum_{i=1}^{N}\int_{-\infty}^{t_{\rm max}} dt\, z^2(t;\bar{t}_i)e^{i\omega t}\,. \tag{4.320}$$

Since $z(t;\bar{t}_i)$ depends only on the combination $\bar{t}_i - t$, inside each integral we can shift the integration variable $t \to t + \bar{t}_i$. For large $t_{\rm max}$ this does not change appreciably the upper integration limit, and we get

$$\begin{aligned}\tilde{M}_{33}(\omega) &= \delta m \sum_{i=1}^{N}\int_{-\infty}^{t_{\rm max}} dt\, z^2(t;0)e^{i\omega(t+\bar{t}_i)} \\ &= \left[(\delta m)N\int_{-\infty}^{t_{\rm max}} dt\, z^2(t;0)e^{i\omega t}\right]\left[\frac{1}{N}\sum_{i=1}^{N}e^{i\omega\bar{t}_i}\right]\,.\end{aligned} \tag{4.321}$$

Since $(\delta m)N$ is the total mass of the system, the first bracket gives the value of $\tilde{M}_{33}(\omega)$ in the point-like approximation.[38] The second bracket is the form factor, and we denote it by $F(\omega)$,

$$F(\omega) = \frac{1}{N}\sum_{i=1}^{N}e^{i\omega\bar{t}_i}\,. \tag{4.322}$$

In eq. (4.319) we choose t_0 as the time when the center-of-mass of the star crosses the tidal radius, so it is still an undeformed sphere. At $t = t_0$ the i-th constituent is located at $z_i = r_{\rm tidal} + \delta z_i$, with $-a < \delta z_i < a$ and $|\delta z_i| \ll r_{\rm tidal}$. Then eq. (4.319) becomes

$$\begin{aligned}\bar{t}_i &= t_0 + \frac{2(r_{\rm tidal}+\delta z_i)^{3/2}}{3cR_S^{1/2}} \\ &\simeq \left[t_0 + \frac{2r_{\rm tidal}^{3/2}}{3cR_S^{1/2}}\right] + \left(\frac{r_{\rm tidal}}{R_S}\right)^{1/2}\frac{\delta z_i}{c}\,.\end{aligned} \tag{4.323}$$

The term in bracket does not depend on the index i and gives just a constant phase in eq. (4.322), which cancels when we take the modulus squared. Then

$$F(\omega) = \frac{1}{N}\sum_{i=1}^{N}\exp\{i\omega(r_{\rm tidal}/R_S)^{1/2}\delta z_i/c\}\,. \tag{4.324}$$

Passing to the continuum limit we get, for a system of uniform density,

$$F(\omega) = \frac{1}{V}\int_V d(\delta z)d^2x_\perp\,\exp\{i\omega(r_{\rm tidal}/R_S)^{1/2}\delta z/c\}\,, \tag{4.325}$$

where the integration is over the volume V of the system at time t_0, when it is an undeformed sphere or radius a and $V = (4/3)\pi a^3$. At

[38] As we discussed in the previous subsection, the integral in $\tilde{M}_{33}(\omega)$ is actually divergent. For the purpose of computing the form factor this is irrelevant; we can repeat the argument with $\ddot{\tilde{M}}_{33}(\omega)$, which converges, or we can just regularize the integral in $\tilde{M}_{33}(\omega)$, since anyway the form factor factorizes.

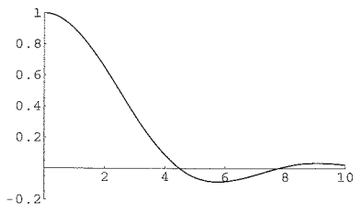

Fig. 4.20 The form factor $F(A(\omega))$, plotted as a function of $A = (\omega a/c)(r_{\rm tidal}/R_S)^{1/2}$.

fixed δz the radius of the circle in the transverse direction is given by $|x_\perp|^2 = a^2 - (\delta z)^2 = a^2(1-u^2)$, where we have written $\delta z = au$, with $-1 < u < 1$. Then the integration over the transverse plane of the sphere at fixed u gives $\pi a^2(1-u^2)$, and

$$F(\omega) = \frac{1}{(4/3)\pi a^3}\,\pi a^3 \int_{-1}^{1} du\,(1-u^2)\exp\{i(\omega a/c)\,(r_{\rm tidal}/R_S)^{1/2}u\}\,. \tag{4.326}$$

We see that the combination $A(\omega) = (\omega a/c)\,(r_{\rm tidal}/R_S)^{1/2}$ appears in the exponential and governs the form factor, as we expected from the physical arguments presented above. Then

$$\begin{aligned} F(\omega) &= \frac{3}{4}\int_{-1}^{1} du\,(1-u^2)e^{iA(\omega)u} \\ &= \frac{3}{A^2(\omega)}\left[\frac{\sin A(\omega)}{A(\omega)} - \cos A(\omega)\right]\,. \end{aligned} \tag{4.327}$$

The form factor f is shown in Fig. 4.20 as a function of A. Since $dE/d\omega$ is proportional to $|\tilde{M}_{33}(\omega)|^2$, the spectrum for a real star is related to the point-like spectrum by

$$\left(\frac{dE}{d\omega}\right)^{\rm real\ star} = |F(\omega)|^2\,\left(\frac{dE}{d\omega}\right)^{\rm point-like}\,. \tag{4.328}$$

4.4 Radiation from accelerated masses

In electrodynamics, a prototype example is the radiation emitted by an accelerated charge. In this section we examine the corresponding gravitational radiation emitted by an accelerated mass. Beside possible applications to astrophysical situations, this exercise is quite instructive by itself, and in particular it will allow us to understand that, while electromagnetic radiation from accelerated particles is beamed in a narrow cone in the forward direction, this is not the case for the GWs produced by an accelerated mass.

4.4.1 GWs produced in elastic collisions

We begin by considering the gravitational radiation produced during the elastic deflection of an object by a fixed scattering center (or, equivalently, a two-body collision in the center-of-mass frame). We denote the initial and final four-momenta of the object by p^μ and p'^μ, respectively.

The energy–momentum tensor of a particle of mass m is given in eq. (3.121). In principle, given the interaction between the object and the scattering center, and the initial conditions, we should compute the classical trajectory $x_0^\mu(t)$, plug it in eq. (3.121), and then perform the Fourier transform. However, in general this is neither practically feasible nor really necessary. We can instead approximate the collision as

instantaneous, and we consider an elastic scattering, so $p'^0 = p^0$. Then we write, using eq. (3.120),

$$T^{\mu\nu}(\mathbf{x},t) = \frac{p^\mu p^\nu}{\gamma m}\,\delta^{(3)}(\mathbf{x}-\mathbf{v}t)\,\theta(-t) + \frac{p'^\mu p'^\nu}{\gamma m}\,\delta^{(3)}(\mathbf{x}-\mathbf{v}'t)\,\theta(t)\,, \tag{4.329}$$

where $\theta(t)$ is the step function: $\theta(t) = 1$ if $t > 0$ and $\theta(t) = 0$ if $t < 0$. In a collision that lasts for a time Δt are generated frequencies up to $\omega_{\rm max} \sim 2\pi/\Delta t$ and therefore, when we approximate the collision as instantaneous, we are introducing spurious contributions at arbitrarily high frequencies. To recover the correct physical result it is sufficient to estimate the time Δt actually taken by the collision. In a collision with impact parameter b and relative velocity v, we have $\Delta t \sim b/v$, and we must cutoff the spectrum at $\omega_{\rm max} \sim 2\pi v/b$. At $\omega \ll \omega_{\rm max}$ the spectrum is well reproduced by the instantaneous approximation.

The four-dimensional Fourier transform of (4.329) is

$$\begin{aligned} \tilde{T}^{\mu\nu}(\mathbf{k},\omega) &= \int_{-\infty}^{\infty} c\,dt \int d^3x\,T^{\mu\nu}(\mathbf{x},t)\,e^{i\omega t - i\mathbf{k}\cdot\mathbf{x}} \\ &= \frac{p^\mu p^\nu}{\gamma m}\int_{-\infty}^{0} c\,dt\,e^{i\omega t - i\mathbf{k}\cdot\mathbf{v}t} + \frac{p'^\mu p'^\nu}{\gamma m}\int_{0}^{\infty} c\,dt\,e^{i\omega t - i\mathbf{k}\cdot\mathbf{v}'t}\,. \end{aligned} \tag{4.330}$$

In the first integral we add a factor ϵt at the exponent, with $\epsilon \to 0^+$, to assure the convergence at $t = -\infty$, while in the second we add $-\epsilon t$, to assure the convergence at $t = +\infty$. Then

$$\tilde{T}^{\mu\nu}(\mathbf{k},\omega) = \frac{c}{i\gamma m}\left[\frac{p^\mu p^\nu}{\omega - \mathbf{k}\cdot\mathbf{v} - i\epsilon} - \frac{p'^\mu p'^\nu}{\omega - \mathbf{k}\cdot\mathbf{v}' + i\epsilon}\right]\,. \tag{4.331}$$

If the particle which is being deflected is not massless, the denominators are never zero and we can set $\epsilon = 0$. We compute first in the non-relativistic limit and then in the general case.

Non-relativistic limit

In this case in the denominators we approximate $\gamma \simeq 1$ and we neglect the terms $\mathbf{k}\cdot\mathbf{v}$ and $\mathbf{k}\cdot\mathbf{v}'$, so we find simply

$$\tilde{T}_{ij}(\omega) \simeq -\frac{ic}{m\omega}(p_i p_j - p'_i p'_j)\,. \tag{4.332}$$

We use a reference frame where the scattering plane is the (x,y) plane; the initial velocity is $\mathbf{v} = v(1,0,0)$ and the final velocity is

$$\mathbf{v}' = v\,(\cos\vartheta_s, \sin\vartheta_s, 0)\,, \tag{4.333}$$

where ϑ_s is the scattering angle and $|\mathbf{v}'| = |\mathbf{v}| = v$ since we are considering elastic scattering. Let (θ,ϕ) be the polar angles which identify the direction of the unit vector $\hat{\mathbf{n}}$ in this frame (i.e. the angles that describe the angular distribution of the gravitational radiation), so

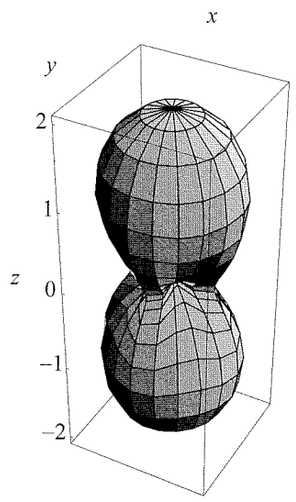

Fig. 4.21 The angular distribution of the gravitational radiation in the non-relativistic limit. The scattering plane is $z = 0$ and we have taken $\vartheta_s = \pi/2$.

$\hat{\mathbf{n}} = (\sin\theta\cos\phi, \sin\theta\sin\phi, \cos\theta)$. Then, performing explicitly the contraction $\Lambda_{ij,kl}\tilde{T}_{ij}(\omega)\tilde{T}^*_{kl}(\omega)$ in eq. (3.16), we find

$$\frac{dE}{d\omega d\Omega} = \frac{Gm^2v^4}{\pi^2c^5}\sin^2\vartheta_s\left[\cos^2\theta + \frac{1}{4}\sin^2(\vartheta_s - 2\phi)\sin^4\theta\right]. \quad (4.334)$$

The emission pattern is shown in Fig. 4.21, for the case $\vartheta_s = \pi/2$. Observe that the radiation is emitted mostly along the z axis, i.e. in the direction perpendicular to the scattering plane. Integrating over the solid angle $d\Omega = d\cos\theta d\phi$ we get

$$\frac{dE}{d\omega} = \frac{8G}{5\pi c^5}m^2v^4\sin^2\vartheta_s\,. \quad (4.335)$$

For the corresponding two-body problem, m is the reduced mass, v the relative velocity and ϑ_s is the scattering angle in the center-of-mass.

Actually, if one is interested only in the radiated energy, integrated over the solid angle, and not in its angular distribution, it can be computed more quickly observing that in the non-relativistic approximation $\tilde{T}_{ij}$ is independent of the angle (all the angular dependence was in the terms $\mathbf{k}\cdot\mathbf{v}$ and $\mathbf{k}\cdot\mathbf{v}'$ that we dropped), and therefore

$$\int d\Omega\,\Lambda_{ij,kl}\tilde{T}_{ij}\tilde{T}^*_{kl} = \tilde{T}_{ij}\tilde{T}^*_{kl}\int d\Omega\,\Lambda_{ij,kl}\,. \quad (4.336)$$

The integral is performed using eq. (3.74), and we get back eq. (4.335).

The frequency spectrum found in eq. (4.335) is flat up to the cut-off frequency $\omega_{\max} \sim 2\pi v/b$, and the total radiated energy is obtained integrating up to $\omega_{\max}$, so

$$\begin{aligned} E_{\rm rad} &\sim \frac{16Gm^2}{5b}\left(\frac{v}{c}\right)^5\sin^2\vartheta_s \\ &= \frac{8}{5}mc^2\left(\frac{R_S}{b}\right)\left(\frac{v}{c}\right)^5\sin^2\vartheta_s\,, \end{aligned} \quad (4.337)$$

where $R_S = 2Gm/c^2$ is the Schwarzschild radius of an object of mass m. Therefore the total energy radiated is suppressed, with respect to the rest-mass energy mc^2 of the particle, both by the by-now familiar factor $(v/c)^5$ (compare, e.g. with eqs. (3.319) or (3.340)) and by the ratio R_S/b.

Relativistic limit

In the general relativistic case we repeat the same steps using the full expression for $\tilde{T}^{\mu\nu}(\mathbf{k},\omega)$ given in eq. (4.331), with $p^i = \gamma m v^i$, and setting $\mathbf{k} = \omega\hat{\mathbf{n}}/c$ (see eq. (3.16)). We then find

$$\begin{aligned} \frac{dE}{d\omega d\Omega} &= \frac{Gm^2\gamma^2v^4}{\pi^2} \\ &\times\left[f_1(v,\vartheta_s;\theta,\phi) - f_2(v,\vartheta_s;\theta,\phi)\sin^2\theta + f_3(v,\vartheta_s;\theta,\phi)\sin^4\theta\right], \end{aligned} \quad (4.338)$$

where

$$\begin{aligned} f_1(v,\vartheta_s;\theta,\phi) &= ab\,\sin^2\vartheta_s + \frac{1}{4}(a-b)^2\,, \\ f_2(v,\vartheta_s;\theta,\phi) &= \frac{a(a+b)}{2}\cos^2\phi + \frac{b(a+b)}{2}\cos^2(\phi-\vartheta_s) \\ &\quad -2ab\cos\vartheta_s\cos\phi\cos(\phi-\vartheta_s)\,, \\ f_3(v,\vartheta_s;\theta,\phi) &= \frac{1}{4}\left[a\cos^2\phi - b\cos^2(\phi-\vartheta_s)\right]^2, \end{aligned} \quad (4.339)$$

and

$$\begin{aligned} a \equiv a(v;\theta,\phi) &= \frac{1}{1-\hat{\mathbf{n}}\cdot\mathbf{v}/c} \\ &= \frac{1}{1-(v/c)\sin\theta\cos\phi}\,, \end{aligned} \quad (4.340)$$

$$\begin{aligned} b \equiv b(v,\vartheta_s;\theta,\phi) &= \frac{1}{1-\hat{\mathbf{n}}\cdot\mathbf{v}'/c} \\ &= \frac{1}{1-(v/c)\sin\theta\cos(\phi-\vartheta_s)}\,. \end{aligned} \quad (4.341)$$

In the non-relativistic limit we have $a \to 1, b \to 1$ and, making use of the identities

$$\cos^2\phi + \cos^2(\phi-\vartheta_s) - 2\cos\vartheta_s\cos\phi\cos(\phi-\vartheta_s) = \sin^2\vartheta_s\,, \quad (4.342)$$

$$\cos^2\phi - \cos^2(\phi-\vartheta_s) = \sin(\vartheta_s-2\phi)\sin\vartheta_s\,, \quad (4.343)$$

we recover eq. (4.334). Instead, in the ultra-relativistic limit, the factors a and b bend the radiation in the direction of the motion (more precisely, in a direction determined by a combination of the initial and final velocity). The resulting pattern function is shown in Fig. 4.22 for the case $v = 0.8$. The distribution is tilted in the direction of motion but the radiation is not focused in a very narrow cone, contrary to what happens in electrodynamics. We examine this point in detail in the simpler geometrical setting of the next subsection.

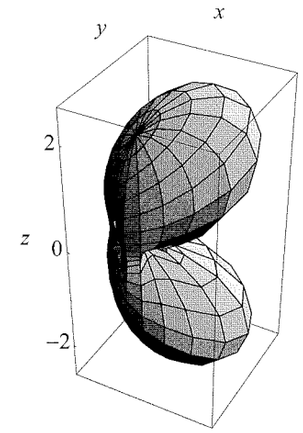

Fig. 4.22 The angular distribution of the gravitational radiation in the relativistic limit. The scattering plane is $z = 0$ and we have taken $\vartheta_s = \pi/2$ and $v = 0.8$.

4.4.2 Lack of beaming of GWs from accelerated masses

In order to examine this effect eliminating irrelevant complications, let us consider an inelastic scattering in which a particle of mass m initially at rest, is accelerated in time Δt to a velocity v.[39]

As in the previous problem, we assume that the acceleration is instantaneous and we then cut off the spectrum at $\omega_{\max} \sim 2\pi/\Delta t$. The energy–momentum tensor is again given by eq. (4.331), where now the first term vanishes (since the initial velocity is zero) and in the second term $\mathbf{v}'$ is the final velocity, which we now denote by $\mathbf{v}$. Therefore

$$\begin{aligned} \tilde{T}^{ij}(\omega\hat{\mathbf{n}}/c,\omega) &= \frac{ic\gamma m}{\omega}\frac{v^iv^j}{1-\hat{\mathbf{n}}\cdot\mathbf{v}/c} \\ &= \frac{ic\gamma m}{\omega}\frac{v^iv^j}{1-(v/c)\cos\theta}\,. \end{aligned} \quad (4.344)$$

[39] In principle our formalism is valid only if we have a closed system, so the total $T^{\mu\nu}$ is conserved. However, we can imagine for instance that the particle of mass m is electrically charged, and is accelerated by the electric field inside a capacitor. To this closed system we can apply our formalism. If the arms of the capacitor are infinitely heavy, they do not contribute to the gravitational radiation because a heavy object of mass M, in the scattering process, acquires a recoil velocity $V \sim 1/M$ and its contribution to $dE/d\omega$, according to eq. (4.335), is $dE/d\omega \sim M^2V^4 = O(1/M^2)$. Thus, in practice we can just consider the particle of mass m on the accelerated trajectory.

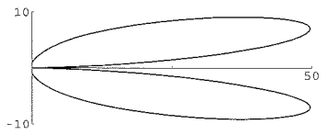

Fig. 4.23 The function $p_{\rm em}(\theta)$, in polar coordinates, for a charged particle with acceleration parallel to the velocity, and $v = 0.99$.

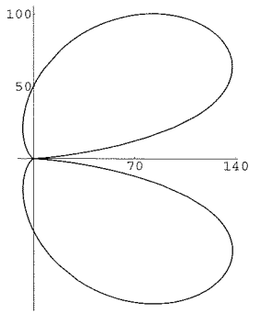

Fig. 4.24 The function $p_{\rm gw}(\theta)$ for a particle with acceleration parallel to the velocity, and $v = 0.99$. Observe the difference in shape compared to Fig. 4.23.

From eq. (3.16) we find

$$\frac{dE}{d\Omega d\omega} = \frac{Gm^2\gamma^2}{2\pi^2 c^5}\Lambda_{ij,kl}\frac{v^i v^j v^k v^l}{[1-(v/c)\,\cos\theta]^2}\,. \tag{4.345}$$

Using eq. (1.39) and performing the contractions, we get

$$\frac{dE}{d\Omega d\omega} = \frac{Gm^2\gamma^2}{4\pi^2 c}\left(\frac{v}{c}\right)^4\frac{\sin^4\theta}{[1-(v/c)\cos\theta]^2}\,, \tag{4.346}$$

or

$$\boxed{\frac{dE}{d\Omega d\omega} = \frac{Gm^2}{4\pi^2 c}\left(\frac{v}{c}\right)^4 p_{\rm gw}(\theta)\,,} \tag{4.347}$$

where

$$\boxed{p_{\rm gw}(\theta) = \gamma^2\frac{\sin^4\theta}{[1-(v/c)\,\cos\theta]^2}} \tag{4.348}$$

describes the angular pattern. It is interesting to compare this result with the electromagnetic radiation produced by a charged particle suddenly accelerated from rest to velocity v. This is given by (see Jackson 1975, eq. (15.65))

$$\left.\frac{dE}{d\Omega d\omega}\right|_{EM} = \left(\frac{e^2}{4\pi^2 c}\right)\left(\frac{v}{c}\right)^2 p_{\rm em}(\theta)\,, \tag{4.349}$$

where

$$p_{\rm em}(\theta) = \frac{\sin^2\theta}{[1-(v/c)\cos\theta]^2}\,. \tag{4.350}$$

Both the gravitational and the electromagnetic radiations are tilted forward, because of the factor $[1-(v/c)\cos\theta]^2$ in the denominator. However, the different power of $\sin\theta$ in the numerator produces a crucial difference in the overall shape. In fact, $p_{\rm em}(\theta)$ has a maximum at an angle $\bar\theta$ given by $\cos\bar\theta = v/c$ so, for large γ, $\bar\theta \simeq 1/\gamma$; at the same time, the width of this maximum is $\Delta\theta = O(1/\gamma)$. Therefore, for $\gamma\to\infty$, the electromagnetic radiation is not only tilted asymptotically toward the forward direction, but is also beamed into a very narrow cone.

The angular pattern for GW is very different. First of all, the angle $\bar\theta$ that maximizes $p_{\rm gw}(\theta)$ is given by $\cos\bar\theta = c(\gamma-1)/(v\gamma)$ which, in the large γ limit, becomes $\bar\theta \simeq (2/\gamma)^{1/2}$; therefore $\bar\theta$ goes to zero only as $O(1/\sqrt{\gamma})$. Second, and more important, one easily checks from the explicit expression that the width of the maximum of $p_{\rm gw}(\theta)$ is $\Delta\theta = O(1)$, to be compared with $\Delta\theta = O(1/\gamma)$ for the electromagnetic case. This is due to the fact that the value of $p_{\rm em}$ at its maximum is γ^2, and it drops to values $O(1)$ if we move away from the maximum by $\Delta\theta = O(1/\gamma)$; for the gravitational radiation, it is still true that the value of $p_{\rm gw}$ at its maximum is $O(\gamma^2)$ just because of the factor γ^2 in front of it, but it remains $O(\gamma^2)$ if we move away from the maximum by a $\Delta\theta = O(1)$.

Therefore, *even in the limit $\gamma\to\infty$, the gravitational radiation is not beamed in a narrow cone, but it is extended over a solid angle comparable to 4π.* The electromagnetic and gravitational radiation pattern are shown in Figs. 4.23 and 4.24, respectively, for $v = 0.99$. The origin of the difference is the factor $\sin^4\theta$ in the numerator of eq. (4.348), which reflect the spin-2 nature of the gravitational field, compared to the $\sin^2\theta$ in the numerator of eq. (4.350), which reflect the spin-1 nature of the electromagnetic field.

To understand this point better, it is instructive to rederive this angular distribution, that we have obtained from a purely classical treatment, using the language of quantum field theory. This can be done evaluating Feynman diagrams such as that in Fig. 4.25, that describe the emission of a graviton by an accelerated particle. The angular dependence is easily understood observing that the propagator of the massive particle gives a contribution to the amplitude proportional to

$$\frac{1}{(p+k)^2+m^2} = \frac{1}{2(pk)}\,, \tag{4.351}$$

where p is the final four-momentum of the massive particle and k of the graviton, (pk) denotes the scalar product of the two four-vectors, and we used $p^2 = -m^2$ and $k^2 = 0$. We write $p^\mu = (E_p/c, |\mathbf{p}|, 0, 0)$, with $|\mathbf{p}| = E_p v/c^2$, while the graviton four-momentum is

$$k^\mu = (E_g/c, |\mathbf{k}|\cos\theta, |\mathbf{k}|\sin\theta, 0)\,, \tag{4.352}$$

where $|\mathbf{k}| = E_g/c$. Then

$$(pk) = -\frac{1}{c^2}E_p E_k[1-(v/c)\cos\theta]\,. \tag{4.353}$$

This gives a factor $[1-(v/c)\cos\theta]$ in the denominator, in the amplitude $\mathcal{M}$, and therefore a factor $[1-(v/c)\cos\theta]^2$ in the emission probability, which is $\sim|\mathcal{M}|^2$. This is independent of whether the wavy line in Fig. 4.25 is a photon or a graviton, as long as it is a massless particle, and elucidates why, both in $p_{\rm em}(\theta)$ and in $p_{\rm gw}(\theta)$, the angular dependence of the denominators is the same, $[1-(v/c)\cos\theta]^2$.

The numerator is instead fixed by the emission vertex. For a photon, the external line carries its wavefunction $\epsilon^*_\mu(k)$. Recall that physical photons are transverse, $\epsilon_\mu(k)k^\mu = 0$. With k^μ given by eq. (4.352), this equation has two linearly independent solutions

$$\epsilon^{(1)}_\mu(k) = (0, \sin\theta, -\cos\theta, 0)\,, \qquad \epsilon^{(2)}_\mu(k) = (0,0,0,1)\,, \tag{4.354}$$

which corresponds to the two physical polarizations (plus the pure gauge mode $\epsilon^\mu\sim k^\mu$). The amplitude is proportional to[40]

$$\sum_{\lambda=1,2}\epsilon^{(\lambda)}_\mu(k)p^\mu = |\mathbf{p}|\sin\theta\,. \tag{4.355}$$

Therefore in the numerator, in the amplitude, we have a factor $\sin\theta$, which gives a factor $\sin^2\theta$ in $p_{\rm em}(\theta)$, in agreement with eq. (4.350).

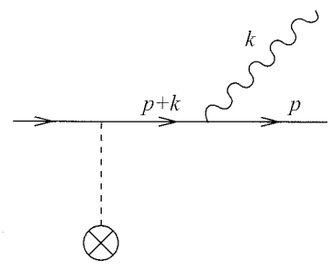

Fig. 4.25 A Feynman diagram corresponding to graviton emission by an accelerated mass. The cross denotes the external field that accelerates the mass. The wavy line represents the graviton.

[40] The fact that the Lorentz index carried by ϵ_μ is saturated by p^μ can be obtained writing explicitly the interaction vertex in quantum electrodynamics, but in fact it is evident from the fact that the amplitude must be linear in ϵ_μ, so we cannot saturate the index μ contracting ϵ_μ with a second polarization vector ϵ^μ, neither we can contract it with k^μ, since $\epsilon_\mu(k)k^\mu$ vanishes. Then $\epsilon_\mu(k)p^\mu$ is the only possible Lorentz scalar. Note also that, according to the Feynman rules of QED, an outgoing photon is actually associated to a factor ϵ^*_μ, but we have chosen a real basis for the polarization vectors.

Similarly, an external graviton line is associated to the polarization tensor $e_{\mu\nu}(k)$ of the graviton, and the physical polarizations correspond to the plus and cross polarization tensors $e^{(+)}_{\mu\nu}(k)$ and $e^{(\times)}_{\mu\nu}(k)$, that satisfy the condition $e_{\mu\nu}(k)k^\mu = 0$. As before, the Lorentz indices can be saturated only by p^μ, so this factor contributes to the amplitude as[41]

$$\sum_{\lambda=+,\times} e^{(\lambda)}_{\mu\nu}(k) p^\mu p^\nu = -|\mathbf{p}|^2 \sin^2\theta \,. \tag{4.356}$$

This produces a factor $\sin^4\theta$ in the modulus squared of the amplitude, and therefore in $p_{\rm gw}(\theta)$, in agreement with eq. (4.348).

Coming back to eq. (4.346) and integrating over the solid angle we get

$$\frac{dE}{d\omega} = \frac{2Gm^2}{3\pi c}\left[\gamma^2\left(6 - \frac{4v^2}{c^2}\right) - \frac{3c}{v}\log\frac{c+v}{c-v}\right] . \tag{4.357}$$

In the non-relativistic limit $v \to 0$, this reduces to

$$\frac{dE}{d\omega} \simeq \frac{8}{15\pi c^5} G m^2 v^4 \,, \qquad (v/c \to 0) \,, \tag{4.358}$$

while in the ultra-relativistic limit

$$\frac{dE}{d\omega} \simeq \frac{4}{3\pi c} G m^2 \gamma^2 \left[1 - \frac{3\log\gamma^2}{2\gamma^2} + O\left(\frac{1}{\gamma^2}\right)\right] , \qquad (v/c \to 1) \,. \tag{4.359}$$

This spectrum is flat up to the maximum frequency $\omega_{\rm max} \sim 2\pi/\Delta t$, and the total radiated energy is therefore obtained multiplying by $\omega_{\rm max}$.

[41] The computation is faster if we orient the axes so that the z axis is in the direction of the graviton momentum $\mathbf{k}$, and the scattering plane in Fig. 4.25 is identified with the (y,z) plane. In this frame $k^\mu = (E_g/c)(1,0,0,1)$ and $p^\mu = (E_p/c, 0, |\mathbf{p}|\sin\theta, |\mathbf{p}|\cos\theta)$. The advantage is that in this frame the polarization tensors have the simple form

$$e^{+}_{\mu\nu} = \begin{pmatrix} 0 & 0 & 0 & 0 \\ 0 & 1 & 0 & 0 \\ 0 & 0 & -1 & 0 \\ 0 & 0 & 0 & 0 \end{pmatrix}_{\mu\nu}$$

and

$$e^{\times}_{\mu\nu} = \begin{pmatrix} 0 & 0 & 0 & 0 \\ 0 & 0 & 1 & 0 \\ 0 & 1 & 0 & 0 \\ 0 & 0 & 0 & 0 \end{pmatrix}_{\mu\nu} ,$$

see eq. (1.56). Then $e^{+}_{\mu\nu}p^\mu p^\nu = -|\mathbf{p}|^2\sin^2\theta$ and $e^{\times}_{\mu\nu}p^\mu p^\nu = 0$.

4.5 Solved problems

Problem 4.1. Fourier transform of the chirp signal

In this problem we compute the Fourier transform of the amplitudes given in eqs. (4.31) and (4.32). We consider first h_+, and we write it in the form

$$h_+(t) = A(t_{\rm ret})\cos\Phi(t_{\rm ret}) \,, \tag{4.360}$$

where

$$A(t_{\rm ret}) = \frac{1}{r}\left(\frac{GM_c}{c^2}\right)^{5/4}\left(\frac{5}{c(t_c - t_{\rm ret})}\right)^{1/4}\left(\frac{1+\cos^2\iota}{2}\right) , \tag{4.361}$$

and, in this problem, t_c is the value of *retarded* time at coalescence. The Fourier transform is

$$\begin{aligned}\tilde h_+(f) &= \int dt\, A(t_{\rm ret})\cos\Phi(t_{\rm ret}) e^{i2\pi f t} \\ &= \frac{1}{2}\, e^{i2\pi f r/c}\int dt_{\rm ret}\, A(t_{\rm ret})\left(e^{i\Phi(t_{\rm ret})} + e^{-i\Phi(t_{\rm ret})}\right) e^{i2\pi f t_{\rm ret}} ,\end{aligned} \tag{4.362}$$

and now in the last integral we rename $t_{\rm ret} \to t$. We have not written explicitly the limits of integration since we will compute this integral with the stationary phase method. Then, all we need is that the stationary point be within the integration domain $t < t_c$, and the fact that $A(t_{\rm ret})$ diverges at the limit of integration $t - t_c$ becomes irrelevant, as long as the stationary phase method is justified (see below). We take $f > 0$, since the value at $f < 0$ can be obtained from $\tilde h_+(-f) = \tilde h^*_+(f)$. Then, observing that $\dot\Phi = \omega_{\rm gw}(t) > 0$, we see that only the term proportional to $e^{-i\Phi(t)+i2\pi f t}$ has a stationary point, while the term proportional to $e^{i\Phi(t)+i2\pi f t}$ is always oscillating fast, and integrates to a negligibly small value. Therefore

$$\tilde h_+(f) \simeq \frac{1}{2} e^{i2\pi f r/c}\int dt\, A(t) e^{i[2\pi f t - \Phi(t)]} \,. \tag{4.363}$$

Since $\log A(t)$ varies slowly in comparison with $\Phi(t)$, the stationary point $t_*(f)$ is determined by the condition $2\pi f = \dot\Phi(t_*)$, However $\dot\Phi = \omega_{\rm gw}$, so this condition expresses the rather natural fact that the largest contribution to the Fourier component $\tilde h_+(f)$ with a given f is obtained for the values of t such that the chirping frequency $\omega_{\rm gw}(t)$ is equal to $2\pi f$. Expanding the exponential to order $(t - t_*)^2$ we find

$$\tilde h_+(f) \simeq \frac{1}{2} e^{i2\pi f r/c} A(t_*) e^{i[2\pi f t_* - \Phi(t_*)]}\left(\frac{2}{\ddot\Phi(t_*)}\right)^{1/2}\int_{-\infty}^{\infty} dx\; e^{-ix^2} . \tag{4.364}$$

The latter integral is a Fresnel integral, and is given by

$$\int_{-\infty}^{\infty} dx\; e^{-ix^2} = \sqrt{\pi}\, e^{-i\pi/4} \tag{4.365}$$

(see Gradshteyn and Ryzhik 1980, 8.25). Therefore

$$\tilde h_+(f) = \frac{1}{2}\, e^{i\Psi_+} A(t_*)\left(\frac{2\pi}{\ddot\Phi(t_*)}\right)^{1/2} , \tag{4.366}$$

where

$$\Psi_+ = 2\pi f(t_* + r/c) - \Phi(t_*) - (\pi/4) \,. \tag{4.367}$$

Using $2\pi f = \omega_{\rm gw}(t_*)$ and the explicit expression of $\omega_{\rm gw}(t)$ given in eq. (4.19), we can eliminate $\tau_* = t_c - t_*$ in favor of f, obtaining

$$\tau_*(f) = \frac{5}{256}(GM_c/c^3)^{-5/3}(\pi f)^{-8/3} \,. \tag{4.368}$$

Inserting this into the expressions for $A(\tau)$, given in eq. (4.361), and for $\ddot\Phi$, obtained differentiating twice eq. (4.30), we find

$$\frac{1}{2} A(t_*)\left(\frac{2\pi}{\ddot\Phi(t_*)}\right)^{1/2} = \left[\left(\frac{5}{24}\right)^{1/2}\frac{1}{\pi^{2/3}}\right]\frac{c}{r}\left(\frac{GM_c}{c^3}\right)^{5/6} f^{-7/6}\left(\frac{1+\cos^2\iota}{2}\right) , \tag{4.369}$$

and therefore we get the result given in the text, see eq. (4.34). Similarly, inserting the value of $t_* = t_c - \tau_*$ given by eq. (4.368) into eq. (4.367) we get the phase $\Psi_+(f)$ given in eq. (4.37). Repeating the same steps for $h_\times$ we get the same prefactor, apart for the different dependence on ι, and $\Psi_\times = \Psi_+ + (\pi/2)$.

To compute the energy spectrum we need the quantity

$$|\tilde h_+(f)|^2 + |\tilde h_\times(f)|^2 = \frac{5}{24\,\pi^{4/3} r^2 c^3}\frac{(GM_c)^{5/3}}{f^{7/3}}\, g(\iota) \,, \tag{4.370}$$

where the function $g(\iota)$ is defined in eq. (4.9). Using eq. (4.10), we see that the angular average of $|\tilde{h}_+(f)|^2 + |\tilde{h}_\times(f)|^2$ is

$$\int \frac{d\Omega}{4\pi} |\tilde{h}_+(f)|^2 + |\tilde{h}_\times(f)|^2 = \frac{1}{6\,\pi^{4/3} r^2 c^3} \frac{(GM_c)^{5/3}}{f^{7/3}} \,. \tag{4.371}$$

It should be observed that the stationary point approximation that we have used is less and less good as f grows. In fact, as f grows, the stationary point t_* approaches the coalescence time t_c. Since the function $A(t)$ diverges as $t \to t_c$, the approximation that $\log A(t)$ varies slowly in comparison with $\Phi(t)$ becomes less and less accurate. To check the validity of the stationary point approximation for $\tilde{h}_{+,\times}(f)$, we compare the total radiated energy computed using the saddle point approximation, eq. (4.43), with an exact numerical evaluation of the time integral in the inspiral phase. Therefore we start from the exact expression

$$\Delta E_{\rm rad} = \frac{r^2 c^3}{16\pi G} \int d\Omega \int_{-\infty}^{t_*} dt \, \left(\dot{h}_+^2 + \dot{h}_\times^2 \right) \,, \tag{4.372}$$

which gives the energy radiated up to time t_*, and we compute numerically the integral. Inserting into this expression the GW amplitude given by eq. (4.29) and performing the integral over $d\Omega$, we find

$$\begin{aligned} \Delta E_{\rm rad} = {} & \frac{(GM_c)^{10/3}}{2^{1/3} G c^5} (GM_c)^{10/3} \\ & \times \int_{-\infty}^{t_*} dt \, \frac{14}{15} \left[\frac{d}{dt} (\omega_{\rm gw}^{2/3} \cos\Phi) \right]^2 + \frac{2}{3} \left[\frac{d}{dt} (\omega_{\rm gw}^{2/3} \sin\Phi) \right]^2 . \end{aligned} \tag{4.373}$$

We now compute the time derivatives, taking into account that $\omega_{\rm gw}$ depends on t, and that $d\Phi/dt = \omega_{\rm gw}$. The result can be written in the form

$$\Delta E_{\rm rad} \simeq \frac{5^{7/5}}{2^{34/5}} M_c c^2 \left[\frac{1}{10} \left(\frac{8}{5} \right)^{12/5} a_1 + \left(\frac{8}{5} \right)^{7/5} a_2 - \frac{1}{30} \left(\frac{8}{5} \right)^{12/5} a_3 \right] , \tag{4.374}$$

with

$$a_1 = \int_{x_*}^{\infty} \frac{dx}{x^{17/5}} \left(\frac{7}{15} \cos^2 x + \frac{1}{3} \sin^2 x \right) , \tag{4.375}$$

$$a_2 = \int_{x_*}^{\infty} \frac{dx}{x^{7/5}} \left(\frac{7}{15} \sin^2 x + \frac{1}{3} \cos^2 x \right) , \tag{4.376}$$

$$a_3 = \int_{x_*}^{\infty} \frac{dx}{x^{12/5}} \sin 2x \,. \tag{4.377}$$

The lower limit of the integrals, x_*, is given by

$$x_* = 2 \left(\frac{5GM_c}{c^3} \right)^{-5/8} \tau_*^{5/8} \,. \tag{4.378}$$

Taking $M_c \simeq 1.21 M_\odot$ (corresponding to two equal masses $M_{\rm NS} = 1.4 M_\odot$), and $\tau_* \simeq 4.6$ ms which, according to eq. (4.20), correspond to taking a cutoff at $f_{\rm max} = 1$ kHz, we have $x_* \simeq 46.1$. Computing numerically the integrals, we find that $a_2 \simeq 0.21$ while $a_1, a_3 = O(10^{-5})$ are negligible. Since a_1, a_3 come from the terms with $\dot{\omega}_{\rm gw}$, the result could have been obtained more simply neglecting the derivatives of $\omega_{\rm gw}$ in eq. (4.373) (this is indeed the reason why the stationary point approximation discussed in the previous problem works well). Putting together the numerical factors, we finally arrive at $\Delta E_{\rm rad} \simeq 4.2 \times 10^{-2} M_\odot c^2$, in full agreement with eq. (4.43).

Problem 4.2. Fourier decomposition of elliptic Keplerian motion

In this problem we compute the Fourier decomposition of the Keplerian motion and of its second mass moment. Using eqs. (4.63), (4.64) and (4.58) we write

$$x(\beta) = a(\cos u - e) \,, \tag{4.379}$$

$$y(\beta) = b \sin u \,, \tag{4.380}$$

where the dependence of u on β is given implicitly by

$$\beta = u - e \sin u \,. \tag{4.381}$$

As shown between eq. (4.83) and eq. (4.93), we can write

$$x(\beta) = \sum_{n=0}^{\infty} a_n \cos(n\beta) \,, \tag{4.382}$$

$$y(\beta) = \sum_{n=1}^{\infty} b_n \sin(n\beta) \,, \tag{4.383}$$

which can be inverted to give, for $n \neq 0$,

$$\begin{aligned} a_n &= \frac{2}{\pi} \int_0^{\pi} d\beta \, x(\beta) \cos(n\beta) \\ &= \frac{2a}{\pi} \int_0^{\pi} d\beta \, (\cos u - e) \cos(n\beta) \,, \end{aligned} \tag{4.384}$$

and

$$\begin{aligned} b_n &= \frac{2}{\pi} \int_0^{\pi} d\beta \, y(\beta) \sin(n\beta) \\ &= \frac{2b}{\pi} \int_0^{\pi} d\beta \, \sin u \sin(n\beta) \,, \end{aligned} \tag{4.385}$$

while, for $n = 0$,

$$a_0 = \frac{1}{\pi} \int_0^{\pi} d\beta \, x(\beta) \,. \tag{4.386}$$

The integrals for $n \neq 0$ can be performed using the integral representation of the Bessel function $J_n(z)$,

$$J_n(z) = \int_0^{\pi} \frac{du}{\pi} \cos(nu - z \sin u) \,, \tag{4.387}$$

(see e.g. Gradshteyn and Ryzhik 1980, 8.411.1). Then we have, for $n \neq 0$,

$$\begin{aligned} a_n &= 2a \int_0^{\pi} \frac{d\beta}{\pi} (\cos u - e) \cos(n\beta) \\ &= \frac{2a}{n} \int_0^{\pi} \frac{d\beta}{\pi} (\cos u - e) \frac{d}{d\beta} \sin(n\beta) \\ &= -\frac{2a}{n} \int_0^{\pi} \frac{d\beta}{\pi} [\frac{d}{d\beta} (\cos u - e)] \sin(n\beta) \\ &= -\frac{2a}{n} \int_0^{\pi} \frac{du}{\pi} [\frac{d}{du} (\cos u - e)] \sin(n\beta) \\ &= \frac{2a}{n} \int_0^{\pi} \frac{du}{\pi} \sin u \sin(nu - ne \sin u) \,. \end{aligned} \tag{4.388}$$

We now use the identity $2\sin x \sin y = \cos(x-y) - \cos(x+y)$, and we get

$$\begin{aligned} a_n &= \frac{a}{n}\int_0^\pi \frac{du}{\pi}\,\cos[(n-1)u - ne\sin u] - \cos[(n+1)u - ne\sin u] \\ &= \frac{a}{n}[J_{n-1}(ne) - J_{n+1}(ne)]\,, \end{aligned} \tag{4.389}$$

where, in the second line, we used eq. (4.387). Using the Bessel functions identity

$$J_{n-1}(z) - J_{n+1}(z) = 2J_n'(z)\,, \tag{4.390}$$

the result can also be rewritten as

$$a_n = \frac{2a}{n}J_n'(ne)\,. \tag{4.391}$$

The integral for a_0 is instead elementary and gives $a_0 = -(3/2)ae$. The computation for b_n is analogous to that of a_n,

$$\begin{aligned} b_n &= -\frac{2b}{n}\int_0^\pi \frac{d\beta}{\pi}\,\sin u \frac{d}{d\beta}\cos(n\beta) \\ &= \frac{2b}{n}\int_0^\pi \frac{du}{\pi}\,\frac{d\sin u}{du}\cos(n\beta) \\ &= \frac{2b}{n}\int_0^\pi \frac{du}{\pi}\,\cos u\cos(nu - ne\sin u) \\ &= \frac{b}{n}\left[J_{n-1}(ne) + J_{n+1}(ne)\right]\,. \end{aligned} \tag{4.392}$$

Using the Bessel functions identity

$$J_{n+1}(z) + J_{n-1}(z) = \frac{2n}{z}J_n(z)\,, \tag{4.393}$$

this result can also be rewritten as

$$b_n = \frac{2b}{ne}J_n(ne)\,. \tag{4.394}$$

We next compute the Fourier decomposition of $x^2(\beta), y^2(\beta)$ and $x(\beta)y(\beta)$. Since $x(\beta)$ is even under $\beta \to -\beta$ while $y(\beta)$ is odd, $x^2(\beta)$ and $y^2(\beta)$ are even while $x(\beta)y(\beta)$ is odd, and therefore we can write

$$x^2(\beta) = \sum_{n=0}^\infty A_n\cos(n\beta)\,, \tag{4.395}$$

$$y^2(\beta) = \sum_{n=0}^\infty B_n\cos(n\beta)\,, \tag{4.396}$$

$$x(\beta)y(\beta) = \sum_{n=1}^\infty C_n\sin(n\beta)\,, \tag{4.397}$$

which can be inverted to give, for $n \neq 0$,

$$A_n = \frac{2}{\pi}\int_0^\pi d\beta\, x^2(\beta)\cos(n\beta) \tag{4.398}$$

$$B_n = \frac{2}{\pi}\int_0^\pi d\beta\, y^2(\beta)\cos(n\beta) \tag{4.399}$$

$$C_n = \frac{2}{\pi}\int_0^\pi d\beta\, x(\beta)y(\beta)\sin(n\beta)\,. \tag{4.400}$$

The calculations are similar to those performed above for a_n and b_n, and the result is

$$A_n = \frac{a^2}{n}\left[J_{n-2}(ne) - J_{n+2}(ne) - 2e(J_{n-1}(ne) - J_{n+1}(ne))\right]\,, \tag{4.401}$$

$$B_n = \frac{b^2}{n}\left[J_{n+2}(ne) - J_{n-2}(ne)\right]\,, \tag{4.402}$$

$$C_n = \frac{ab}{n}\left[J_{n+2}(ne) + J_{n-2}(ne) - e(J_{n+1}(ne) + J_{n-1}(ne))\right]\,, \tag{4.403}$$

while $A_0 = (1+4e^2)/2$ and $B_0 = 1/2$. Observe that these coefficients can be rewritten in many equivalent forms using Bessel function identities.

Further reading

- The radiation from a binary system of two point masses and their frequency spectrum was computed by Peters and Mathews (1963). The Fourier expansion of the Kepler motion is discussed in Watson (1966). The orbit circularization due to radiation of angular momentum was computed by Peters (1964). The chirp amplitude was first computed by Clark and Eardley (1977), see also Thorne (1987), Finn and Chernoff (1993), Cutler and Flanagan (1994).
- The fact that coalescing binaries can be standard candles was discussed by Schutz (1986). The propagation of GWs through a FRW background, in the geometric optics limit, is discussed in Thorne (1983), Section 2.5.4.
- The production of GWs from rotating and precessing rigid bodies is computed in Zimmermann and Szedenits (1979), for axisymmetric bodies and for triaxial bodies with small wobble angle. The radiation from non-axisymmetric bodies rotating and precessing is discussed in Zimmermann (1980) and Van Den Broeck (2005). Rotating fluid stars are studied in Bonazzola and Gourgoulhon (1996). The back-reaction due to wobble radiation is discussed in Bertotti and Anile (1973) and Cutler and Jones (2001). In the latter paper one also finds the correct result for elastic, rather than rigid, neutron stars.
- The production of GWs from a point-like particle falling radially into a black hole is discussed in Davies, Ruffini, Press and Price (1971) and Davis, Ruffini and Tiomno (1972), see also Ohanian and Ruffini (1994). The frequency spectrum is computed in Wagoner (1979). Detweiler and Szedenits (1979) show that, allowing for angular momentum of the test mass, can increase the power output by a large factor, and higher multipoles become more important. The suppression due to the tidal disruption of extended sources is computed by Haugan, Shapiro and Wasserman (1982). Early simulations of head-on black-hole collisions were performed by Smarr (1979).
- The radiation produced in the collision between particles is discussed in Weinberg (1972), Section 10.4. The calculation of the gravitational radiation produced by an accelerated particle, using Feynman diagram techniques, and the fact that the radiation emitted in particle scattering is not beamed, is discussed by Feynman (see Feynman, Morinigo and Wagner 1995, Section 16.4), while our purely classical derivation leading to eq. (4.348) is, as far as we know, original.
- Various examples of production of GWs are discussed in the textbook by Shapiro and Teukolsky (1983), Chapter 16.